ELECTROPHORETIC SEPARATIONS FOR CONTINUOUS FLOW SYNTHESIS

Nikita Ivanov

A DISSERTATION SUBMITTED TO THE FACULTY OF GRADUATE STUDIES

IN PARTIAL FULFILLMENT OF THE REQUIREMENTS

FOR THE DEGREE OF

DOCTOR OF PHILOSOPHY

GRADUATE PROGRAM IN CHEMISTRY

YORK UNIVERSITY

TORONTO, ONTARIO

August 2022

ABSTRACT

The continuous-flow synthesis field has grown considerably in the last several decades. Converting a reaction from its batch synthesis to a continuous-flow alternative offers a long list of potential improvements. The latest advances make it possible for reactions to take place “on the chip’, where microscopic channels are used to propagate and mix different reactants. Continuously propagating discrete volumes of reactants inside a small capillary has the advantage of improved mass and heat transfers. These transport phenomena directly affect the kinetics and thermodynamics of the reaction, two factors that influence reaction yield over time. Having higher yields means that more product is made in a similar or lesser time frame, which can potentially lower the production cost of a pharmaceutical product, resulting in a monetary advantage for the early adopter. Another positive aspect of continuous flow chemistry is safety. By miniaturizing a reactor, we gain another level of control over the system. Since flow-reactor volumes are microscopic, the enthalpy of exothermic reactions can be easily dissipated. This is extremely important when reactions of interest possess high enthalpic contribution, especially if they are self-accelerating decomposition reactions.

Since no reaction can ever achieve a hundred percent yield, a product purification mechanism is required at the end of each synthesis step. It runs naturally that a continuous-flow synthesis system should feed into a continuous-flow separation compliment without breaking the fundamental continuity concept. Up to this day, this remains the most problematic area of continuous-flow chemistry. Available continuous separation methods are either pseudo-continuous (simulated moving bed chromatography, SMBC) or severely limited in the number of concurrently separated analytes (Continuous liquid-liquid extraction, CLLE).

The real solution to this problem are molecular stream separation (MSS) platforms. MSS approach allows for multiple analytes to be separated and analyzed simultaneously without disturbing the synthesis platform's continuous nature. Only two major MSS branches exist today, continuous-flow electrophoresis (CFE) and continuous annular chromatography (CAC). Although CAC has always been developed with the organic synthesis in mind, CFE has historically been reserved for water-soluble biological analytes such as DNA or proteins. By adapting CFE to the world of organic chemistry, we open the door to the field of electrophoretic separations for continuous-flow synthesis.

The following manuscript will touch on the subject of fundamental engineering challenges imposed by the project and will serve to summarize our latest efforts at transforming CFE into a simple yet comprehensive platform for continuous chemistry separations.

DEDICATION

To those who have helped me on my journey

By all ye cry or whisper,
By all ye leave or do,
The silent, sullen peoples
Shall weigh your Gods and you.
Comes now, to search your manhood
Through all the thankless years,
Cold-edged with dear-bought wisdom,
The judgment of your peers.
R. Kipling 1897

Тем, что ты уже сделал
И сделать еще готов,
Молчащий народ измерит
Тебя и твоих Богов.
Теперь твою возмужалость
И непокорность судьбе
Оценит горький и трезвый
Суд равных тебе.
Р. Киплинг 1897

AKNOWLEGMENTS

I would like to thank my parents, who welcomed me into this world despite their youth's political and economic turmoil.

I would like to thank my grandparents for taking care of me when my parents couldn’t.

I would like to thank my primary school teachers for their care and devotion.

I would like to thank my E.S.P. “Le Sommet” teachers for their kindness and patience with my attempts to speak French.

I would like to thank Dr. John Basso for his academic and spiritual mentorship during my time at the University of Ottawa; our conversations soothed my undergraduate pains.

I would like to thank my M.Sc. supervisor, Dr. Paula Ribeiro, for guiding me during my early graduate studies at McGill University.

I would like to thank Dr. Vitalie Samoil for his enthusiastic teaching of hands-on biochemistry techniques and his help running what now feels like a thousand western blots.

I would like to thank Philip Zanet for being my friend and for all the laughs we shared watching dumb Star Wars and Marvel films.

I would like to thank Dr. Sven Kochmann for his mentoring during my doctoral work and for talking to me every time I showed up at his office door to discuss my “great” ideas.

I would like to thank Viktor Galievsky for introducing me to the world of CE repair and helping me with my optical projects.

I would like to thank Dr. Stas Beloborodov for filling the blanks in my general chemistry knowledge, for his experimental advice, and for keeping me company for five years.

I would like to thank Dr. Vasily Panferov for introducing me to the world of point-of-care devices and the many funny stories that he recited.

Finally, I would like to thank Prof. Sergey Krylov for taking a leap of faith six years ago and taking in a biochemistry student for a chemical engineering project.

TABLE OF CONTENTS

ABSTRACT II
DEDICATION IV
AKNOWLEGMENTS V
TABLE OF CONTENTS VII
LIST OF TABLES X
LIST OF FIGURES XI
LIST OF ABRREVIATIONS XIII

CHAPTER 1. INTRODUCTION

1.1. THE OVERVIEW OF CONTINUOUS SEPARATIONS FOR ORGANIC CHEMISTRY 1
1.1.1. One-dimensional continuous separations 6
1.1.2. Two-dimensional continuous separations 7
1.1.2.1. Continuous liquid-liquid extraction 7
1.1.2.2. Continuous annular chromatography 8
1.1.2.3. Continuous-Flow Electrophoresis 9
1.2. CONTINUOUS ELECTROPHORETIC SEPARATIONS 10
1.2.1. Analytical separations 10
1.2.2. Preparative separations 11
1.2.2.1. Proteins 11
1.2.2.2. DNA 12
1.2.2.3. Lipids 12
1.2.2.4. Nano-particles 12
1.2.2.5. Small molecules 13
1.3. CONTINOUS ELECTROPHORETIC SEPARATIONS DEVICE 14
1.3.1. Device fabrication and materials 14
1.3.2. Solvent and background electrolyte (BGE) 16
1.3.3. Electrodes 18

CHAPTER 2. DEVELOPING A NON-AQUEOUS CONTINUOUS-FLOW SEPARATION PLATFORM

2.1. INTRODUCTION 20
2.2. MATERIALS AND METHODS 22
2.2.1. Chemicals and materials 22
2.2.2. Instrumentation 22
2.2.3. Chip fabrication 23
2.2.4. General experimental details 23
2.2.5. Mixing behaviour of PC 23
2.2.6. Evaluation procedure for NACFE images 24
2.2.7. Constructing angulagrams from reflectometric images 25
2.2.8. Extracting stream parameters form angulagrams 26
2.2.9. Evaluation of the 10-h separation 26

2.2.10. Electrical current measurements 27
2.3. RESULTS AND DISCUSSION 27
2.3.1. Selection of device material 27
2.3.2. Selection of solvent and charge carrier 28
2.3.3. Assessing the quality of NACFE 29
2.3.4. Assessing the stability of NACFE 34
2.3.5. Obtaning a pure product in NACFE 36
2.4. CONCLUSIONS 37

CHAPTER 3. DETECTING MOLECULAR STREAMS IN CONTINUOUS ELECTROPHORETIC SEPARATION

3.1. INTRODUCTION 39
3.2. MATERIALS AND METHODS 40
3.2.1. Materials and chemicals 40
3.2.2. Instrumentation 40
3.2.3. Chip Fabrication 41
3.2.4. General experimental details 41
3.2.5. Evaluation procedure 42
3.2.6. Constructing angulagrams 42
3.2.7. Estimating limit of detection (LOD) 43
3.2.8. Analyte concentration as a function of signal 44
3.2.9. Estimating the LOD by calculations 46
3.2.10. Minimum channel depth for sub-mM LOD 47
3.2.11. Extracting stream parameters from angulagrams 48
3.3. RESULTS AND DISCUSSION 49
3.3.1. Molecular stream detection 49
3.3.2. FSV imaging system 51
3.3.3. FSV proof-of-concept 52
3.3.4. FSV chip design 54
3.3.5. FSV proof-of-work 56
3.4. CONCLUSIONS 57

CHAPTER 4. IMPROVING THE RESOLUTION THROUGH NON-ORTHOGONAL APPLICATION OF THE ELECTRIC FIELD

4.1. INTRODUCTION 59
4.2. MATERIALS AND METHODS 60
4.2.1. Index of Uniformity calculations 60
4.2.2. Measurements of electrophoretic mobilities in CE 62
4.2.3. Circular CFE device fabrication details 62
4.2.4. Circular CFE experimental details 63
4.2.5. Using Fiji/TrackMate for the circular design flow field Γ calculations 64
4.3. RESULTS AND DISCUSSION 66
4.3.1. From rectangular to circular geometry 66

4.3.2. Ideal device requirements 67
4.3.3. Optimizing the flow-field 68
4.3.4. Optimizing the electric field 70
4.3.5. Optimized device numeric simulations 73
4.3.6. Optimized device experimental flow-field uniformity 75
4.3.7. Optimized device experimental electric field uniformity 76
4.3.8. Optimized device resolution 77
4.4. CONCLUSIONS 80

LIMITATIONS 82
CONCLUDING REMARKS 85
FUTURE PLANS 86

LIST OF PUBLICATIONS 88

REFERENCES 89

APPENDICES 101
APPENDIX A - Supplementary tables and figures for Chapter 2 101
APPENDIX B - Supplementary tables and figures for Chapter 3 108
APPENDIX C - Supplementary tables and figures for Chapter 4 111

LIST OF TABLES

Table 3.1. Chip assemblies and properties for various combinations of quartz, transparent plastic (TP), and fluorescent plastic (FP). 54

Table A2.1. (APPENDIX A) Properties of tested plastic materials 101

Table B3.1. (APPENDIX B) Properties of tested plastic materials..... 108

LIST OF FIGURES

Figure 1.1. Basic one-dimensional separation system with three analytes possessing different proportionality coefficients and resulting terminal velocities 2

Figure 1.2. A) One-dimensional discrete separation system with the separating force acting parallel to the hydrodynamic flow. B) Two-dimensional continuous separation system with the separating force orthogonal to the hydrodynamic flow 4

Figure 1.3. One-dimensional continuous separation system 6

Figure 1.4. Schematic representation of two-phase Continuous Liquid-Liquid Extraction (CLLE) system. 7

Figure 1.5. Schematic representation of Continuous Annular Chromatography (CAC) system 8

Figure 1.6. Schematic representation of Continuous-Flow Electrophoresis (CFE) system 9

Figure 2.1. Schematic of NACFE seamlessly integrated between two stages (upstream and downstream) of continuous-flow organic synthesis 20

Figure 2.2. Angulagrams of NACFE of fluorescein, α-naphtholbenzein, Sudan black B, and DMAS in 30 mM TBAA in PC at two different electrolyte flowrates 30

Figure 2.3. Angulagrams of NACFE of α-naphtholbenzein, Sudan black B, and DMAS under various concentrations of TBAA in PC 33

Figure 2.4. Stream parameters and an averaged photo of 10-h NACFE in 30 mM TBAA in PC 35

Figure 3.1. Schematics of UV imaging using UV optics and UV camera and fluorescence sublayer visualization (FSV) 49

Figure 3.2. Schematic and photo of the FSV setup designed, assembled, and used in this work 51

Figure 3.3. Feasibility of a quartz-quartz pseudo chip, a PVC-PVC CFE chip, and a quartz-PEI CFE chip for FSV 53

Figure 3.4. Photo and the angulagram of the separation of benzoic acid and styrene in CFE 56

Figure 4.1. Schematic depiction of conventional orthogonal MSS, continuous-flow electrophoresis, and continuous annular chromatography. 59

Figure 4.2. Illustration of the second-order rotational symmetry for conventional rectangular-geometry MSS and the high-order rotational symmetry for hypothetical circular-geometry MSS 67

Figure 4.3. COMSOL-simulated hydrodynamic flow lines of the evolving circular FFE design 69

Figure 4.4. The influence of the electrode length on the uniformity of electric field in the eye-shaped CFE device with 16 electrode segments in total with 71

Figure 4.5. Comparison of field-flow uniformity of circular CFE to that of rectangular CFE 72

Figure 4.6. The effect of the field-to-flow angle on simulated CFE of three species with electrophoretic mobilities μ1 = –1.01 × 10–8, μ2 = –5.66 × 10–9, and μ3 = 0 m2/(V*s) 74

Figure 4.7. Assessment of flow uniformity in circular CFE via flowing fluorescent beads through the device without electric field and with an average flow velocity of 0.09 mm/s in the separation zone 76

Figure 4.8. Indirect assessment of electric-field uniformity in a circular CFE device via evaluation of stream linearity 77

Figure 4.9. Comparison of CFE of fluorescein, α- naphtholbenzein, and Sudan Black with 90° and 112.5° field-to-flow angle 78

Figure A2.1. (APPENDIX A) NACFE chip 103

Figure A2.2. (APPENDIX A) Electric current in NACFE with an electrolyte being TBAA solution in PC 104

Figure A2.3. (APPENDIX A) Formation of brown precipitate at the cathode for the imidazolium-based electrolyte 105

Figure A2.4. (APPENDIX A) Comparing NACFE with weak- and strong-basicity anions in the electrolyte 106

Figure A2.5. (APPENDIX A) Acetonitrile as a solvent in non-aqueous electrolyte 107

Figure B3.1. (APPENDIX B) Quartz-quartz pseudo device 109

Figure B3.2. (APPENDIX B) PEI-quartz pseudo device 110

Figure C4.1. (APPENDIX C) CAC geometry transformation 111

Figure C4.2. (APPENDIX C) Varying the total number of the electrode segments. 112

Figure C4.3. (APPENDIX C) Angulagrams for Figure 4.6a. 113

LIST OF ABBREVIATIONS

BGE	background electrolyte
CAC	continuous annular chromatography
CE	capillary electrophoresis
CFS	continuous-flow synthesis
CFP	continuous-flow purification
CLLE	continuous liquid-liquid extraction
DNA	deoxyribonucleic acid
E	applied electrical field
EOF	electroosmotic flow
f	frictional coefficient
FFE	free-flow electrophoresis
FFIZF	free-flow interval zone electrophoresis
FFITP	free-flow isotachophoresis
FFIEF	free-flow iso-electric focusing
FFZE	free-flow zone electrophoresis
FSV	fluorescence sublayer-based visualization
LOD	limit of detection
μ	electrophoretic mobility
μ_{EOF}	electroosmotic mobility
MEC	micellar electrokinetic chromatography
MBC	moving bed chromatography
μFFE	micro-FFE
MS	mass spectrometry
η	dynamic viscosity of the solution
NACFE	non-aqueous continuous-flow electrophoresis
PEI	polyetherimide
pH	potential of hydrogen
pI	isoelectric point
Q	charge
ρ	density
PMMA	poly(methyl methacrylate)

PC	propylene carbonate
PVC	polyvinyl chloride
R	resolution
R_{hyd}	hydrodynamic radius
SMBC	simulated moving bed chromatography
t	migration times
TBAA	tetrabutylammonium acetate
TMB	true moving bed chromatography
UV	ultraviolet
v	velocity of the molecule
V	applied voltage
V_{EOF}	velocity of electroosmotic flow

CHAPTER 1. INTRODUCTION

1.1. THE OVERVIEW OF CONTINUOUS SEPARATIONS FOR ORGANIC CHEMISTRY

Continuous-flow chemical synthesis has demonstrated its value as a practical tool for organic chemistry by providing the benefits of increased yields, automation capability, and safety[1–4]. Downstream purifications of these processes are crucial to ensure high product purity and high operation efficiency. Naturally, continuous synthesis benefits from continuous purifications. Such an approach requires a continuous-flow separation of compounds with minimal technical complexity and ease of upstream synthesis hyphenation to downstream analysis. This introduction will outline the benefits and requirements of a genuinely continuous separation method.

Fundamentally, the nature of any separations is governed by a limited set of physical parameters that describe its identity. The act of separation is best described as the spatial division of multiple analytes of interest that are co-localized inside an arbitrary starting matrix. This basic description of the task highlights two major underlying requirements for any separation. The first requirement is the need for space of one dimension or higher. A simple line best describes one-dimensional space, and no separation is possible in a zero-order dimension since it's represented by a dot. The second requirement is the difference in physical motion (Δv) of the analytes. When their velocities are uneven, given enough time, the analytes occupy different spatial coordinates(**Figure 1.1**). For this to happen, analytes must obtain a terminal velocity caused by a separating force (F) of arbitrary nature that acts discriminately upon them. The magnitude of analyte velocity caused by this force, regardless of its physical nature, is dissimilar due to the difference in particle-specific proportionality coefficients (c_a, c_b)**Eq1**.

$$\Delta v = (c_a - c_b)F \qquad \textbf{Eq. 1}$$

Depending on the separating force, such coefficients are settling mobility (centrifugation methods), electrophoretic mobility (electric field methods), retention factor (chromatography methods), and magnetophoretic mobility (magnetic field methods).

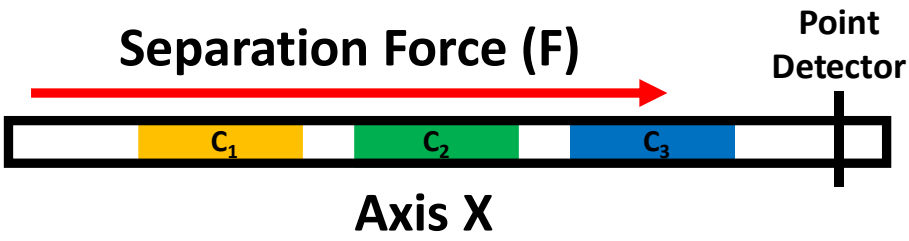

Figure 1.1 Basic one-dimensional separation system with three analytes possessing different proportionality coefficients and resulting terminal velocities.

It is important to note that the complete list of potential forces for a continuous separation is not limited to the four previously mentioned. Selecting the appropriate force for separation lies exclusively with a separation chemist. The best separation results are typically obtained with the force that gives the most considerable difference in the terminal velocity of analytes.

For any one-dimensional separation system, the quality of separation between two analytes is best described by resolution R defined as follows:

$$R = \frac{t_{a2} - t_{a1}}{\frac{1}{2}(W_{a2} + W_{a1})} \qquad \textbf{Eq. 2}$$

Where t is the time that it takes for an analyte to reach the detector and W is the width of the analyte peak. R is a dimensionless number that quantitatively describes how well two analytes are resolved. As evident from the equation, the highest values of R are obtained when the time values are very different. Since the distance to the detector is predetermined for both analytes, it is their velocity that determines the exact value of t. While maximizing the velocity difference, it's essential not to forget the second variable W in the equation that describes the width of a peak. The peak width of both species should be kept minimal. Aspects that can potentially affect W include all parameters that influence molecular transport phenomena. Such parameters are analyte size, matrix viscosity, analyte concentration, and temperature.

The same equation can be used to analyze the separation quality of systems with higher dimensionality. Although possible, such an approach convolutes the data presented to the operator and is by definition flawed. Multi-dimensional separation methods require a different kind of analysis that can't be condensed to a single value without a loss of valuable information. This problem was addressed by S. Kochmann et al.[5]

Let us examine how analytes of interest are eluted to better understand the advantage of two-dimensional over one-dimensional separation systems. Essentially, any one-dimensional separation system is limited to a single spatial axis of coordinates where analytes are resolved. Under hydrodynamic flow, analytes are injected into the apparatus and reach the end at specific times and in discrete volumes (**Figure 1.2A**). This primary limitation creates the analytical bottleneck that forces an operator to wait until the reaction system can be sampled again. In one-dimensional separation systems, the sampling frequency is inherently limited by the elution time of the analyte with the slowest mobility. Low sampling frequency can be a challenge for reactions with high chemical kinetics since the time required to sample the system might reach

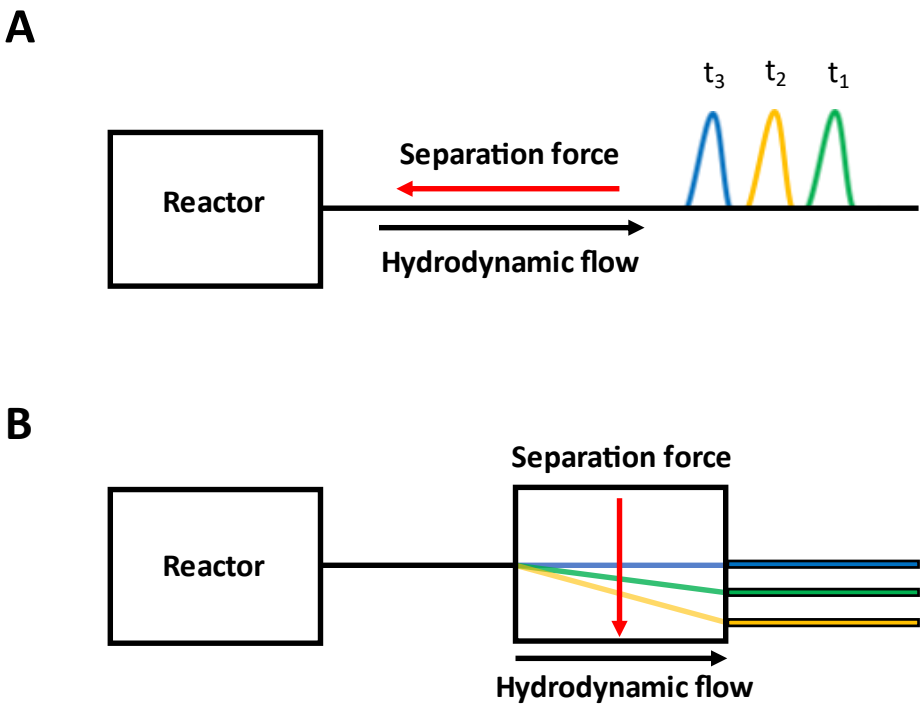

Figure 1.2 A) One-dimensional discrete separation system with the separating force acting parallel to the hydrodynamic flow. **B**) Two-dimensional continuous separation system with the separating force orthogonal to the hydrodynamic flow.

tens of minutes. Because of the previously mentioned limitations, one-dimensional systems can be continuous only under a strict set of conditions that will be described further.

Two-dimensional separation systems circumvent this limitation by incorporating an additional dimension to their separation zone (**Figure 1.2B**). This way, the separation zone obtains a new set of non-overlapping coordinates where multiple analytes can be localized without overlapping. Under the hydrodynamic flow, analytes continuously enter the separation zone and are continuously separated along two axes before reaching the end. This approach allows the operator to sample all analytes simultaneously and doesn't require waiting for the slowest analyte. Only separation systems of the second dimensionality or higher can be genuinely continuous. The sampling rate of a truly continuous two-dimensional system is limited only by the detector's capabilities. By extension, the expanded dimensionality comes at the cost of inherent sampling complexity. Conventional sampling methods that use single-point detectors become a limiting factor when analyzing two-dimensional separations. Intuitively, two-dimensional separation systems require two-dimensional sampling methods. This problem is further addressed in **Chapter 3**.

The last important factor in two-dimensional continuous separations is the angle of the applied separation force. The red arrow in **Figure 1.2** is included to demonstrate how the separating force angle is different in the two cases. One dimensional system can only experience the separating force applied parallel to the flow, once again constrained by its dimensionality. Two-dimensional systems enjoy the possibility of having the force applied at any angle between 0 and 360 degrees to the hydrodynamic flow. This additional degree of freedom is interesting for multiple reasons and is discussed in **Chapter 4**.

1.1.1. One-dimensional continuous separations

Before proceeding to two-dimensional continuous separation methods, it's worth mentioning some exceptional cases that attempt to achieve continuous separation and harness its advantages without expanding their dimensionality. Such strategies attempt to preserve the most vital aspect of one-dimensional systems, their simplicity. Simple designs are generally more robust, cheaper, and easier to model numerically. The most common engineering approach that converts a one-dimensional discrete separation method into a continuous extractor is to achieve differential mobility of analytes. Simply put, the analytes should move in opposite directions. Such a feat is typically accomplished by increasing the separation force to the point where one of the analytes moves against the hydrodynamic flow (**Figure 1.3**). Well-known examples of this approach are moving bed chromatography (MBC or TMB) and simulated moving bed chromatography (SMBC).[6,7] What sets such methods apart from the two-dimensional continuous separations is their fundamental limitation to two or fewer analytes that can be simultaneously separated[8]. In the case of multi-component chemical reactions, this system can only produce one pure analyte.

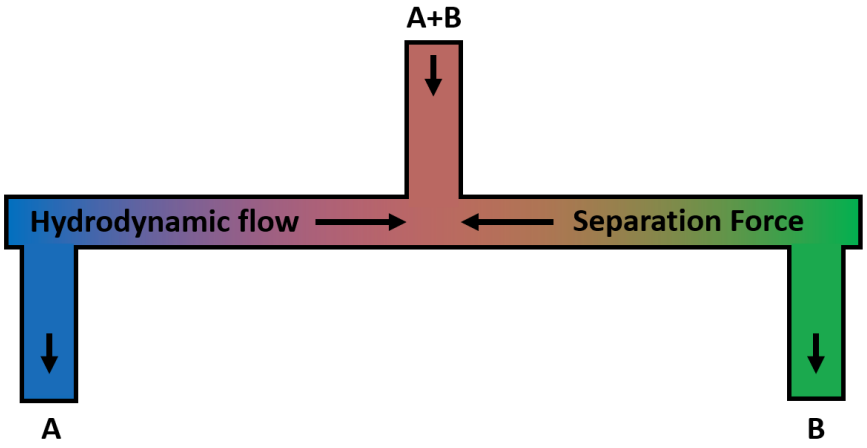

Figure 1.3 One-dimensional continuous separation system.

1.1.2. Two-dimensional continuous separations or molecular stream separations (MSS)

There are three techniques capable of achieving unlabeled multi-component separation of small molecular products, namely continuous liquid-liquid extraction (CLLE), continuous-flow electrophoresis (CFE), and continuous annular chromatography (CAC). All of them exploit the same fundamental principles described in the overview. Each method is a logical extension of its discrete predecessor. Proper continuity for all three is achieved by the introduction of an additional dimension.

1.1.2.1. Continuous liquid-liquid extraction

CLLE is a small part of a more prominent family of continuous Phase-Phase extractions that isn't limited to liquids.[9,10] In CLLE, the target hydrophobic compound is extracted from the aqueous-organic mixture based on its solubility in a particular phase (**Figure 1.4**). Simple extraction with two immiscible liquids is reliable and easy to implement into a continuous system. Rare instances combine three immiscible liquids running side-by-side.[11] In some cases, a solid alternative can replace the third liquid.[12] CLLE application for synthesis is narrowed by its limited ability to separate multiple hydrophobic compounds within the organic phase.

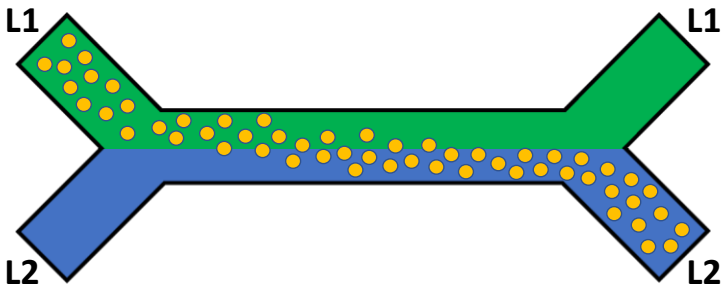

Figure 1.4 Schematic representation of two-phase Continuous Liquid-Liquid Extraction (CLLE) system.

1.1.2.2. Continuous annular chromatography

Continuous annular chromatography (CAC) methods are exciting varieties of the liquid chromatography technique where two additional dimensions were added to achieve continuity[13]. The purpose of the first extra dimension is to create a continuous separations system with all the advantages described in the overview. This modification, however, creates an engineering problem. Chromatographic methods operate based on the difference in interaction times of analytes with stationary and mobile phases. Continuous chromatographic separation in two dimensions would require an infinitely long stationary phase that moves orthogonally to the flow. Creators have solved the problem by further expanding the dimensionality of the method. They created a pseudo-two-dimensional continuous separation platform by folding a two-dimensional stationary plane into a rotating cylinder (**Figure 1.5**).

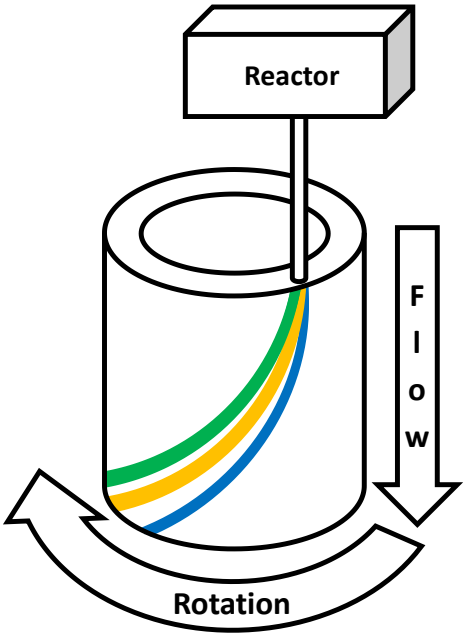

Figure 1.5 Schematic representation of Continuous Annular Chromatography (CAC) system.

1.1.2.3. Continuous-Flow Electrophoresis

Continuous-flow electrophoresis (CFE) is the method on which the following chapters will focus. Over the past several years, our lab has developed and continuously improved this robust and straightforward separation technique for multiple hydrophobic compounds.[14–16] CFE is based on free-flow electrophoresis (FFE), which utilizes an electric field perpendicular to the input hydrodynamic flow to separate compounds based on their difference in electrophoretic mobility (**Figure 1.6**). Conventional FFE is a continuous method limited to aqueous media for separating water-soluble compounds. Our work presented in **Chapter 2** expands the scope of FFE to hydrophobic compounds to better accommodate the needs of continuous organic synthesis.

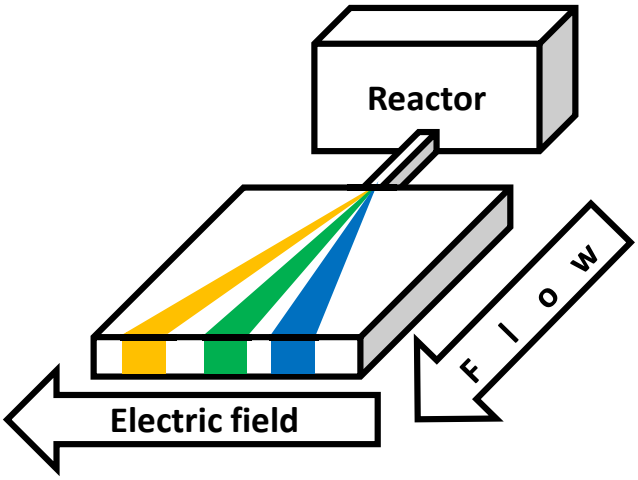

Figure 1.6 Schematic representation of Continuous-Flow Electrophoresis (CFE) system.

1.2. CONTINUOUS ELECTROPHORETIC SEPARATIONS

This section covers two significant classes of continuous electrophoretic separations, namely separations performed for analysis and separations performed for analyte collection and later use. Although this isn't the only way of classifying continuous electrophoretic separations, this approach is simple and streams from the general demand imposed by the experimental design.

1.2.1. Analytical separations

The simplest engineering case of analytical continuous electrophoretic separations are separations performed without collecting the molecular streams at the end of the separation zone. In devices solely designed for analytical separation, all streams converge to a single outlet. Such devices are used to sample batch and continuous flow reactors by assessing the conversion rate and yield. The lack of need for stream collection allows such devices to operate on a microscopic scale. The typical internal volume of such devices is measured in tens or hundreds of microliters.[17,18] Because of the smaller size, Joule heating is less of an issue, and the high electric field strength is easier to attain. For this reason, most analytical platforms achieve a higher resolution of analytes than standard preparative methods. The most common detection methods used in continuous analytical separations are UV-Vis and laser-induced fluorescence (LIF).[17,19,20] Optical analysis doesn't require analyte collection and can be performed directly on the chip.[21] When a platform is capable of stream collection, but no collection is needed, some destructive detection methods such as Mass Spectrometry (MS) can be performed.[16,18,22] Although more expensive, MS hyphenated analytical platforms can be used for advanced sample analysis such as top-down proteomics.[23,24]

1.2.2. Preparative separations

Preparative electrophoretic separations typically require a higher level of engineering than those found in standard analytical devices. Preparative platforms usually end with multiple outlets equally spaced before the exit from the separation zone. Depending on the device, separation analysis might happen continuously on the chip or at the molecular stream collecting outlets. Alternatively, collected fractions can be analyzed discretely after the separation has ended. However, this approach is sub-optimal since continuous separation and reactor optimization, in this case, is impossible.[25] Because the purpose of any preparative method is to maximize the amount of collected analytes, such devices are typically larger and have higher internal volumes. Joule heating plays a significant role by causing convection and destroying the laminar flow profile in the separation zone. Special care must be taken not to overheat the device. Because of this fundamental limitation caused by its size, preparative continuous electrophoretic methods typically attain a lower resolution of analytes than purely analytical techniques.

1.2.2.1. Proteins

Proteins are the most routinely studied macromolecules due to their omnipresence, abundance, and relevance. The same reasons make them the most frequent analytes collected by continuous electrophoretic methods. More than fifty years ago, their water solubility made them a perfect candidate for earlier attempts at continuous collections.[26] Proteins can be separated based on their size-to-charge ratio by the classical method or isoelectric point by isoelectric point focusing[27,28]. Collected proteins can be easily worked up from the separation buffer by filtration.

1.2.2.2. DNA

DNA collections by continuous electrophoretic methods are substantially less frequent than protein collections, mainly because DNA fragments possess the same size-to-charge ratio regardless of their base-pair count. This property makes achieving good separation quality for double-stranded DNA molecules challenging. Additional matrix modifications are required to separate double-stranded DNA based on molecular size.[29] Working with single-stranded DNA is easier since single-stranded molecules typically fold into various shapes. This folding makes their size-to-charge ratio substantially different and allows them to be separated. Potential applications include clinical sample separations and preparation of aptamer libraries.[30,31]

1.2.2.3. Lipids

Another rare case of continuous electrophoretic separations is lipid collection experiments. Contrary to proteins and DNA, lipids are not water-soluble. The carrier solution matrix must be modified with large fractions of methanol and chloroform not to cause aggregation. Proof of work experiments have examined the lipid composition of separated liposomes and their internal molecular content.[32,33]

1.2.2.4. Nano-particles

Recent applications of continuous electrophoretic separations involve nano-particle collection. The metallic core of a nanoparticle is electrically neutral, but for solubility and protection, it is encased inside an organic monolayer. This monolayer is negatively charged and creates a Zeta potential that keeps nanoparticles from aggregating. Nanoparticles migrate with

different electrophoretic mobilities depending on their size. Multiple reports show how well suited CFE is for obtaining monodisperse fractions.[17,34,35]

1.2.2.5. Small molecules

This kind of preparative electrophoretic separation attempts to collect small molecular weight (<1000 Da) organic synthesis products for medical or technological applications.[15,36] Small molecule CFE is limited by the low solubility of relevant molecular compounds in water. To circumvent this problem, researchers have explored the possibility of non-aqueous continuous electrophoretic separations. Some previous attempts at supplementing electrolyte solutions with organic solvent show promise.[37] Unfortunately, this method doesn't work with organic solvents that don't mix well with water. The introduction of water-free organic solvent creates several engineering challenges, such as device degradation and electrolyte incompatibility. **Chapter 2** expands upon our work of bridging continuous electrophoretic separations and the world of chemical synthesis.

1.3. CONTINOUS ELECTROPHORETIC SEPARATIONS DEVICE

The primary descriptive parameters of all continuous electrophoretic separations are the magnitude of the hydrodynamic flow and the magnitude of the electric field. Those two parameters can coexist only due to the research community's elaborate engineering of CFE devices. Even though the primary duo has been studied and modelled[38], multiple CFE engineering aspects are left to be explored and improved. Many CFE devices contain extensive secondary engineering modifications that make them stand out. Such changes allow the corresponding device to be better at something than a reference configuration. Frequently modified factors include but are not limited to electrodes, ion-selective membranes, and background electrolyte solution (BGE). The following chapter will cover important engineering aspects of CFE and interesting new takes on the old technology.

1.3.1. Device fabrication and materials

The central physical part of CFE is the separation zone accommodating geometry that contains all the elements required to support the electric field over some conducting solution that is pushed through the separation zone by differential pressure. Historically, the most common way to fabricate the device involves a reductive manufacturing method known as photolithography[39–43]. This method creates geometrical features with micrometer precision and is frequently used to fabricate microfluidic devices. Glass is the most common substrate for photolithography. The material is popular due to its transparency and chemical inertness, allowing harsh cleaning conditions. The lithography process begins with silicon oxide wafers being spin-coated with a photoresist. The wafer is then exposed to a UV light source through a photomask. Regions that absorb UV radiation become resistant to the development process that

removes the excess photoresist. The resulting geometry is then etched with a chemical agent that removes the substrate where photoresist coating is absent. Even though this method produces very fine geometrical features, it requires a clean microfluidic fabrication room. Such facilities are rare and expensive. In addition, the etching process typically requires highly harmful chemicals capable of reacting with glass, such as hydrofluoric acid.

Some researchers have suggested using alternative fabrication methods that can potentially be faster, cheaper, and less harmful. One of the proposed methods is the NC milling of polymer substrates.[44] This method can produce CFE devices from various polymer substrates and doesn't require expensive machinery or a clean room facility. Additionally, this method can fabricate more intricate geometries of non-uniform depth that are significantly harder to make with photolithography. The major disadvantage of machining is its struggle to produce geometries of low micrometer scale. Another disadvantage is the low compatibility of this method with some popular microfluidic substrate materials, such as glass. In addition, only expensive varieties of polymers (e.g. PEEK or PEI) can match the degree of chemical resistance offered by glass substrates.

The rise of the popularity of additive manufacturing has slowly trickled into the area of microfluidics. Significant advantages of additive manufacturing are material economy and its ability to produce hollow geometries that are otherwise impossible to make with reductive methods. Some groups have made CFE geometries using this method[17,45–47]. 3D printers are quickly evolving into prevalent prototyping and manufacturing platforms. Cheaper models are typically limited to printing with thermoplastics. This deposition method is simple but suffers from low precision caused by thermoplastic expansion due to temperature changes. Geometries made with fused deposition require additional workup in acetone vapor to reduce surface non-

uniformity.[47] High-end models and engineering prototypes of 3D jet printers can print with acrylic polymers and even glass.[48] Typical precision of these methods surpasses fused deposition printing and rivals NC micro milling capabilities but is far from precision obtained with photolithography. The major disadvantages of current high-end methods are high equipment and material cost and low diversity of material substrate.

1.3.2. Solvent and background electrolyte (BGE)

As mentioned in **Chapter 1.1,** the velocity of an analyte in CFE is predetermined by its proportionality coefficient to the applied force. In the case of electrophoretic separations, this force is the electric field, and the proportionality coefficient is the ratio of analyte's charge (Q) to size ($6\pi r$) and medium viscosity (η) **Eq.3**.

$$\mu = \frac{Q}{6\pi r\eta} \qquad \boldsymbol{Eq.3}$$

This coefficient (μ) is typically referred to as electrophoretic mobility. The actual value of electrophoretic mobility depends on three physical factors. The analyte's molecular structure influences the size and charge. A BGE additionally affects the charge. Finally, the solvent viscosity is directly accounted for in the equation. We can directly influence the coefficient and improve analyte resolution by experimenting with electrolytes and solvents. This approach has been long known in water as Isoelectric Focusing, Field-Step Electrophoresis, and Isotachophoresis.[49,50]

Another approach to separating analytes in CFE is by conferring a charge through secondary interactions with BGE components, as shown by **Eq. 4** where $X^{\mp}$ is an arbitrary charged component of the electrolyte pair with an unspecified affinity constant (K^f) for the analyte A, and $AX^{\mp}$ is the product complex that will migrate in the electric field.

$$X^{\mp} + A = AX^{\mp} \qquad \boldsymbol{Eq.4}$$

The mobility equation (**Eq.3**) then must be modified to account for the increased particle radius of the formed complex between $X^{\mp}$ and A. As well as for the affinity constant ($K^f_{AX^{\mp}}$) that predicts the extent of heteroconjugation between $X^{\mp}$ and A.[51]

$$\mu_{AX^{\mp}} = \frac{Q_{X^{\mp}}}{6\pi r_{AX^{\mp}}\eta} \cdot \frac{K^f_{AX^{\mp}}[X^{\mp}]}{K^f_{AX^{\mp}}[X^{\mp}] + 1} \qquad \boldsymbol{Eq.5}$$

This method can be further expanded to separating neutral analytes by Micellar Electrokinetic Chromatography (MEC).[52] It is worth noting that MEC has yet to be adapted for continuous separations. **Chapter 2** explores a similar approach for non-aqueous CFE separations since the absence of organic solvent's self-dissociation renders most analytes neutral under typical conditions.

1.3.3. Electrodes

Electrodes are another critical factor in CFE engineering. Under normal circumstances, most solvents undergo electrolysis when sufficient voltage is applied. Water electrolysis happens at voltages of 1.2V and higher. Two gas varieties evolve on the surface of electrodes. Hydrogen gas is made by cathodic reduction, and oxygen is produced by oxidation on the anode. Gas production is a significant engineering problem that plagues all aqueous CFE devices. Gas bubbles interfere with laminar flow profiles inside the chip and cause the separation to fail if not timely removed. Technical means that mediate this problem include the introduction of special electrode channels isolated from the separation zone by intricate flow engineering and physical barriers. Commonly, such barriers are ion-permeable membranes that separate the flow but don't interfere with the electric field by allowing ions to migrate.[53] The disadvantage of this method is the relatively high cost of porous membranes and the difficulty of assembly. Another way to remove the gas is by introducing special venting openings that allow it to leave.[14] This method is disadvantageous due to the system's openness to the surrounding environment and flow-rate limitations. Non-aqueous CFE (NACFE) presented in **Chapter 2** doesn't use water and has a significantly lower electric current, making it substantially more resistant to gas generation-related problems than aqueous methods. In NACFE, gas is removed by normal solvent flow and no additional modifications are necessary.

CHAPTER 2. DEVELOPING A NON-AQUEOUS CONTINUOUS-FLOW SEPARATION PLATFORM

The presented material was published previously and reprinted with permission from "Ivanov, N.A.; Liu, Y.; Kochmann, S.; Krylov, S.N. Non-aqueous continuous-flow electrophoresis (NACFE): separation complement for continuous-flow organic synthesis. *Lab on Chip* 2019, 19, 2156–2160." Copyright 2019 Royal Chemical Society.

My contributions to the article were: (i) performing presented experiments, (ii) preparing figures, (iii) interpreting the results, and (iv) writing the manuscript. NACFE image evaluations were prepared by Dr. Sven Kochmann.

ABSTRACT

We introduce non-aqueous continuous-flow electrophoresis (NACFE) in which the electrolyte is a solution of an organic salt in an aprotic organic solvent. NACFE can maintain the steady-state separation of multiple hydrophobic organic species into individual molecular streams. It is a potential separation complement for continuous-flow organic synthesis. This proof-of-concept work will serve as a justification for efforts towards making NACFE a practical tool in flow chemistry.

2.1. INTRODUCTION

Continuous-flow organic synthesis has a number of important advantages over its batch counterpart.[1,54–56] Continuous-flow separation of multiple components of the reaction stream (e.g. products, intermediates, excess reactants, catalysts, etc.) from each other is often required between the stages of continuous-flow organic synthesis.[3] Liquid-liquid extraction that segregates molecules through their partitioning between organic and aqueous phases is the most common continuous-flow separation method.[57,58] Yet, it can hardly separate hydrophobic organic molecules with similar partition coefficients from each other.[9] Continuous-flow electrophoresis (CFE), which is also called free-flow electrophoresis, can support much more selective

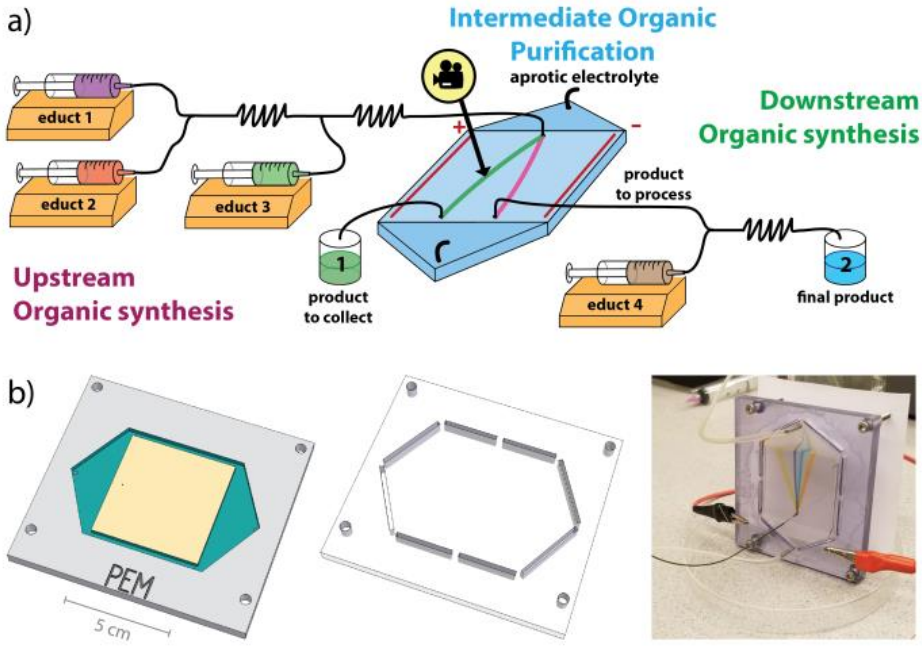

Figure 2.1 a) Schematic of NACFE seamlessly integrated between two stages (upstream and downstream) of continuous-flow organic synthesis. b) Geometry of the bottom part (left) and top part (middle) of the NACFE chip used in this study as well as its photo in operation (right).

separation.[40,59,60] Its ability to separate multiple molecular streams in a single phase could potentially facilitate its seamless integration with continuous-flow organic synthesis. However, practical CFE has been so far limited to aqueous electrolytes; with an exception of a single work by Bowser and co-authors reporting the use of a non-aqueous electrolyte including a protic organic solvent (methanol).[37] Aqueous electrolytes are incompatible with continuous-flow organic synthesis, as the synthesis often involves reaction components insoluble in water or sensitive to aqueous media.[61] An additional problem with aqueous electrolytes is intensive gas formation during water electrolysis; hardly avoidable accumulation of gas bubbles in the separation chamber makes steady-state operation of CFE a technical challenge (protic organic solvents suffer from the same problem).[14,62,63] On the contrary, non-aqueous continuous-flow electrophoresis (NACFE) could potentially use aprotic organic solvents, which are not only compatible with solvents utilized in continuous-flow organic synthesis but also could reduce gas formation and make separation stable without elaborate technical solutions. Owing to these two anticipated advantages, NACFE utilizing aprotic organic solvents appears to be a highly attractive separation complement for continuous-flow organic synthesis (**Figure 2.1a**). Devices for NACFE are simple and can be easily custom fabricated (**Figure 2.1b**). Therefore, it is rather surprizing that there have been no reports on this technique while aprotic non-aqueous electrolytes, e.g. based on cyclic carbonates, are widely used in batteries,[64] and have been used in discontinuous separation by capillary electrophoresis.[65] The goal of this work was to prove the feasibility of NACFE with aprotic electrolytes and test its suitability for steady-state separation of multiple molecular streams in the organic phase.

2.2. MATERIALS AND METHODS

2.2.1. Chemicals and materials

All solutions were prepared using analytical grade reagents. Acetonitrile, α-naphtholbenzein, 2-[4-(dimethylamino)styryl]-1-methylpyridinium iodide, fluorescein sodium salt, imidazolium ethyl sulfate, PC, rhodamine 6G, Sudan black B, and TBAA were purchased from Sigma Aldrich (Oakville, ON, Canada). Electrolytes were solutions of imidazolium or tetrabutylammonium salts in PC or acetonitrile. Stock solutions of analytes were prepared in respective electrolytes as solvents. All chip materials listed in **APPENDIX A, Table A2.1** were purchased from McMaster Carr (Elmhurst, IL, USA).

2.2.2. Instrumentation

The electrolyte was delivered to the NAFCE chip with an NE-9000G peristaltic pump from New Era Pump Systems, Inc. (Farmingdale, NY, USA). The pump was equipped with a Masterflex pulse dampener from Cole Palmer (Vernon Hills, IL, USA) to suppress flow pulsation. Analyte solutions were delivered to the NACFE chip with a Model 11 syringe pump from Harvard Apparatus (Holliston, MA, USA). Separation voltage was applied to the platinum electrodes inside the separation zone from an EPS 3501 XL power supply from GE Healthcare (Chicago, IL, USA). NACFE chips were fabricated using a MODELA MDX-540 Benchtop Milling Machine from Roland DGA (Irvine, CA, USA).

2.2.3. Chip fabrication

NACFE chips were designed in Solid Edge (see model files in geometry.zip) and fabricated of PVC Type I according to our previously developed fabrication procedure for PMMA chips (*J. Sep. Sci.* 2011, 34, 556−564, DOI: **10.1002/jssc.201000758**; *Lab Chip* 2017, 17, 256-266, DOI: **10.1039/C6LC01381C**). Details on chip fabrication and chip components used (apart from the chip material) may be found in these two previous works.

2.2.4. General experimental details

Electrolyte and analyte flow rates were in the ranges of 2−4 mL/min and 1−2 µL/min, respectively. 30−150 V were applied as separation voltages resulting in field strengths of 5−28 V/cm (distance between electrodes = 5.5 cm), respectively. Recycling for the 10-h separation was done in discrete steps transferring the electrolyte from the outlet container to the source container (feeding the peristaltic pump) roughly every 2.5 h.

2.2.5. Mixing behavior of propylene carbonate (PC)

PC and water are not miscible at similar ratios (e.g. 50:50). Therefore, water can be used to extract Tetrabutylammonium acetate (TBAA) or other salts from the PC phase; aqueous workup of TBA-salts is a common technique (see e.g. DOI: **10.1021/ol063113h**). The organic compounds will remain mainly in the PC phase (extraction coefficients can be further tuned by adding acid or base to water or by washing with diethyl ether):

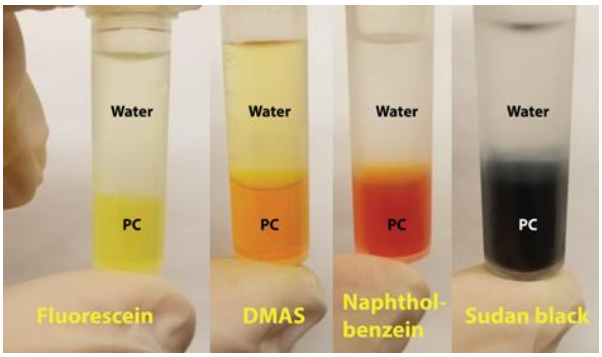

PC (boiling point at 1 atm ≈ 240 °C) can then be removed by rotary evaporation to yield pure organic compounds. Note that at high concentrations of TBAA (1 M), water and PC phases become miscible, and no phase separation can be observed. Similarly, at low PC:water ratios (lower than 20:80, see DOI: **10.1021/je00028a012**), PC and water mix and form a one-phase system. However, any organic compound previously dissolved in PC will precipitate; the precipitate can be further washed with cold water to remove the remaining TBAA (and other salts). PC is also not miscible with hexane; therefore, hexane can be used to extract the organic compounds from PC if applicable directly (see e.g. DOI: **10.1021/cr900393d**). A continuous separation method such as CLLE can potentially work up the product without resorting to conventional batch methods.

2.2.6. Evaluation procedure for NACFE images

The following procedures are mostly an implementation and extension of the concepts and programs in our previous work: *Anal. Chem.* 2018, 90, 9504−9509, DOI: **10.1021/acs.analchem.8b02186**. The basic idea is to represent molecular stream separation by a single plot called angulagram. In an angulagram, every stream is represented by a single peak.

Peak properties, such as position and shape, contain all information required to calculate quantitative stream characteristics: stream deflection, stream width, and stream linearity. The source code of all programs described here can be found in the Supplementary Files on Github (DOI: **10.5281/zenodo.2592588**) and ChemRxiv (DOI: **10.26434/chemrxiv.7840937**).

2.2.7. Constructing angulagrams from reflectometric images

The general procedure of angulagram construction is the same as the one used for fluorescence images in the previous work, namely i) aligning the image (rotation/mirroring), ii) cropping the region of interest (separation zone), iii) transferring the data from Cartesian to polar coordinates, and iv) integrating the signal over the radius. In contrast to fluorescence images, a reflectometric input image naturally includes a high background, which can be filtered out by lowering the color saturation and extracting only the hue levels of interest. The respective parameters were manually determined in Photoshop using the ruler tool (rotation angle, inlet position, and separation zone size) and adjustments tools (Image → Adjustments → Hue/saturation; Image → Adjustments → Levels); these parameters were then fed into a Python program (**angureflexin.py**) that performed the construction (see source code for details). The generated output consisted of an angulagram, a parameter file that listed all used parameters, an image of the separation zone in polar coordinates, and a preview image that was used as the thumbnail for the angulagrams in this work.

2.2.8. Extracting stream parameters form angulagrams

Another Python script (**evolutin.py**) was used to find the stream peaks in the angulagrams and determine their parameters (deflection, width, linearity, and resolution), as described in our previous work. See the source code for details.

2.2.9. Evaluation of the 10-h separation

Angulagrams for all 3587 images (taken every 10 s) were created using batch processing by a Python script (**angulagrams10h.py**, processing time: 8.5 h) using the Python script (**angureflexin.py**) and the method described above. Parameters (rotation angle, color saturation, hue levels, etc.) were pre-determined for a set of 38 images across the whole separation (see **sampleparameters.csv**). They were found to be similar for these 38 images; therefore, their averages were used for the whole set of 3587 images. The resulting angulagrams were subsequently evaluated, and stream parameters were extracted (**streameval10h.py** and **streampara10h.py**, processing times: about 45 min each) using the Python script (**evolutin.py**) and the method described above. Parameters needed for evaluation (background, window size for extrema finding, etc.) were pre-determined for a sample set. Before extracting stream parameters from the angulagrams, angulagrams were smoothened by a Savitzky-Golay filter (window size = 31, polynomial order = 3) to ensure the stability of the used numerical methods for finding minima/maxima etc. Finally, an integrated image based on all 3587 images was calculated (**integrate10h.py**) and presented in Figure 4d. A video file was generated by reducing the resolution of the images and encoding them with the XVID codec (**makevideo10h.py**).

2.2.10. Electrical current measurements

An EPS 3501 XL Electrophoresis Power Supply was used to set the electrophoresis voltage and measure the current. However, this device has no direct output (RS232 or the like) to sample the current data. Therefore, we used a camera to observe the display and then used an optical character recognition (OCR) approach to extract the current values. This was implemented as another Python script (**extract_currents.py**) using OpenCV (Open Source Computer Vision Library, https://opencv.org/) and Google's Tesseract engine (https://github.com/tesseract-ocr/tesseract). See source code for details. A video file was generated by reducing the resolution of the images and encoding them with the XVID codec (**makevideo10h.py**).

2.3. RESULTS AND DISCUSSION

2.3.1. Selection of device material

The following Continuous-flow separation (as an integral part of continuous-flow synthesis) must operate under steady-state conditions. We, thus, aimed at developing steady-state NACFE confirmed by stable, uninterrupted operation during e.g. a 10-h shift. Separation instability in CFE is caused by the gradually growing distortion of the hydrodynamic flow and/or electric field during the course of operation. The major and very persistent cause of such distortion is the hardly-avoidable accumulation of gas bubbles in the device.[14,62,63] The most straightforward long-term solution for this problem is bubble evacuation to the atmosphere through an open-electrolyte approach.[14] This approach should, however, be avoided for non-aqueous electrolytes due to safety concerns. Thus, we limited ourselves to closed NACFE devices. In NACFE, one can foresee another potential source of growing distortion of

hydrodynamic flow: deterioration of the electrophoretic device under the influence of an organic solvent. Hence, a NACFE device must be made of a solvent-resistant material. We chose propylene carbonate (PC) as an aprotic organic solvent and had to use a device material resistant to it. While silica glass is arguably the best choice of a solvent-resistant optically-transparent material, making prototype NACFE devices of HF-etched glass is not as practical as making them of mechanically-machined plastics. We tested a set of 18 plastics, commercially available in sheets, for their machinability, optical clarity, and resistance to PC (**APPENDIX A, Table A2.1**). Three of them, fluorinated ethylene propylene, polyvinyl chloride (PVC) Type I, and polysulfone, were found potentially suitable based on these three parameters. Of these three plastics, we chose PVC Type I for its optical clarity, cost efficiency, and full suitability for device-fabrication procedures previously developed for poly(methyl methacrylate).[44,66] A NACFE chip of basic geometry (**Figure 2.1b** and **APPENDIX A, Figure A2.1**) was fabricated and used for all experiments described below.

2.3.2. Selection of solvent and charge carrier

A key component of any electrolyte is a charge carrier, which is typically a well-soluble non-reactive salt giving a free cation and a free anion upon dissociation. Two types of organic salts have been previously used as charge carriers in non-aqueous aprotic electrolytes in capillary electrophoresis: tetraalkylammonium salts and imidazolium salts (ionic liquids).[67,68] Their use in capillary electrophoresis did not guarantee transferability to NACFE for two reasons. In contrast to capillary electrophoresis, electrodes in NACFE are inside the separation chamber, making NACFE susceptible to instability associated with the electrochemistry of electrolyte components. In addition, capillary electrophoresis runs take only a few minutes, and long-term stability is not

a requirement in contrast to NACFE. Therefore, we first tested NACFE for the long-term stability of the electric current and optical properties of the chip. The experiment was done for two electrolytes: solutions of tetrabutylammonium acetate (TBAA) and imidazolium ethyl sulfate in PC. We found that the electrical current was stable for TBAA during a 10-h run (**APPENDIX A, Figure A2.2**). No gas bubble accumulation was evident. Minor precipitation could be noticed at the cathode side of the NACFE chip, likely due to an electrochemical reaction involving tetrabutylammonium. This precipitate did not affect the optical clarity of the chip. In contrast, we found the excessive formation of a brown precipitate at the cathode side of the chip for the imidazolium electrolyte (**APPENDIX A, Figure A2.3**). The precipitate was most likely an insoluble product of an electrochemical reaction involving imidazolium.[69] This precipitate affected the optical clarity of the chip and could interfere with optical detection; accordingly, we ruled out imidazolium-based electrolytes from our further consideration. Hence, a solution of TBAA in PC was chosen as a default electrolyte for the rest of this NACFE study.

2.3.3. Assessing the quality of NACFE

Next, we tested the separation of multiple molecular streams in NACFE (**Figure 2.2**). As molecules to be separated, we used 2-4-(dimethylamino)styryl-1-methylpyridinium (DMAS), Sudan black B, α-naphtholbenzein, and fluorescein (the first three are hydrophobic and poorly soluble in water). All of them are chromophores visible to the naked eye, facilitating easy stream detection in this proof-of-feasibility work.

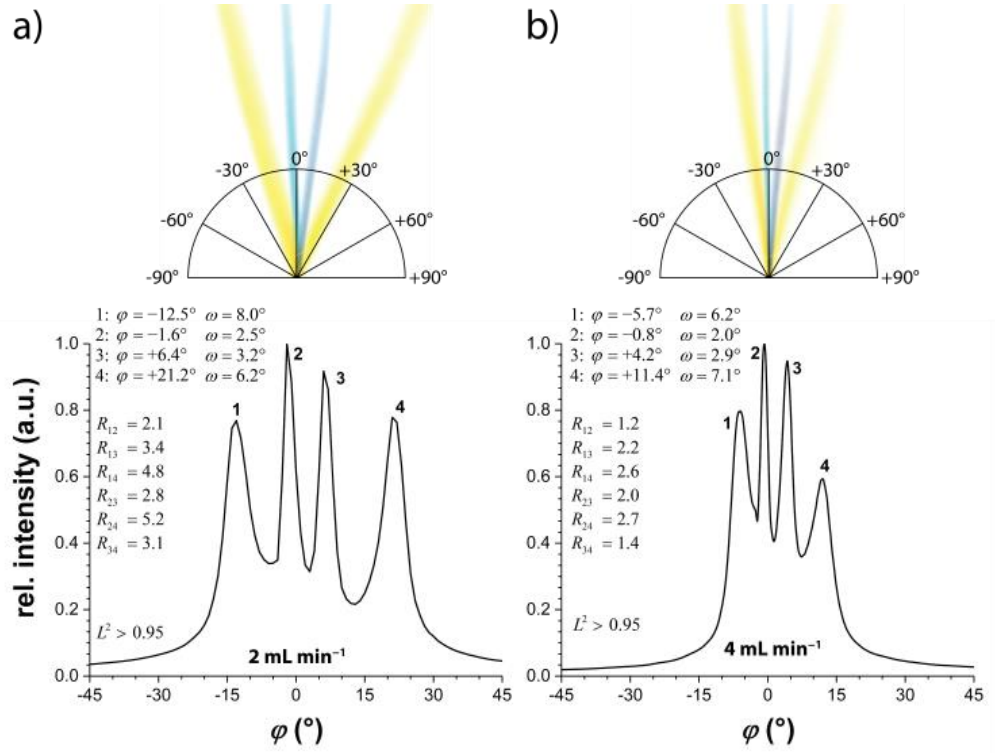

Figure 2.2 Angulagrams of NACFE of fluorescein (1), α-naphtholbenzein (2), Sudan black B (3), and DMAS (4) (1.25 mM each) in 30 mM TBAA in PC at two different electrolyte flowrates: a) 2 and b) 4 mL/min. The values in the graph are stream deflection (φ), stream width (ω), stream linearity (L^2), and resolution of stream n from stream m (R_{nm}). NACFE was run with E = 27.3 V/cm (I = 8.3 mA) and a sample flowrate of 2 µL/min. The anode and cathode are towards negative and positive angles, respectively.

The quality of NACFE was assessed using a recently introduced approach based on angulagram representation of molecular stream separation and four quantitative characteristics: stream deflection, stream width, stream linearity, and resolution of two streams.[5] Images of molecular streams in NACFE were recorded with a consumer photo camera. These images were

processed automatically to construct angulagrams and compute the quantitative characteristics of the streams (see materials and methods for details on these procedures and corresponding custom-designed software).

All molecular streams shown in **Figure 2.2** were deflected as predicted by the previously proposed separation mechanism based on heteroconjugation.[70,71] Briefly, small anions (e.g. acetate) form heteroconjugates with hydrogen-bond donors. The effective charge of a heteroconjugate is negative, and its magnitude depends on the degree of heteroconjugation; this dependency is advantageous as it allows, for instance, the separation of different phenols.

In our case, α-naphtholbenzein (phenol) and fluorescein (carboxylic acid and phenol) formed negatively charged heteroconjugates, which were deflected towards the anode. DMAS is not a hydrogen-bond donor but possesses one quaternary nitrogen atom with a positive charge. Hence, DMAS was deflected towards the cathode. Sudan black B has no positive charge and is assumed to be a very weak hydrogen-bond donor, which, however, still can experience a low degree of heteroconjugation. Therefore, its stream was expected to be deflected slightly towards the anode, i.e. negative angles in the angulagram in **Figure 2.2**. In fact, it was deflected towards the cathode, i.e. positive angles. This small deflection was due to the presence of the electroosmotic flow[72–74] (from anode to cathode) and affected deflection of other streams as well. This unexpected presence of EOF can potentially be explained by errors during the polymerization process where wrong monomers are added to the polymer chain or by the presence of unknown plasticizers. Ideally, one would compare the experimental deflection angles to theoretical ones;[5] however, the theory for calculating electrophoretic mobilities (which define deflection angles) is not straightforwardly applicable to non-aqueous electrophoresis. All streams in **Figure 2.2** are linear ($L2 > 0.95$) and narrow (< 10° in width). The worst stream resolution (R

> 1.2) in **Figure 2.2** is still sufficient for collecting any individual stream with hardly any overlap with any other stream ($R \geq 1.0$ is our threshold for collectible streams[5]);

in the particular case in **Figure 2.2b**, α-naphtholbenzein and sudan black B can be collected with ≈ 98% purity assuming normal distributed stream profiles at the end of the chip. Increasing the concentration of the charge carrier in the electrolyte expectedly led to improved separation, confirmed by decreasing stream width and increasing linearity (**Figure 2.3**).

Unsurprisingly, no separation could be observed when the electrolyte was replaced with pure PC without any charge carrier. Adding a charge carrier at a concentration (3.3 mM) similar to the analyte concentrations (1.67 mM) resulted in one broad stream (width: 9.8°) in which the individual analytes started to separate. Increasing the charge carrier concentration from 3.3 to 10 mM (an order of magnitude higher than the analyte concentrations) turned this broad stream into individual narrow ones (widths of 4.4 to 6.8°); further increase to 30 mM narrowed the streams even more (widths of 2.3 to 4.5°). The carrier concentration had only minimal effect on the linearity; linearity increased from 0.90 to 1.00 with carrier concentration increasing from 0 to 30 mM. An increase in the carrier concentration progressively suppresses the electroosmotic flow directed towards the cathode.[75] Hence, stream deflections changed towards the anode with increasing carrier concentration. For instance, the stream deflection of Sudan black B changed from +13.4 to +3.0° (i.e. became less deflected) when the carrier concentration was increased from 0 to 30 mM. Increasing the carrier concentration above 100 mM, e.g. for increasing the concentrations of separated species, will be associated with increased Joule heating and worsening quality of separation.

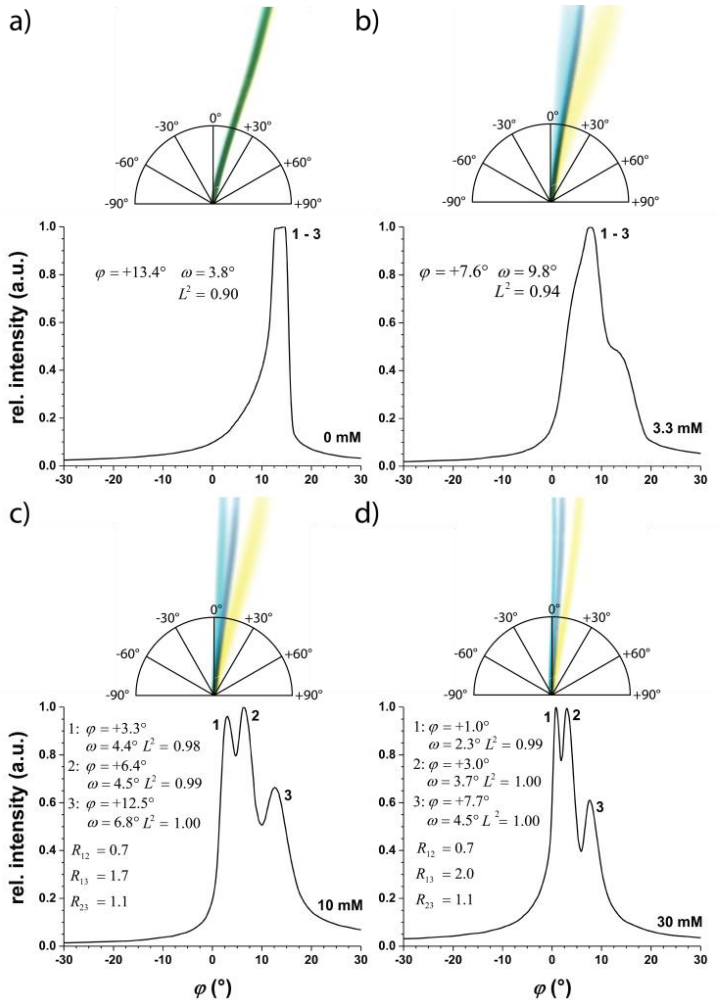

Figure 2.3 Angulagrams of NACFE of α-naphtholbenzein (1), Sudan black B (2), and DMAS (3) (1.67 mM each) under various concentrations of TBAA in PC: a) 0, b) 3.3, c) 10 and d) 30 mM. Given are stream deflection (φ), stream width (ω), stream linearity (L^2), and resolution of stream n from stream m (R_{nm}). E = 27.3 V/cm was used in all experiments and resulted in currents of 0.07 (a), 1.26 (b), 3.69 (c), and 9.9 mA (d). The flowrates were 3 mL/min for the electrolyte and 2 µL/min for the sample. The anode and cathode are towards negative and positive angles, respectively.

The quality of separation depended on the nature of the anion in the charge carrier. A weak-base anion (e.g. hydrogen sulfate) could not support the separation of α-naphtholbenzein from Sudan black B, while a strong base (e.g. acetate) could separate them (**APPENDIX A, Figure A2.4**). All results discussed above are consistent with the aforementioned separation mechanism in NACFE, in which heteroconjugation of electrolyte anions with hydrogen-bond donors plays a key role (see above).[70,71]

2.3.4. Assessing the stability of NACFE

Finally, we examined whether steady-state NACFE could be maintained (e.g. stable separation during a 10-h shift), which is the key requirement for integrating NACFE with continuous-flow synthesis. Three hydrophobic analytes were used in this experiment: α-naphtholbenzein, Sudan black B, and DMAS. The electrolyte was recycled roughly every 2.5 h to minimize material waste; we did not interrupt separation for electrolyte recycling. Our results show no significant deterioration in stream deflection, width, or linearity during the 10-h NACFE with the exception of stream width for α-naphtholbenzein, which drifted from 5 to 12° (**Figure 2.4**). However, this degree of stream widening would not significantly affect stream collection for the observed magnitudes of resolution and stability of deflection.

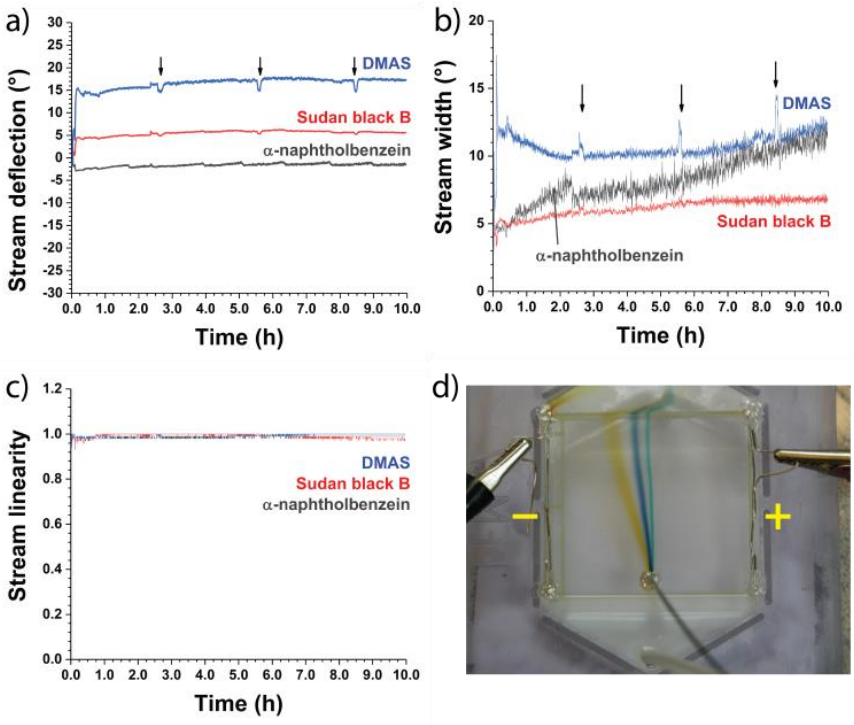

Figure 2.4 a−c) Stream parameters and d) an averaged photo (3587 images were integrated for visual assessment of separation stability) of 10-h NACFE of α-naphtholbenzein, Sudan black B, and DMAS (1.67 mM each) in 30 mM TBAA in PC. Recycling was done roughly every 2.5 h (marked with arrows).

In the frame of the present work, we also explored the option of using acetonitrile instead of PC in NACFE. Our results demonstrate that separation in acetonitrile-based electrolytes is possible in principle (**APPENDIX A, Figure A2.5**). However, electrolytes based on PC beneficially allowed lower flowrates (due to lesser gas bubble formation) and higher electric fields (due to lower currents and Joule heating). Furthermore, PC is a less toxic, less volatile, and more viscous solvent than acetonitrile (Propylene carbonate, MSDS No. O43314, Thermo Fisher Scientific; Acetontrile, MSDS No. A9981, Thermo Fisher Scientific). Thus, we did not further

investigate acetonitrile in the frame of this work. However, the interested reader is referred to an excellent work by the Belder group that was published after the original submission of our manuscript and which completely focuses on acetonitrile as a solvent in NACFE.[36]

2.3.5. Obtaining a pure product in NACFE

Finally, we would like to address the issue of obtaining a pure product after the separation by NACFE, using our specific case as an example. The solvent outflow collected at the terminal end of the separation zone contains a product mixed with an excess of electrolyte. Both the electrolyte (TBAA) and the solvent (PC) need to be removed to yield a pure product. Based on our practical experience with PC (materials and methods 2.2.5), we see three options to achieve this goal. The first option is a liquid-liquid extraction of the electrolyte from propylene carbonate with an equal volume (50:50 v/v) of water, followed by vacuum-assisted rotary evaporation of the remaining propylene carbonate. The second alternative is to precipitate a product from the PC-TBAA mixture with an excess of water (higher than 4:1 volume ratio). The precipitated product can then be filtered and washed with cold water to remove all remaining TBAA. The third option is a liquid-liquid extraction of the product directly from PC using hexane or the like. For this, of course, the product has to be soluble in hexane. Hexane can then be removed by vacuum-assisted rotary evaporation. Obviously, the choice of the most suitable option depends on the properties of the product to be separated and purified. Furthermore, the in-flow implementation is not as straightforward and requires some engineering.

2.4. CONCLUSIONS

In conclusion, we proved the feasibility of NACFE with an aprotic electrolyte, namely TBAA in PC, by demonstrating steady-state separations of multiple molecular streams. This proven feasibility should stimulate efforts to implement integrated NACFE/continuous-flow synthesis. Here, we would like to outline what is required for such an implementation. First, any NACFE device must have outputs for multiple molecular streams; such devices have been successfully fabricated and used in the past.[39,76,77] Second, the optimization of device operation, e.g. adjustment of electric field and flowrate, requires visualization/ detection of separated molecular streams. Most organic molecules are not chromophores visible to the naked eye but absorb UV light; therefore, UV-imaging of a large area of the NACFE chip is required. Belder and co-authors have recently demonstrated deep-UV fluorescence imaging of UV-absorbing molecular streams in a small CFE chip.[21,78] This is a promising approach toward UV-imaging of larger chips. However, significant increases in scanning speed and covered area are required to apply this approach to real-time imaging of larger chips. We foresee that solving this challenging detection issue will open the way for the practical use of NACFE in combination with continuous-flow synthesis. It is important to emphasize that in contrast to liquid-liquid extraction, which has no intrinsic detection capability and requires secondary analysis, e.g. by HPLC, CFE has a unique capability of real-time quantitative detection, which makes such secondary analyses unnecessary.

CHAPTER 3. DETECTING MOLECULAR STREAMS IN CONTINUOUS ELECTROPHORETIC SEPARATION

The presented material was published previously and reprinted with permission from "Ivanov, N.A.; Kochmann, S.; Krylov, S.N. Visualization of Streams of Small Organic Molecules in Continuous-Flow Electrophoresis. *Analytical Chemistry* 2020, 92, 2907–2910."

My contributions to the article were: (i) performing presented experiments (ii) preparing figures, (iii) interpreting results and (v) writing the manuscript. Image evaluations were prepared by Dr. Sven Kochmann.

ABSTRACT

Continuous-flow electrophoresis (CFE) separates a stream of a multi-component mixture into multiple streams of individual components inside a thin rectangular chamber. CFE will be able to benefit flow chemistry when it is both compatible with non-aqueous solvents utilized in organic synthesis and capable of generically detecting streams of small organic molecules. While stable non-aqueous CFE has been demonstrated, generically detecting molecular streams has not been achieved yet. Here we propose a general approach for molecular stream visualization *via* analyte-caused obstruction of excitation of a fluorescent layer underneath the separation chamber – fluorescent sublayer-based visualization (FSV). We designed and fabricated a CFE device with one side made of quartz and another side made of UV-absorbing, visibly-fluorescent, chemically-inert, and machinable plastic. This device was demonstrated to support non-aqueous CFE of small organic molecules and quantitative detection of their streams in real-time with a limit of detection below 100 μM. Thus, CFE may satisfy the conditions required for its seamless integration with continuous flow organic synthesis in flow chemistry.

3.1. INTRODUCTION

Continuous-flow electrophoresis (CFE) separates a stream of a multi-component mixture into multiple streams of individual components inside a thin rectangular chamber with an electric field perpendicular to the hydrodynamic flow.[59,60,62] CFE can potentially benefit flow chemistry, which currently lacks in-line multi-component separation in a single organic phase.[3,61] To become useful for flow chemistry, CFE must be compatible with non-aqueous solvents utilized in organic synthesis and capable of generically detecting multiple molecular streams of small organic molecules in real-time. While stable non-aqueous CFE (NACFE) has been demonstrated,[36,79] generically detecting molecular streams in real-time has not been achieved yet. Detection of streams in CFE usually relies on analyte fluorescence;[21,45,66,78,80–82] however, fluorescence is not a universal property of molecules. Mass spectrometry (MS) is a generic detection approach, but it can only be interfaced with CFE off-line,[16,83,84] and, thus, cannot detect multiple molecular streams in real-time. In addition, MS detection is prohibitively expensive for use as an on-board detector in CFE. Our current work was motivated by the insight that being a very common feature of organic molecules, UV absorbance in the range of 200−300 nm can potentially be a basis for a generic way of real-time detection of multiple streams of small organic molecules in CFE.

3.2. MATERIALS AND METHODS

3.2.1. Materials and chemicals

Analytical grade propylene carbonate (PC), styrene, and benzoic acid were purchased from Sigma Aldrich (Oakville, ON, Canada). Double-sided polished JGS1 (= transparent in UV region) fused silica quartz glass sheets (50 mm × 50 mm × 1 mm) were purchased through eBay (Shop: *pickbestforyou*, China). Technical grade tetra butyl ammonium acetate (TBAA) was purchased from TCI America (Portland, OR, United States). The electrolyte was a solution of tetrabutylammonium acetate salt in propylene carbonate. Stock solutions of analytes were prepared in respective electrolytes as solvents. All chip materials listed in **APPENDIX B, Table B3.1** were purchased from McMaster Carr (Elmhurst, IL, USA).

3.2.2. Instrumentation

The electrolyte was delivered to the CFE chip with a NE-1010 syringe pump from New Era Pump Systems, Inc. (Farmingdale, NY, USA). Analyte solutions were delivered to the

Supplementary method figure 3.1. Imaging setup as described in the Instrumentation chapter (3.3.2.) of Materials and Methods.

NACFE chip with a NE-300 syringe pump from New Era Pump Systems, Inc. (Farmingdale, NY, USA). Separation voltage was applied to the platinum electrodes inside the separation zone from an EPS 3501 XL power supply from GE Healthcare (Chicago, IL, USA). The plastic parts of all chips were fabricated using a MODELA MDX-540 Benchtop Milling Machine from Roland DGA (Irvine, CA, USA). A customary hand-held UV lamp (UVGL−25 Compact UV lamp, UVP, Cambridge, UK; 4 W of lamp power consumption; 254 nm excitation) was used as a light source and a mirrorless camera (Panasonic Lumix DMC-G85 with 12−60 mm objective; UV and polarisation filter) as the detector for the visible emission light (>400 nm). The following picture shows the whole setup, including the pumps.

3.2.3. Chip Fabrication

NACFE chips were designed in Solid Edge (see model files in **models.zip**) and fabricated of PVC Type I or PEI according to our previously developed fabrication procedure (*Lab Chip* **2019**, *19*, 2156−2160, DOI: **10.1039/C9LC00460B**). More details on chip fabrication and chip components may be found in this previous work.

3.2.4. General experimental details

Electrolyte and analyte flow rates were 1 mL/min and 3 µL/min, respectively. 250 V were applied as separation voltages resulting in field strength of 45 V/cm (distance between electrodes = 5.5 cm).

3.2.5. Evaluation procedure

The evaluation procedure was the same as described in our previous papers (*Lab Chip* **2019**, *19*, 2156−2160, DOI: **10.1039/C9LC00460B**, *Anal. Chem.* **2018**, *90*, 9504−9509, DOI: **10.1021/acs.analchem.8b02186**). Raw evaluation files, a copy of the programs, and evaluated data can be found in **evaluation.zip**.

The basic idea is to represent molecular stream separation by a single plot called angulagram. In an angulagram, every stream is represented by a single peak. Peak properties, such as position and shape, contain all information required to calculate quantitative stream characteristics: stream deflection, stream width, and stream linearity. The source code of all programs described here can be found on Github (DOI: **10.5281/zenodo.2592588**) and ChemRxiv (DOI: **10.26434/chemrxiv.7840937**).

3.2.6. Constructing angulagrams

The general procedure of angulagram construction is i) aligning the image (rotation/mirroring), ii) cropping the region of interest (separation zone), iii) transferring the data from Cartesian to polar coordinates, and iv) integrating the signal over the radius. A reflectometric input image taken with a consumer camera naturally includes a high background, which can be decreased by lowering the color saturation and extracting only the hue levels of interest. The respective parameters were manually determined in Photoshop using the ruler tool (rotation angle, inlet position, and separation zone size) and adjustments tools (Image → Adjustments → Hue/saturation; Image → Adjustments → Levels); these parameters were then fed into a Python program (**angureflexin.py**) that performed the construction (see source code for details). The generated output consisted of an angulagram, a parameter file that

listed all used parameters, an image of the separation zone in polar coordinates, and a preview image that was used as the thumbnail for the angulagrams in this work.

3.2.7. Estimating limit of detection (LOD)

The LODs of the quartz-quartz pseudo device and the quartz-PEI device were estimated by i) constructing the respective angulagrams (see above), ii) determining the peak height of the stream, iii) determining an average background signal, iv) determining the noise of this background signal, v) calculating the signal-to-noise (*S*/*N*) ratios for several concentrations of styrene (100, 500, and 1000 µM), and vi) using linear regression to determine the concentration of styrene at *S*/*N* = 3. The average background signal was determined by selecting a small region of constant signal just left to the stream peak in the angulagram; for good measure, the left side was used in our case since it was higher and, thus, would result in "more" background (*i.e.* worse than the right side). The standard deviation of the same region of background was used as noise. For the linear regression, the following linear equation with an intercept of *S*/*N* = 1 was used:

$$\frac{S}{N} = m \times c_{\text{styrene}} + 1$$

The intercept of *S*/*N* = 1 was chosen since, in practice, *S* = *N* for a zero concentration of styrene. Consequently, the LOD concentration (*S*/*N* = 3) of styrene was calculated by

$$\text{LOD}_{\text{styrene}} = c_{\text{styrene, } S/N=3} = \frac{S/N - 1}{m} = \frac{3-1}{m} = \frac{2}{m}$$

See **Excel-files** in **evaluation.zip** for details.

3.2.8. Analyte concentration as a function of signal

The signal *S* is the "blank" fluorescence in the non-shaded area (*i.e.* without analyte) minus the fluorescence in the shaded areas (*i.e.* with analyte):

$$S = F_{\text{blank}} - F_{\text{shaded}} \tag{1}$$

Fluorescence intensity *F* can be expressed by Parker's law (Parker, C. A.; Rees, W. T. *Analyst 1960*, 85, 587-600. DOI*:* **10.1039/AN9608500587**.):

$$F = I_{\text{ex}} k \phi_{\text{f}} \varepsilon_{\text{f}} c d = I_{\text{ex}} k' \tag{2}$$

where I_{ex} is the excitation light intensity, k is a parameter reflecting specific optical geometry of the instrument, ε_{f} is the excitation coefficient, ϕ_{f} is the quantum yield of the fluorophore, c is the concentration of the fluorophore, and d is the depth of the fluorescent layer. Since all these parameters except for I_{ex} are constant they can be combined to a single constant *k'*. F_{blank} and F_{shaded} only differ in the excitation light intensity, which depends on light absorption of a potential analyte. Using the Lambert-Beer's law, light intensity I decreased due to the absorption by the analyte relates to the intensity of incident light I_0 as:

$$I = I_0 10^{-A} \tag{3}$$

For the non-shaded areas, no light is absorbed and I_0 is the intensity of light that excites fluorescence of the fluorescent sublayer. For the shaded areas, light is absorbed and the intensity of light that excites fluorescence of the fluorescent sublayer is $I = I_0 10^{-\text{A}}$. Then, intensities of fluorescence produced by the non-shaded and shaded areas can be expressed using **Eq. 2** and **3**:

$$\begin{aligned} F_{\text{blank}} &= k' I_0 \\ F_{\text{shaded}} &= k' I = k' I_0 10^{-A} \end{aligned} \tag{4}$$

Combining **Eq. 4** and **1** yields:

$$\begin{aligned} F_{\text{blank}} - F_{\text{shaded}} &= S \\ k' I_0 - k' I_0 10^{-A} &= S \\ k' I_0 (1 - 10^{-A}) &= S \\ F_{\text{blank}} (1 - 10^{-A}) &= S \end{aligned} \tag{5}$$

where A is the absorption of the analyte. Solving for A yields:

$$\begin{aligned} 1 - 10^{-A} &= \frac{S}{F_{\text{blank}}} \\ 10^{-A} &= 1 - \frac{S}{F_{\text{blank}}} \\ A &= -\log_{10}\left(1 - \frac{S}{F_{\text{blank}}}\right) \end{aligned} \tag{6}$$

The absorption is defined as the product of analyte concentration, an extinction coefficient of the analyte, and path length (here: the depth of the separation channel). Solving **Eq. 6** for the concentration yields:

$$\begin{aligned} c_{\text{analyte}} \varepsilon_{\text{analyte}} d_{\text{channel}} &= -\log_{10}\left(1 - \frac{S}{F_{\text{blank}}}\right) \\ c_{\text{analyte}} \varepsilon_{\text{analyte}} d_{\text{channel}} &= -\log_{10}\left(\frac{F_{\text{blank}} - S}{F_{\text{blank}}}\right) \end{aligned} \tag{7}$$

and ultimately in:

$$\begin{aligned} c_{\text{analyte}} &= \frac{1}{\varepsilon_{\text{analyte}} d_{\text{channel}}} \log_{10}\left(\frac{F_{\text{blank}}}{F_{\text{blank}} - S}\right) = \\ &= \frac{1}{\varepsilon_{\text{analyte}} d_{\text{channel}}} \log_{10}\left(\frac{F_{\text{blank}}}{F_{\text{shaded}}}\right) \end{aligned} \tag{8}$$

Eq. 8 allows calculating the concentration of analytes in the separation channel using the fluorescence intensity F_{blank} of non-shaded areas as a reference, the fluorescence intensity F_{shaded} of the analyte stream, the extinction coefficient, and the channel depth.

3.2.9. Estimating the LOD by calculations

Using **Eq. 8** it is possible to calculate a rough estimate for the LOD of a particular molecule by using the relation $S = 3N$: the noise N is simply the standard deviation of F_{blank}. We used ImageJ to get the mean intensity value as well as the standard deviation in areas around the stream (on **raw 100 µM styrene.jpg** for both quartz-quartz and quartz-PEI chips), *e.g.*:

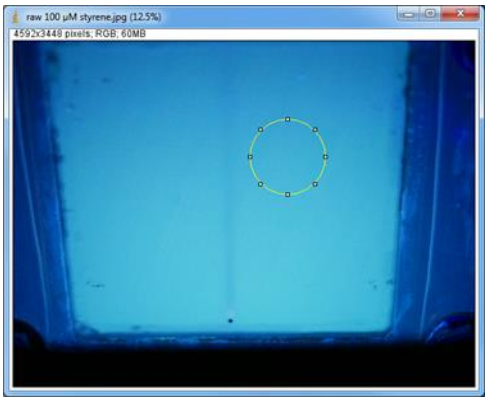

Supplementary method figure 3.2. Raw image used in Estimating the LOD by calculations chapter (3.2.9.) of Materials and Methods.

In this example, the mean is 122.308 AU, and the standard deviation is 5.501 AU. Along with the extinction coefficient ($1.47 \times 10^4\ M^{-1}\ cm^{-1}$ at around 250 nm, see Rodebush, W.H.; Feldman, I., *J. Am. Chem. Soc.* **1946**, *68*, 896) and the depth of the channel (200 µm) in **Eq. 8**,

the LOD is 214 µM. Since the illumination of the images is not homogeneous, different areas will lead to different mean values and standard deviations and, in turn, to different LODs. We evaluated the LOD of styrene for the total non-shaded region and different sub-regions to be in the range of 50−250 µM for both chips.

These LODs are overall greater than the experimental ones from before due to an underestimation of the extinction coefficient $\varepsilon_{\text{analyte}}$. $\varepsilon_{\text{analyte}}$ is a measure of the amount of light being absorbed over a certain path length (per cm) and a certain concentration (per M) for a certain wavelength with a relatively narrow window. However, the UV lamp emits a broad band around 254 nm, and the analyte (styrene) is likely to absorb more light resulting in an effective extinction coefficient $\varepsilon_{\text{analyte,eff}}$ that is 2−5 times larger than $\varepsilon_{\text{analyte}}$ used for the calculation above. Consequently, the estimated LOD would be 2−5 lower. Conclusively, an optimized optical setup will lead to more precise LOD estimations.

Note that this computational method is an estimate of the LOD based on one data point (blank measurement) and without any analyte (effects); experimental estimates from a series of concentrations are a more reliable measurement method (see above).

3.2.10. Minimum channel depth for sub-mM LOD

Our goal is to find the minimum channel depth for a LOD of 1 mM at *S*/*N* of 3. Solving **Eq. 8** for the channel depth yields:

$$d_{\text{channel}} \geq \frac{1}{\varepsilon_{\text{analyte}} c_{\text{analyte,LOD}}} \log_{10}\left(\frac{F_{\text{blank}}}{F_{\text{blank}} - 3N}\right)$$

The typical extinction coefficient of small aromatic molecules (*e.g.* styrene, see above) at 250 nm is about 1.5×10^4 M^{-1} cm^{-1}. If we assume (based on the values from the LOD estimation above) that the noise is about 5% of the fluorescence signal ($N = 0.05 \times F_{blank}$), then the minimum channel depth to achieve a LOD of 1 mM is 108 µm. The channel depth of the present chip(s) is 200 µm, *i.e.* the chips are suitable for sub-mM LODs of small molecules.

3.2.11. Extracting stream parameters from angulagrams

Another Python script (**evolutin.py**) was used to find the stream peaks in the angulagrams and determine their parameters (deflection, width, linearity, and resolution), as described in our previous work. See the source code for details. (DOI: **10.26434/chemrxiv.7840937**)

3.3. RESULTS AND DISCUSSION

3.3.1. Molecular stream detection

UV detection of streams in a mesoscale CFE chip (with separation chamber dimensions being 5 cm × 5 cm × 0.2 mm) is not a trivial task. The most straightforward approach is to use UV absorbance imaging with a UV-transparent CFE chip positioned between a UV light source and a UV camera (**Figure 3.1A**). This approach is very expensive as it requires a difficult-to-

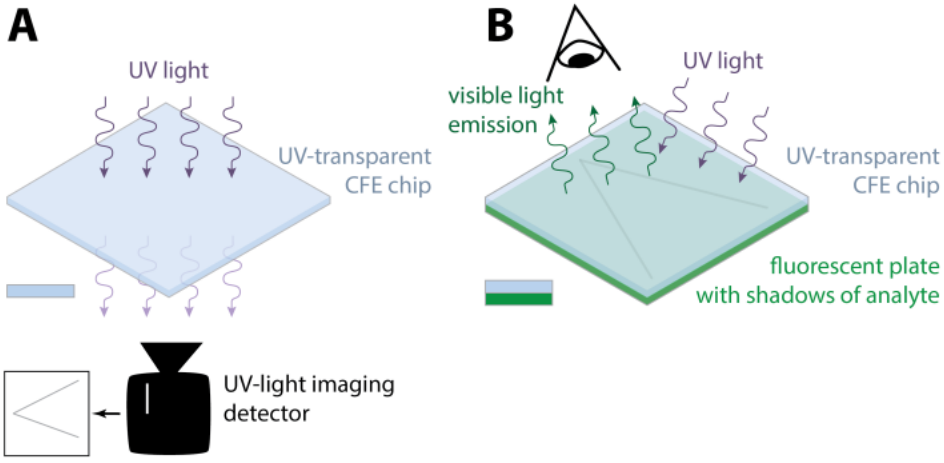

Figure 3.1 Schematics of UV imaging using UV optics and UV camera (**A**) and fluorescence sublayer visualization (FSV) (**B**). **A:** UV light passes through the transparent CFE chip in which analytes absorb some of UV light. A UV camera positioned on the opposite side of the chip images UV absorbing streams. **B:** UV light passes through the transparent CFE chip in which analytes absorb some of UV light. The remaining UV light excites fluorescence of a UV-absorbing visible-fluorescent plate positioned on the opposite side of the chip. Absorption of UV light by the analytes decreases fluorescence in the shadowed areas. The fluorescence and, thus, the shadows are visible to the naked eye and common photo/video cameras.

make all-quartz chip, expensive UV optics, and a very expensive UV camera. The high cost of this solution will most likely make it prohibitive for practical use. Here we propose a more elaborate but much less expensive alternative to UV absorbance imaging, namely, stream visualization *via* analyte-caused obstruction of excitation of a fluorescent sublayer placed underneath the separation chamber. We term this approach fluorescence sublayer-based visualization (FSV). Conceptually, a source of UV light and a visible-range camera are positioned on one side of the CFE chip, while a sublayer capable of fluorescing in the visible range upon UV excitation is positioned on the opposite side (**Figure 3.1B**). If an analyte in the CFE chip absorbs UV light, it decreases the intensity of UV light reaching the sublayer and, thus, decreases fluorescence intensity from the shadowed area. Additionally, fluorescence is visible to the naked eye and, thus, in principle, no camera is needed provided that the eye is protected from stray UV light.

This FSV approach has been successfully used to detect small organic molecules in thin-layer chromatography (TLC) and nucleic acids in gel electrophoresis.[85–87] In TLC, separation of organic molecules occurs right on the fluorescent TLC plate making their FSV trivial. Using FSV for visualizing nucleic acids within the gel is also simple as it only requires that a UV-transparent gel be placed on a fluorescent plate. Using a fluorescent sublayer for stream visualization in CFE is much more complicated as the streams are within a CFE device. Accordingly, the whole device should be placed on the fluorescent plate, and the device should thus be UV-transparent. Such requirements impose significant technical challenges in CFE-device fabrication and optical-setup design. The goal of our work was to find a practical solution for these technical challenges and prove the feasibility of the FSV of molecular streams in CFE.

3.3.2. FSV imaging system

We have previously developed an imaging system and image-analysis software for the detection and characterization of streams of fluorescent analytes in CFE.[5,66] In principle, FSV could utilize the same setup and software provided that the visible-range fluorescence excitation light source be replaced with a UV one. However, for this work, we assembled a new setup with a typical hand-held UV lamp (254 nm) and a mirrorless micro four-thirds camera as the detector (**Figure 3.2**). We did this because our previous setup used a light emitting diode (LED) as a light source, and we could not find a powerful replacement for UV excitation (>1 mW); in contrast, the hand-held UV lamp used in the new setup has a bright bulb with 254 nm primary band excitation (4 W of power consumption).

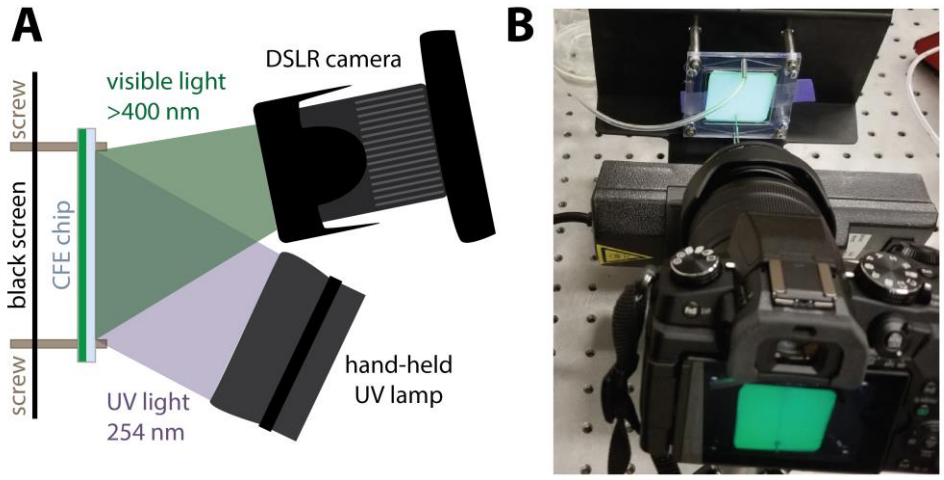

Figure 3.2 Schematic (**A**) and photo (**B**) of the FSV setup designed, as-sembled, and used in this work. The chip is mounted against a black background. A customary hand-held UV lamp (254 nm main band excitation) is used as a UV light source and a mir-rorless camera (Panasonic Lumix DMC-G85 with 12−60 mm objective; UV and polarization filter) is used as a detector for visible-light fluorescence of the fluorescent sublayer (>400 nm).

To demonstrate that FSV is a practical stream-visualization method for non-aqueous CFE, we aimed to reliably image organic molecules in our mesoscale CFE device with a 200 µm thickness (height) of the separation chamber.[79] As CFE should benefit flow chemistry and flow chemistry deals with relatively high concentrations in the millimolar range,[3,61] our goal was to achieve sub-mM LOD (concentration providing a signal-to-noise ratio of 3) in a 200-µm-thick CFE chamber.

3.3.3. FSV proof-of-concept

An optically ideal CFE device for FSV must be made of quartz, the best UV-transparent material. However, making a mesoscale CFE device of pure quartz is technically challenging; we did not have the capabilities to make such a device. On the other hand, our imaging experiments required neither a fully functional nor a pure quartz CFE device. Therefore, we simply emulated an optically-ideal CFE device by assembling a pseudo-device with a 200 µm-thick chamber between two quartz plates but without electrodes. The quartz plates were fixed together by a custom-fabricated plastic frame (**APPENDIX B, Figure B3.1**). We filled the chamber with propylene carbonate and propagated a stream of a small organic molecule solution, styrene in propylene carbonate at concentrations varying between 100 µM and 1 mM, through the chamber. The pseudo-device was placed on a fluorescent TLC plate and imaged with the FSV setup depicted in **Figure 3.2**. We could reliably visualize 100 µM of styrene (**Figure 3.3A**), and the LOD was estimated to be approximately 30 µM. Since the LOD was sufficiently low, the next logical step was to attempt FSV in a real CFE device made of PVC Type I (PVC, chemically-inert plastic suitable for fabrication via milling).[79] The device with a 200-µm-thick chamber was placed on a fluorescent TLC plate and imaged with the setup depicted in **Figure 3.2**. Since PVC

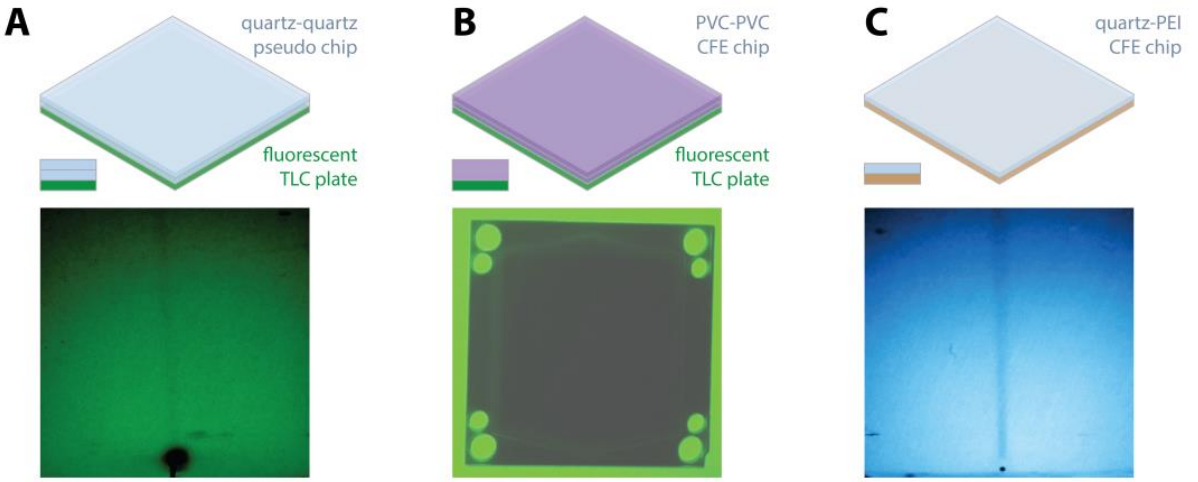

Figure 3.3 Feasibility of a quartz-quartz pseudo chip (**A**), a PVC-PVC CFE chip (**B**), and a quartz-PEI CFE chip (**C**) for FSV. **A**: A stream of sty-rene solution (100 µM) is forwarded into the pseudo chip and visualized by a shadow on the fluorescent TLC plate under it. The con-trast of the photo here was increased to improve visibility of the stream to the human eye. **B**: PVC blocks basically all UV light; there-fore, fluorescence is only visible at the eight openings (fixing holes) and the area around the chip. No streams could be visualized in this chip. The brightness of the photo here was increased to visualize the chip geometry better. **C**: A stream of styrene solution (100 µM) is forwarded into the quartz-PEI CFE chip and visualized by a UV shadow brought onto the fluorescent PEI part. The contrast of the photo here was increased to improve visibility of the stream to the human eye.

plastic is poorly UV transparent, the CFE chip blocked most UV light from reaching the fluorescent TLC plate resulting in one single large shadow in the form of the chip (**Figure 3.3B**). No stream shadows could be visualized or analyzed in such a device. These experiments with a

quartz pseudo-device and a PVC-made CFE device led us to the conclusion that FSV could be used for visualizing a stream of organic molecules in CFE, but this approach required a UV-transparent CFE device.

3.3.4. FSV chip design

We considered a set of *a priori* options for device design with three criteria in mind: feasibility of device fabrication, UV transparency of the device, and chemical inertness of device material (**Table 3.1**). Our procedure for fabricating a mesoscale CFE device with a large area (5 cm × 5 cm) but a shallow (200 μm) separation chamber involves machining the bottom and

	Top	Bottom	TLC plate required	Optical clarity[a]	Machin-ability[b]	Chemical resistivity[c]
1	quartz	quartz	yes	●●●	●	●●●
2	TP	TP	yes	●	●●●	●●
3	quartz	TP	yes	●●	●●●	●●
4	quartz	FP	no	●●●	●●●	●●

[a]Optical clarity in UV-region (200−300 nm) of the optical spectrum.
[b]Ability to mill plastics using our established protocols for PVC.
[c]Compatibility with propylene carbonate.

Table 3.1 Chip assemblies and properties for various combina-tions of quartz, transparent plastic (TP), and fluores-cent plastic (FP).

top pieces of the device and bonding both pieces together; machining the top piece can be avoided if the material possesses an even and smooth surface (on the microscale) by nature. This fabrication approach immediately rules out the option of an all-quartz chip (**1**), which is optically and chemically ideal but technically challenging to fabricate due to the poor machinability of quartz. As our classical CFE devices are made solely of plastic, a logical option to consider was a device with the top and bottom pieces made of UV-transparent plastic (**2**). UV-transparent plastics, however, have much worse UV transparency than quartz, suggesting a combination of a quartz top piece and a UV-transparent-plastic bottom piece (**3**). While improving the optical quality of the top piece to an ideal level (quartz), this combination does not improve the optical quality of the plastic bottom one. Further, UV transparent plastics give fewer choices for compatibility with organic solvents; in fact, we found only polymethylpentene (PMP) to be suitable for this approach.

The limitations of the transparent-plastic bottom piece suggested us to drop our first FSV approach with a stand-alone fluorescence plate under the CFE device and consider embedding a fluorescence layer into the bottom piece. Further, we realized that the self-fluorescence of UV-absorbing plastics, which was previously viewed as an additional optical obstacle, provided a way of "integrating" a fluorescence sublayer with the plastic bottom piece. If the bottom piece is machined from a UV-absorbing visibly-fluorescent plastic, then the top piece could be simply an unprocessed quartz plate (in a PVC-plastic frame) (**4**). Such a device has optical properties even better than those of the quartz-quartz setup due to the absence of any intermediate layer separating the analyte from the fluorescent sublayer. In addition, most UV-absorbing plastics fluoresce in the visible range giving us a good choice of materials for satisfying the requirement of chemical inertness (see **APPENDIX B, Table B3.1** for details).

3.3.5. FSV proof-of-work

We fabricated a fully functional CFE chip with a bottom piece made of polyetherimide (PEI; a fluorescent plastic) and a top piece made of quartz in a PVC-plastic frame. In essence, the top piece was made out of PVC with a quartz central piece; this central piece functioned as a window (**APPENDIX B, Figure B3.2**). This approach allowed us to use our established protocols for machining plastics while incorporating a quartz window without the need to machine quartz itself. The chip could be imaged with the FSV setup depicted in **Figure 3.2** without an additional fluorescent TLC plate under the chip. We could clearly see a stream of

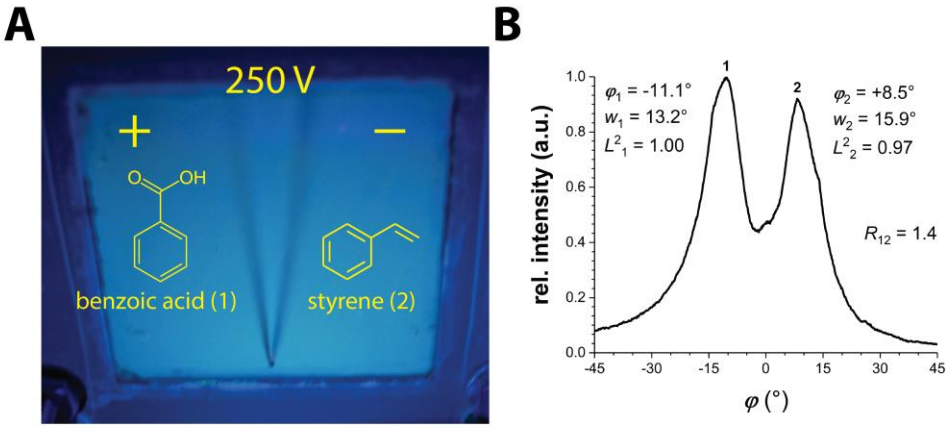

Figure 3.4 Photo (**A**) and the angulagram (**B**) of the separation of benzoic acid (**1**) and styrene (**2**) in CFE. **A**: Both streams are clearly visi-ble by naked eye and can be evaluated using our imaging system (**Figure 3.2**) using angulagrams. **B**: The evaluated angulagram shows the extracted stream parameters (deflection φ, width w, linearity L², and resolution R) for benzoic acid and styrene. Conditions: background electrolyte flow rate = 1 mL min−1, sample flow rate = 3 μL min−1, sample concentration = 2.5 mM each in propylene carbonate. See Materials and Methods for more details.

100 µM styrene (**Figure 3.3C**). The LOD for styrene in this chip was estimated to be 30 µM, *i.e.* identical to the LOD obtained for the ideal quartz-quartz pseudo-device.

Since the quartz-PEI chip was a fully functional CFI device, we subsequently used it to separate a mixture of benzoic acid and styrene using our established NACFE protocol,[79] and detect the streams with FSV. Both molecular streams were clearly visible by the naked eye and detectable with the camera (**Figure 3.4**). The streams were evaluated with our 'angulagrams' analysis method.[66] Our evaluation revealed that the two streams could be separated with a good resolution (R = 1.4) and were highly linear (L^2 > 0.96 for both streams). These results emphasize that not only does the quartz-PEI chip allow FSV in principle but it is also a *practical* CFE device.

3.4. CONCLUSIONS

In conclusion, we showed that FSV is a feasible and practical approach for visualizing molecular streams in CFE. In this work, we demonstrated the real-time and quantifiable imaging of UV-absorbing small organic molecules with a sub-mM LOD that is suitable for integrating CFE into flow chemistry for continuous synthesis and separation. As FSV is a universal visualization technique, we also foresee applications in visualizing unlabeled biomolecules such as proteins and DNA in CFE.

CHAPTER 4. IMPROVING THE RESOLUTION THROUGH NON-ORTHOGONAL APPLICATION OF THE ELECTRIC FIELD

The presented material was published previously and reprinted with permission from "Kochmann, S.; Ivanov, N.; Le Blanc J.C.Y.; Gorin, B.I.; Krylov, S.N. Circular Geometry in Molecular Stream Separation to Facilitate Nonorthogonal Field-to-Flow Orientation. *Analytical Chemistry* 2022, 2022, 94, 27, 9519–9524." American Chemical Society.

My contributions to the article were: (i) performing presented experiments, (ii) preparing figures, (iii) interpreting results, and (iv) writing the manuscript. The image evaluation software was prepared by Dr. Sven Kochmann.

ABSTRACT

Molecular stream separation (MSS) is a promising complement for continuous-flow synthesis. MSS is driven by forces exerted on molecules by a field applied at an angle to the stream-carrying flow. MSS has only been performed with a 90° field-to-flow angle because of a rectangular geometry of canonic MSS; the second-order rotational symmetry of a rectangle prevents any other angle. Here, we propose a non-canonic circular geometry for MSS, which better aligns with the polar nature of MSS and allows changing the field-to-flow. We conducted in silico and experimental studies of circular geometry for continuous-flow electrophoresis (CFE, an MSS method). We proved two advantages of circular CFE over its rectangular counterpart. First, circular CFE can support better flow and electric-field uniformity than rectangular CFE. Second, the non-orthogonal field-to-flow orientation, achievable in circular CFE, can result in a higher stream resolution than the orthogonal one. Considering that circular CFE devices are not more complex in fabrication than rectangular ones, we foresee that circular CFE will serve as a new standard and a testbed for the investigation and creation of new CFE modalities.

4.1. INTRODUCTION

Continuous-flow organic synthesis has several important advantages over its batch counterpart,[2,4,88] and continuous separation is its logical extension.[3,78,89] There are several continuous-separation methods; however, the only widely used one is liquid-liquid extraction, which can hardly separate multiple species from each other.[9,10] In contrast, molecular stream separation (MSS) can continuously separate multiple species; though, its early stage of development hinders the efficient combination with continuous-flow synthesis.[13,36,79] MSS is driven by a force exerted discriminatively on the separated species by a force field oriented at an angle to the hydrodynamic flow carrying the streams. The interplay of the separating force and

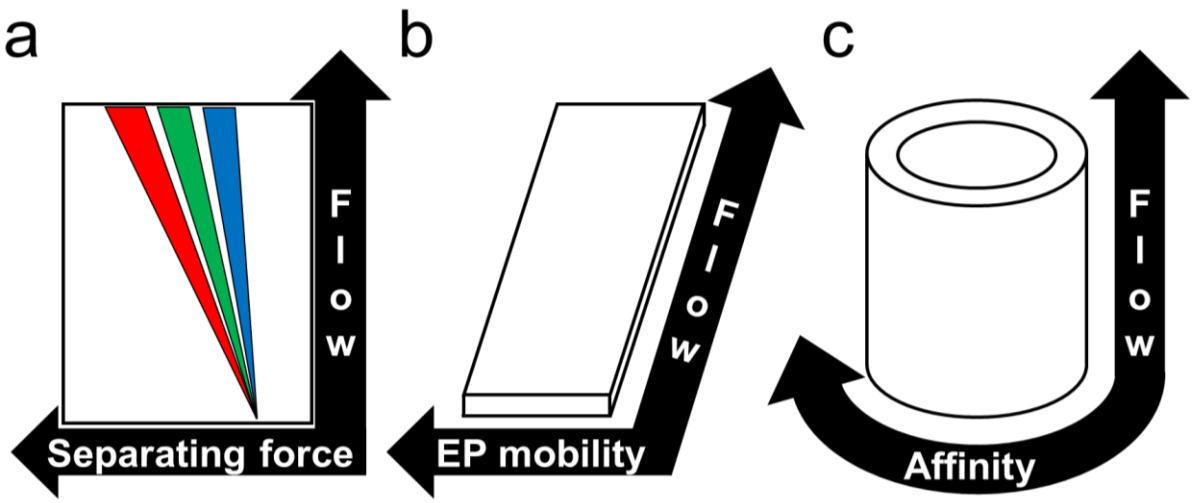

Figure 4.1 Schematic depiction of conventional orthogonal MSS: **a)** general principle and its implementation in **b)** continuous-flow electrophoresis (CFE) with differential electrophoretic (EP) mo-bility of molecules being the driving force of MSS, and **c)** continuous annular chromatography (CAC) with differential affinity to the solid phase driving MSS.

the hydrodynamic flow causes the splitting of the stream of mixed species into their individual molecular streams (**Figure 4.1a**).

Fundamentally, MSS is defined by three variables: the field-to-flow angle, the field strength, and the flow rate. The influence of the varying magnitudes of field strength and flow rate on MSS has been extensively studied, and these parameters are used to control separation.[90] On the opposite, the field-to-flow angle has always been 90° owing to the apparent obviousness that the 90°-angle is optimal as well as conceptual challenges and technical difficulties associated with the non-orthogonal field-to-flow orientation within the canonic rectangular paradigm of MSS (as will be discussed below).[91] The aim of this work was to understand if the field-to-flow orientation can be included as a degree of freedom, thus, facilitating non-orthogonal MSS for exploration and potential use.

4.2. MATERIALS AND METHODS

4.2.1. Index of Uniformity calculations

A two-dimensional vector field is exported as a four-column data set consisting of two-number coordinates and corresponding X,Y vector components. The sum of all X vector components and the sum of all Y vector components are used to find the average flow vector for the entire device (**Eq.1**). This average vector points in the general direction of the flow within the device.

$$\text{Average flow vector} = \left(\sum X_{\text{components}}, \sum Y_{\text{components}}\right) \quad (1)$$

The angle φ from **Eq. 2** calculates the angular deflection of the average vector from the *X*-axis.

$$\varphi = -arctan\left(\frac{\sum Y_{\text{components}}}{\sum X_{\text{components}}}\right) \quad (2)$$

This angle is then used to rotate the entire vector field using **Eq. 3** and **Eq. 4** along the *X*-axis for further calculations. *X*' and *Y*' are the newly obtained vector components after the rotation:

$$X' = X_{\text{component}}\, cos\, \varphi - Y_{\text{component}}\, sin\, \varphi \quad (3)$$

$$Y' = X_{\text{component}}\, sin\, \varphi - Y_{\text{component}}\, cos\, \varphi \quad (4)$$

The homogeneity factor (Γ) is then calculated as in **Eq. 5**. In any real device, rotation of the general flow direction in the direction of the *X* axis allows the ratio component of **Eq. 5** to always be between 0 and 1. In the ideal case of a perfect homogenous flow, Γ will be equal to 1. All flow non-homogeneities would increase the $\left|\boldsymbol{Y'_{components}}\right|$ part and decrease the Γ value.

$$\Gamma = 1 - \frac{\sum|Y'_{\text{components}}|}{\sum|X'_{\text{components}}|} \quad (5)$$

Examples of Γ values for different geometries are shown in **APPENDIX C, Note C4.1**.

4.2.2. Measurements of electrophoretic mobilities in CE

All CE experiments were done with a P/ACE MDQ instrument from Sciex (Concord, ON, Canada). Light absorption at 240 nm was used for analyte detection using the direct absorbance method. An uncoated fused silica capillary with an inner diameter of 75 μm, total length of 30 cm, and distance from the inlet to the detection point of 20 cm were used for all CE experiments when measuring μ (electrophoretic mobility) of fluorescein (FLU), Sudan Black (SBL) and α-naptholbenzein (NAP). The background electrolyte was 30 mM tetrabutylammonium acetate (TBAA) in propylene carbonate. An EOF marker (1.0 mM toluene dissolved in the background electrolyte) was injected along with 1 mM of each analyte into the anode end of the capillary by a pressure pulse of 0.4 psi for 2.5 s. CE separation was carried out at an electric field of 1000 V/cm (30 kV across 30 cm) with a capillary temperature set to 25°C. Analyte migration velocities (m/s) were calculated from the corresponding electropherograms based on characteristic times required for the analyte to reach the UV detector. Experimental electrophoretic mobilities ($m^2/(V*s)$) were calculated by dividing experimental analyte velocities (m/s) by the applied electric field (V/m).

Electropherogram and corresponding data table are shown in **APPENDIX C, Note C4.3.**

4.2.3. Circular CFE device fabrication details

Circular devices were designed in Solid Edge and fabricated of PEI (polyetherimide) and PVC (polyvinylchloride) plastics according to our previously developed fabrication procedure for PMMA chips (*J. Sep. Sci.* **2011**, *34*, 556−564, DOI: 10.1002/jssc.201000758; *Lab Chip* **2017**, *17*, 256–266, DOI: 10.1039/C6LC01381C). Details on chip fabrication and chip components used (apart from the chip material) may be found in these two previous works. Circular devices

were fabricated using MODELA MDX-540 Benchtop Milling Machine from Roland DGA (Irvine, CA, USA). Short Π-shaped palladium wires were inserted into the PEI device to create electrode segments surrounding the separation zone **(APPENDIX C, Note C4.4a)**. Π-shaped nickel wires with gold-coated crimps attached on both sides **(APPENDIX C, Note C4.4b)** were used to connect multiple segments into a single electrode array **(APPENDIX C, Note C4.4c)**. After electrode assembly, the PEI device was covered with a flat-machined piece of PVC plastic **(APPENDIX C, Note C4.4d)**.

4.2.4. Circular CFE experimental details

Flow rates of the background electrolyte and analyte were in the ranges of 2−4 mL/min and 1−2 μL/min, respectively. 150 V was applied from an EPS 3501 XL power supply (GE Healthcare, Chicago, IL, USA) to the platinum electrodes around the separation zone resulting in electric field strength of 25 V/cm (distance between the electrodes was 6 cm). Depending on the electrolyte concentration, the conductivity of our background electrolyte solution was 2 to 8 μS/m. The electrolyte solution was delivered to the circular device with a NE-9000G peristaltic pump from New Era Pump Systems, Inc. (Farmingdale, NY, USA). The pump was equipped with a Masterflex pulse dampener from Cole Palmer (Vernon Hills, IL, USA) to suppress flow pulsation. Analyte solutions were delivered to the circular device with a Model 11 syringe pump from Harvard Apparatus (Holliston, MA, USA). A mixture of analytes (1.25 mM each; 3.75 mM combined) was prepared in the 30 mM of the electrolyte solution (exactly the same as the background electrolyte) to maintain homogenous conductivity in the separation zone. Note, in Non-aqueous CFE, analytes do not have an intrinsic change and, accordingly, do not change the

overall conductivity. The analytes acquire electrophoretic mobility through their association with the background electrolyte.

4.2.5. Using Fiji/TrackMate for the circular design flow field Γ calculations

The recorded video **flowstream.mp4** (about 13.4 GB) was edited in the following way using **ffmpeg 3.4.8** software to remove background, improve particle tracking conditions, and significantly reduce file size while maintaining high resolution:

```
# Remove audio from video
ffmpeg -i flowstream.mp4 -c copy -an flowstream_noaudio.mp4

# Remove color (reduces file size to 1/3)
ffmpeg -i flowstream_noaudio.mp4 -vf format=gray flowstream_noaudio_gray.mp4

# Cut the first 5 seconds (shaking camera)
ffmpeg -i flowstream_noaudio_gray.mp4 -ss 5 -c copy flowstream_noaudio_gray_cut.mp4

# Add overlay (removes all the chip background)
ffmpeg -i flowstream_noaudio_gray_cut.mp4 -i flowstream_overlay.png -filter_complex
    "[0:v][1:v] overlay=0:0" -pix_fmt yuv420p -codec h264_nvenc
    flowstream_noaudio_gray_cut_overlay.mp4

# Change curves to improve contrast
ffmpeg -i flowstream_noaudio_gray_cut_overlay.mp4 -vf "curves=all='0.04/0.0 0.08/1.0'" -
    pix_fmt yuv420p -codec h264_nvenc flowstream_noaudio_gray_cut_overlay_curved.mp4

# Crop the video (removes more background, reduces the memory per frame size/requirement);
    the original video is 3840x2160; also, use gray pixel format to turn everything to an
    8bit image
ffmpeg -i flowstream_noaudio_gray_cut_overlay_curved.mp4 -vf "crop=1600:2160:1000:0'" -
    pix_fmt gray -codec h264_nvenc flowstream_noaudio_gray_cut_overlay_curved_cropped.mp4

# Create a set of tiff files with lzw compression out of this movie file; "gray" format is
    important, otherwise tiffcp will not work (subsampling)
ffmpeg -i flowstream_noaudio_gray_cut_overlay_curved_cropped.mp4 -compression_algo lzw -
    pix_fmt gray tiffs/flowstream%05d.tif
```

The result is a set of tiff-files, **flowstream00001.tif** to **flowstream38246.tif**, that can be used in **Fiji/ImageJ2 1.53f51** with the **TrackMate 7.6.0** plugin.[92–94] We found that using the video file directly or other image formats (*e.g.*, tiff-stacks) caused importing the files to fail.

Tracking the particles in TrackMate was done by using every 10th image and selecting *t*-axis ("Swaping *z* and *t*"). The **Difference of Gaussian** (DoG) detector (estimated diameter: 5 px,

quality threshold: 30, subpixel localization) was used for particle recognition in all images. Subsequently, all detected particles were forwarded to the **Simple Linear Assignment Problem** (Simple LAP) tracker for generating the tracks (linking max distance: 15 px; gap-closing distance: 18 px; max-frame gap: 2). The resulting information was exported to **flowstream_tracks.xml**.

Further processing was done with developed Python scripts (see the protocol on the next page) to find the marker positions on the image (calculating the resolution and the center point), calculate, and select the flow vectors. All Python scripts can be found in the ChemRxiv depository (DOI: 10.26434/chemrxiv-2022-3w7gt).

```
# Markers found using a randomly selected single image => Center point at 810, 1024;
    average distance between markers is 1408 (1415 and 1401 pixels) => 60 mm real units
    between them => 0.0426 mm/pixel
findmarkers.py --area 3600 --markers 3 --showimage flowstream01694.tif

# Calculate velocity vectors; removing zero-length vectors (usually artifacts from
    tracking); removing tracks with small number of points (everything below 10); average
    the track data for one vector (reduces the impact of high errors in track
# detection between two time points)
track_velocities.py --skipzero --average --minpoints 10 flowstream_tracks.xml
    flowstream_tracks_processed.csv

# Filter velocity vectors by position (center of chip is at 810 1024 pixels, center area
    is 40 by 40 mm²
# 940 x 940 px², at 0.0426 mm/px => rectangle from 340, 554 to 1280, 1494)
filter_velocities.py --skip 1 flowstream_tracks_processed.csv
    flowstream_tracks_processed_and_filtered.csv 344 554 940 940
```

The resulting file **flowstream_tracks_processed_and_filtered.csv** was further processed in Excel to calculate Γ (see **trackmate flow field Γ calculations.xlsx**). Note that on the image, the *y*-axis is the hydrodynamic flow axis; to keep consistency with our calculations (in which *x*-axis is the hydrodynamic flow axis), we swapped *x* and *y* labels in the Excel file.

4.3. RESULTS AND DISCUSSION

4.3.1. From rectangular to circular geometry

There are two major MSS methods: continuous-flow electrophoresis (CFE, **Figure 4.1b**) and continuous annular chromatography (CAC, **Figure 4.1c**).[95,96] Both CAC and CFE utilize a rectangular geometry; the rectangle is planar for CFE and folded into a cylinder for CAC. In CFE, two straight parallel electrodes constitute two sides of a thin rectangular separation zone in which the electric field is perpendicular to the hydrodynamic flow. In CAC, a thin cylindrical layer of the stationary chromatographic phase is rotating orthogonally to the hydrodynamic flow creating an infinitely long stationary phase and a continuous force field.

The rectangular geometry of canonic MSS does not allow the change of the field-to-flow angle because of the 2^{nd}-order rotational symmetry of a rectangle (**Figure 4.2a**). A rectangle has only two equivalent rotational positions and allows only orthogonal field-to-flow orientation. To allow all field-to-flow angles, the geometry must be of the infinite-order symmetry, *i.e.*, circular rotational symmetry (**Figure 4.2b**). This symmetry would be in alignment with the polar system of coordinates and angulagrans recently introduced for the description of MSS.[5]

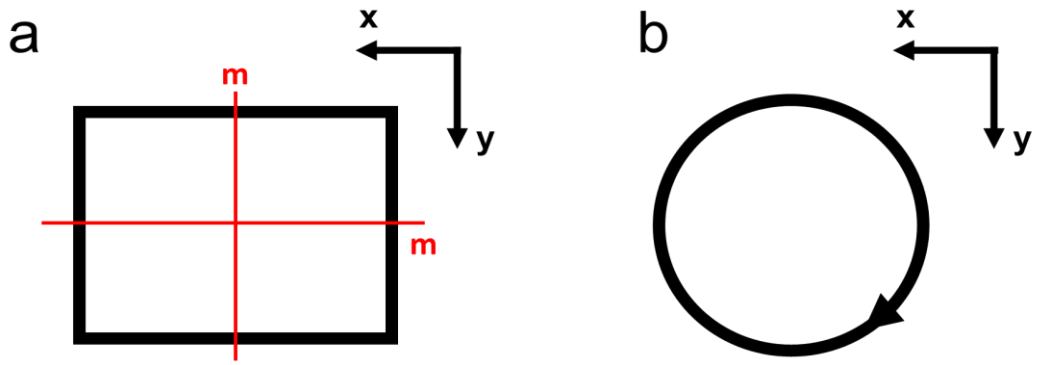

Figure 4.2 Illustration of **a)** the second-order rotational symmetry for conventional rectangular-geometry MSS and **b)** the high-order rotational symmetry for hypothetical circular-geometry MSS. A rectangle has two mirror axes, and a circle has an infinite number of mirror axes in the x-y plane.

Note that the circular symmetry transforms into spherical symmetry for CAC due to CAC's utilizing a folded rectangle (**APPENDIX C, Figure C4.1**). The relative simplicity of a planar circular MSS device over a spherical one predefined our choice of circular CFE over spherical CAC for this experimental work.

4.3.2. Ideal device requirements

In an ideal CFE device, the electric field and the hydrodynamic flow should be uniform, *i.e.*, field and flow lines must be straight, parallel, and uniformly spaced inside most of the separation zone. Intuitively, a classic rectangular device with straight and parallel electrodes and a rectangular separation zone between them is best to satisfy the uniformity condition. In contrast, a circular device, having arc-shaped electrodes circularly oriented around a circular

separation zone, *a priori* appeared to be completely incompatible with the uniformity requirement. The major goal of our investigation was to understand if circular-geometry CFE was feasible, *i.e.* a working proof-of-concept device could be created with the same simple-to-use fabrication process that we developed before.[44]

Developing a circular CFE device with both a uniform field and a uniform flow requires a quantitative measure of uniformity. We used an index of uniformity Γ which provides the relative degree of uniformity inside the separation zone of our CFE device with a maximum value of Γ being unity (see **Materials and Methods**).

This study requires evaluating multiple hypotheses *via* testing multiple CFE device designs. We use a milling process to fabricate CFE devices.[44] Making one device takes a day and incurs a non-negligible cost in materials and supplies. Accordingly, this study could become impractically long and/or cost-prohibitive if carried out experimentally only. To keep the project within a reasonable time- and cost scales, we investigated multiple virtual devices within COMSOL Multiphysics software. Modeling in COMSOL allowed us to assess the feasibility of circular CFE and optimize the design of a CFE device before fabricating it. The details of our COMSOL model can be found in **APPENDIX C, Note C4.2**.

4.3.3. Optimizing the flow-field

The hydrodynamic flow and the electric field do not interfere with each other in the first approximation. Hence, we consider their uniformity separately, starting with the flow uniformity. As an initial point, we selected the design with a circular separation zone of uniform thickness, a single source, and a drain for the flow (**Figure 4.3a**). Expectedly, the flow in a virtual design

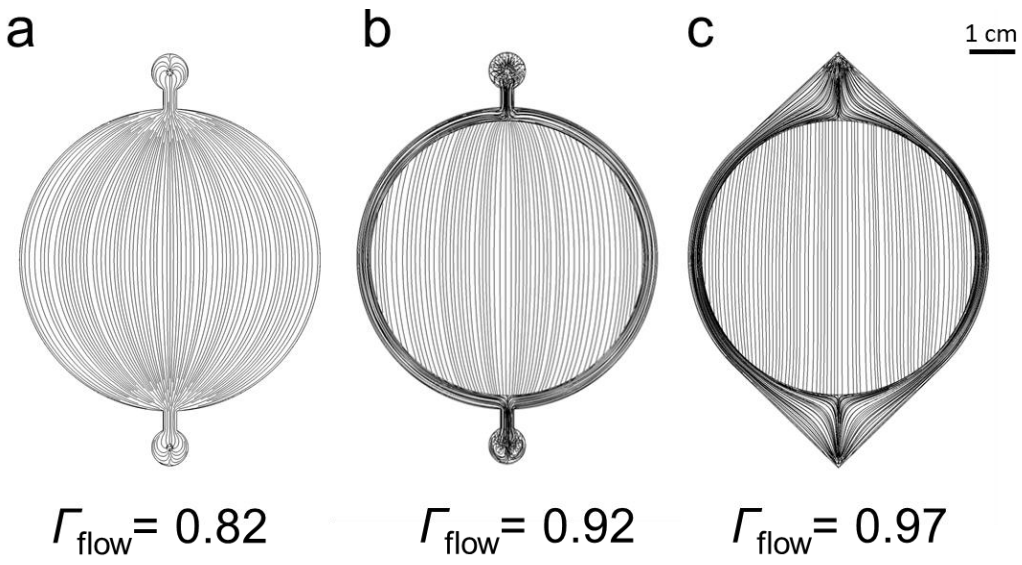

Figure 4.3 COMSOL-simulated hydrodynamic flow lines of the evolving circular FFE design: **a)** a simple circular design with a constant depth of 250 μm, **b)** a device with a 3-mm-deep electrode-containing sacrificial channel around the 60-mm diameter of the separation zone, and **c)** an eye-shaped device with the electrode-containing channel and deepened entrance and exit zones. The values of the corresponding uniformity index Γ_{flow} are shown in the graph.

with such features diverges from the source and converges to the sink. The flow lines are visibly curved, resulting in the uniformity index Γ_{flow} = 0.82.

When developing rectangular CFE devices, we identified and successfully used two device features as a means of flow uniformization: (*i*) deep sacrificial channels around the separation zone, which also serve for placing electrodes, and (*ii*) deep and large entry and exit zones.[14] We decided to explore these two features in a circular CFE device before even looking for any other means of flow uniformization.

As in a rectangular design, adding sacrificial channels to a circular design drastically improved flow uniformity. We gradually increased the depth of the channels to reach flow uniformity of $\Gamma_{flow} > 0.9$ (**Figure 4.3b**). We did not proceed with further depth increase as it started causing an unjustifiable decrease of the flow velocity in the separation zone. Instead, we explored adding the entrance and exit zones to the device with the channels, which proved to further increase flow uniformity. The shape of the zones was varied to achieve the maximum value of $\Gamma_{flow} = 0.97$ with an eye-shaped device (**Figure 4.3c**). Notably, this flow uniformity in a circular device was higher than in the best rectangular device previously assessed ($\Gamma_{flow} = 0.95$) and allowed us not to look for any other means of flow uniformization. While the reason for better flow uniformity in a circular device was not further investigated, we attribute this fact to the absence of flow-disturbing corners in the circular device. Solving the flow uniformity issue allowed us to concentrate on electric field uniformity in the eye-shaped device (**Figure 4.3c**).

4.3.4. Optimizing the electric field

We chose segmented arced electrodes with segments spaced by a short distance from each other and occupying the entire perimeter of the separation zone (**Figure 4.4**). Several segments would be connected to each other to form each of the two electrodes on the opposite sides of the separation zone. A voltage would be applied to these electrodes to create an electric field in the separation zone. We varied (*i*) the total number of segments and (*ii*) the length of electrodes (the number of segments per electrode) in our virtual instrument to assess their influence on field uniformity.

Three total numbers of electrode segments were considered 24, 20, and 16. The total length of the electrodes was kept approximately constant by activating approximately half of the

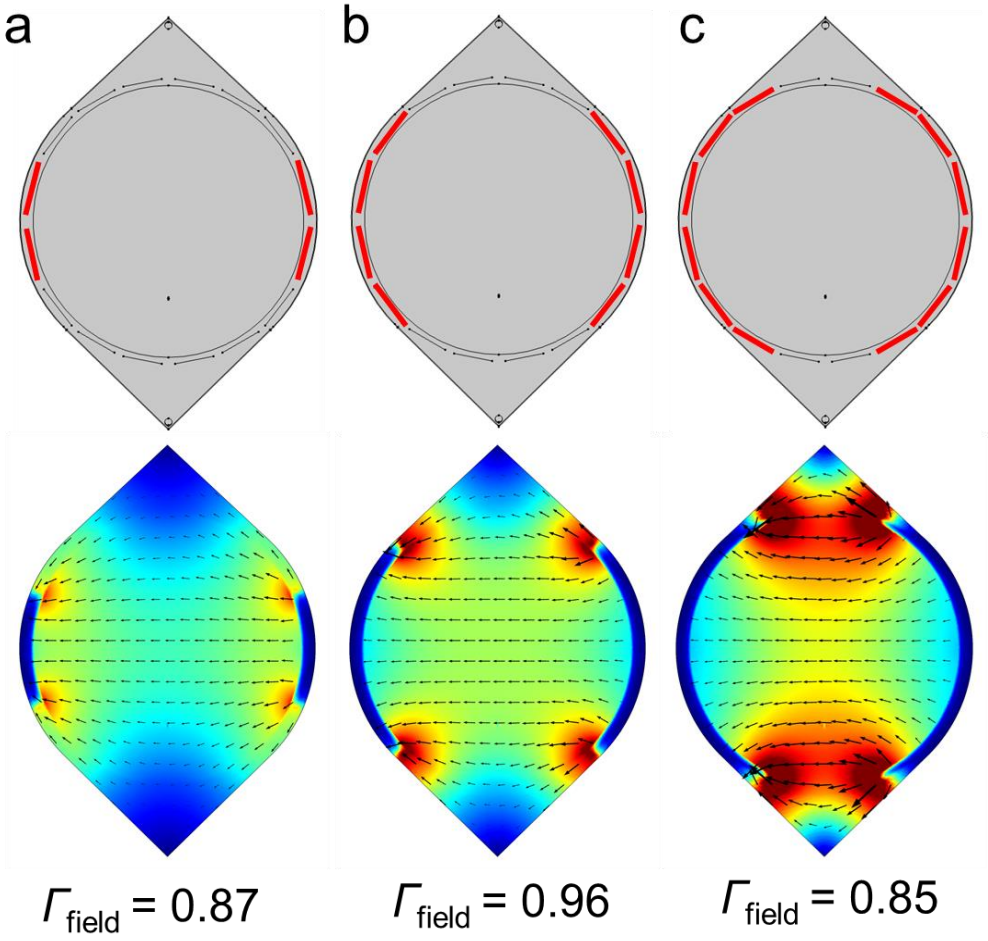

Figure 4.4 The influence of the electrode length on the uniformity of electric field in the eye-shaped CFE device with 16 electrode segments in total with: **a)** two, **b)** four, and **c)** six segments per each electrode. The top panel depicts electrode segmentation; active segments are shown in red. The bottom panel show COMSOL-simulated electric field vectors.

segments. This varying segmentation had a negligible effect on the field uniformity; the index of uniformity was $\Gamma_{\text{field}} \approx 0.96$ for all three cases (**APPENDIX C, Figure C4.2**), allowing us to choose either number of segments. We used a practical consideration to decide between 24, 20, and 16. In theory, a large number of segments provides a high degree of flexibility for setting the direction and magnitude of the electric field. However, in practice, a larger number of segments

creates a greater engineering challenge. Accordingly, we chose 16 segments for our evolving functional circular CFE device.

We then varied the length of electrodes by changing the number of segments per electrode

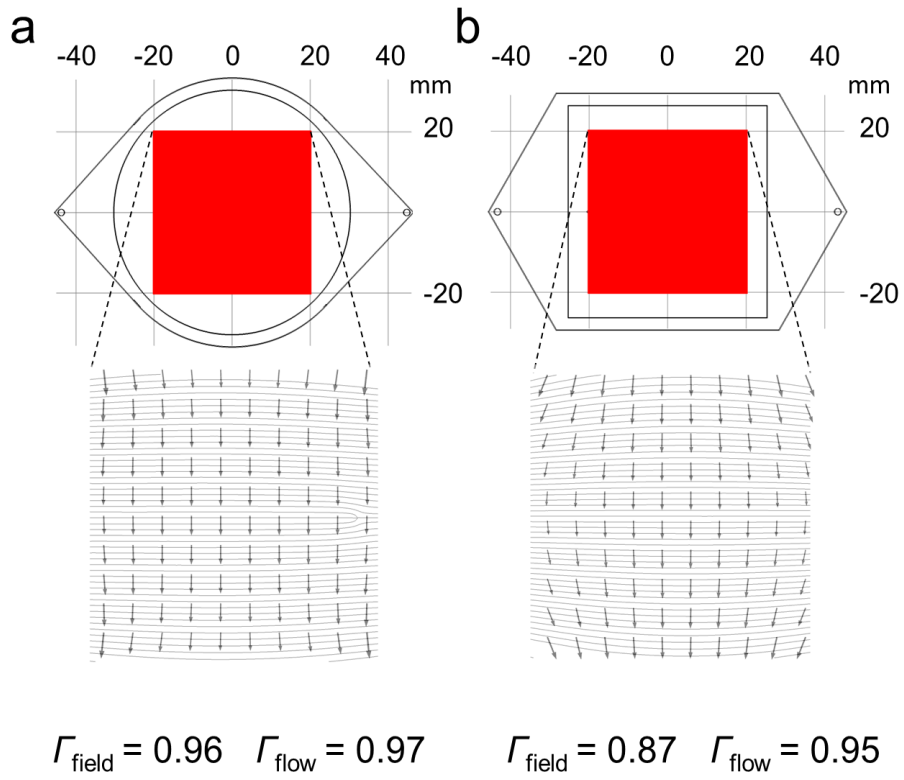

Figure 4.5 Comparison of field-flow uniformity of **a)** circular CFE to that of **b)** rectangular CFE. The top panels show general geometries of the respective devices, and the bottom panels show COMSOL-simulated overlayed flow lines and field vectors in these devices. The red 40 × 40 mm area is where the uniformity index for the circular device in greater than 0.95 for both field and flow. The uniformity indexes within the same square within the rectangular device were lower. The bottom graphs show flow lines and field vectors.

from two to six (**Figure 4.4**). Increasing the electrode length increases the surface area of the electrode, which, in turn, would increase the electric current in a real CFE device. Since high currents are undesirable in electrophoresis (due to Joule heating, bubble generation, etc.), we aimed to find the minimum length needed for field uniformity of $\Gamma_{\text{field}} \geq 0.95$ in the separation zone. We found that four segments per electrode (**Figure 4.4b**) resulted in $\Gamma_{\text{field}} = 0.96$ and, thus, satisfied our criterion. Accordingly, this electrode length was used in our further in-silico and experimental studies.

The above-described COMSOL simulation proved that our circular CFE device could support both a uniform hydrodynamic flow ($\Gamma_{\text{flow}} = 0.97$) and a uniform electric field ($\Gamma_{\text{field}} = 0.96$). It is instructive to compare the overall field-flow uniformity of a circular CFE device to that of a rectangular CFE device (**Figure 4.5**). The shaded areas (16 cm^2) indicate parts of the separation zones in which both the flow and field are uniform with $\Gamma_{\text{field}} > 0.95$. Those parts have similar sizes relative to the total area of separation zones: 57% for the circular device and 64% for the rectangular device. This comparison clearly shows that the overall field-flow uniformity of a CFE device is not compromised when the device's rotational symmetry changes from the 2-nd order to high order.

4.3.5. Optimized device numeric simulations

We then used the circular device optimized for flow and field uniformity to simulate the separation of three analytes: two with negative electrophoretic mobilities and one with zero mobility. The chosen electrode design with 16 segments in total and four segments per electrode allows eight different field-to-flow angles from 0° to 157.5° with a step of 22.5°. Each of them was used to investigate the influence of the angle on CFE separation. The streams for eight

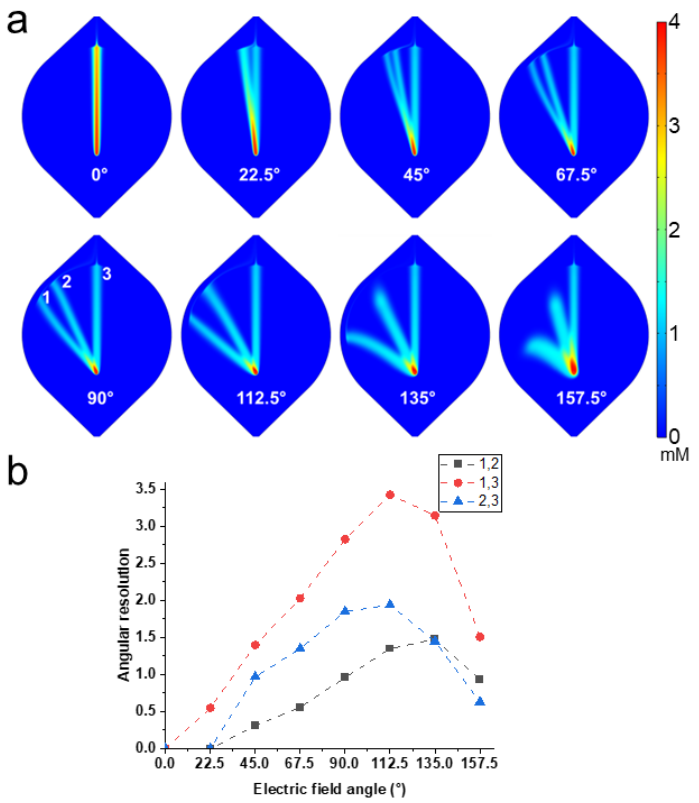

Figure 4.6 The effect of the field-to-flow angle on simulated CFE of three species with electrophoretic mobilities $\mu_1 = -1.01 \times 10^{-8}$, $\mu_2 = -5.66 \times 10^{-9}$, and $\mu_3 = 0$ $m^2/(V*s)$. These mobilities correspond to fluorescein, α-naphtholbenzein, and Sudan Black, respectively, measured in non-aqueous capillary electrophoresis as described in Note S3. Each analyte has a starting concentration of 1.25 mM. **Panel a** show the separated stream at eights different angles, and **panel b** shows the dependence of the angular resolution (calculated from the streams in panel a via intermediate angulagrams) on the field-to-flow angle. The volumetric flow rate and electric field strength were typical for real CFE experiments in a device of this scale: 2 mL/min and 25 V/cm, respectively.

angles are shown in Figure 6a, while the corresponding angulagrams can be found in Figure S3. The angular resolution was calculated from the angulagrams using the previously reported

approach.[5] The resolution was found to depend on the field-to-flow-angle (**Figure 4.6b**). The maximum and minimum resolutions are achieved at angles different from 90°, which agrees with the theory of CFE.[97] The improvement in resolution is obtained only for angles greater than 90°.

Overall, our COMSOL investigation of circular CFE proved its feasibility and provided a pre-optimized design for further fabrication and evaluation of the circular CFE device. No optimization of real CFE devices was necessary. The circular device was fabricated using the same Solid Edge code as the one used for creating device geometry in COMSOL. Using the same code ensured that the physical device was identical to the virtual device within the precision of our fabrication process. The details of the fabrication steps are described in **Materials and Methods 4.2.3. (pictures in APPENDIX C, Note C4.4)** while experimental details on CFE can be found in **Materials and methods 4.2.4.**

4.3.6. Optimized device experimental flow-field uniformity

Flow uniformity in the physical CFE device was tested by flowing fluorescent beads added to the background electrolyte through the device at a zero electric field strength. **Figure 4.7a** demonstrates an image with flow lines derived from a video of fluorescence from the moving beads (**Video S1, DOI: 10.26434/chemrxiv-2022-3w7gt**). The video was used to create a vector field (**Figure 4.7b**) using Fiji/TrackMate,[92–94] which, in turn, was utilized to calculate flow uniformity index $\Gamma_{\text{flow}} \approx 0.91$ (**Materials and methods 4.2.1.**). This value is similar to that predicted in COMSOL, providing cross-validation for COMSOL modeling and experiments in a physical device.

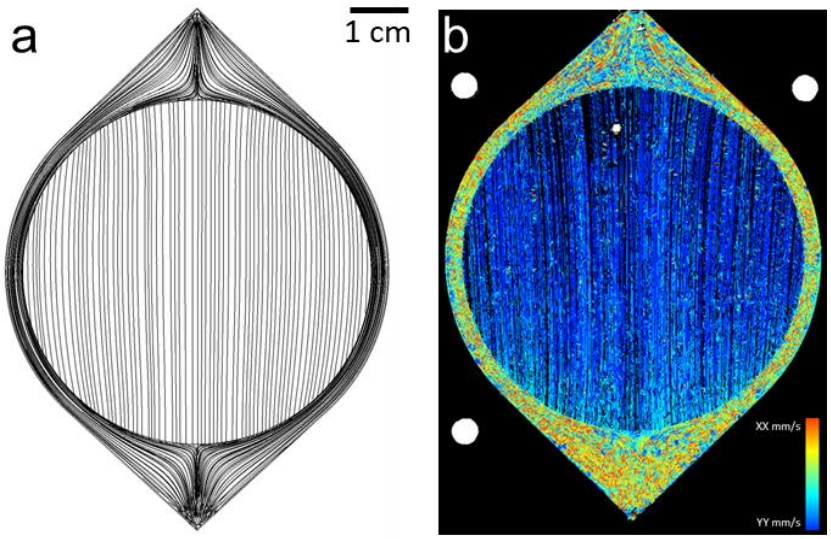

Figure 4.7 Assessment of flow uniformity in circular CFE via flowing fluorescent beads through the device without electric field and with an average flow velocity of 0.09 mm/s in the separation zone. **Panel a** shows the flow field produced by COMSOL software. **Panel b** shows the vector field produced from the video with Fiji/TrackMate and used to calculate uniformity index $\Gamma_{flow} = 0.91$.

4.3.7. Optimized device experimental electric field uniformity

We did not have a direct way of investigating electric field uniformity. Therefore, we assessed it *via* evaluating stream linearity in CFE separation; if the electric field is non-uniform, then streams are non-linear even if the flow is uniform. We ran the separation of four species and found that stream linearity was ≥0.95 for all four streams (**Figure 4.8**). The results of these experiments indirectly proved that the electric field was uniform in a circular CFE device.

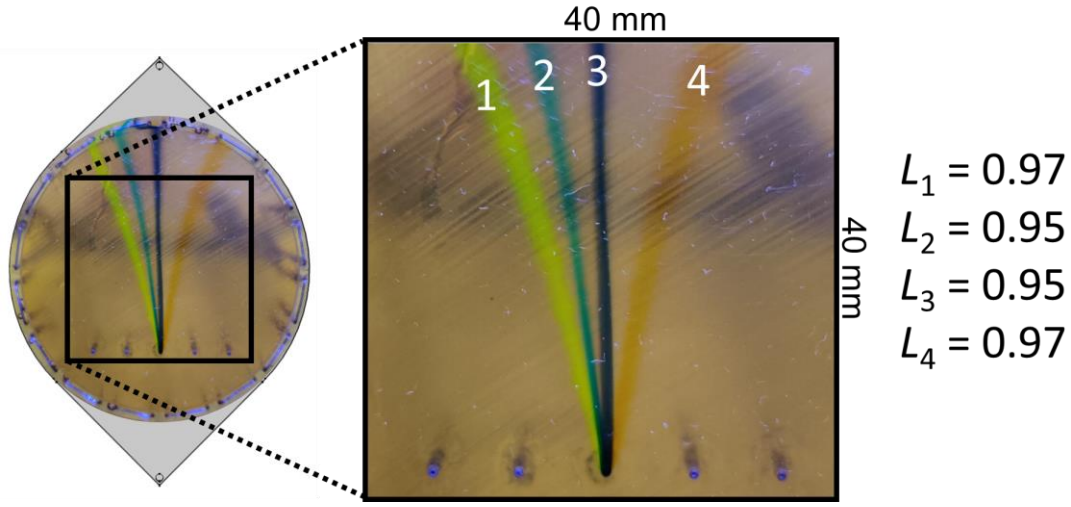

Figure 4.8 Indirect assessment of electric-field uniformity in a circular CFE device via evaluation of stream linearity of fluorescein (stream 1), α-naphtholbenzein (stream 2), Sudan Black B (stream 3) and DMAS (stream 4). The field-to-flow angle was 90°. Experimental details can be found in Note S5. Stream linearities are shown to the right of the image.

4.3.8. Optimized device resolution

Proving that the real circular CFE device supports uniform flow and field allowed us to move to the ultimate goal of this study: an experiment assessing the influence of the field-to-flow orientation on CFE. We used three analytes: negatively charged fluorescein, negatively charged α-naphtholbenzein, and neutral Sudan Black. Note that their mobilities were utilized in simulated CFE shown in Figure 4, and 112.5° was an angle for the best resolution of both fluorescein and α-naphtholbenzein from Sudan Black. Accordingly, in our CFE experiments, separation quality was compared at two field-to-flow angles, *i.e.*, 90° and 112.5° (**Figure 4.9**). The dependence of stream deflection on the angle was in a manner predicted in both COMSOL modeling and in the

theory of CFE. Stream resolution was significantly higher for 112.5° than for 90°. These experiments provided the final proof of concept for circular CFE.

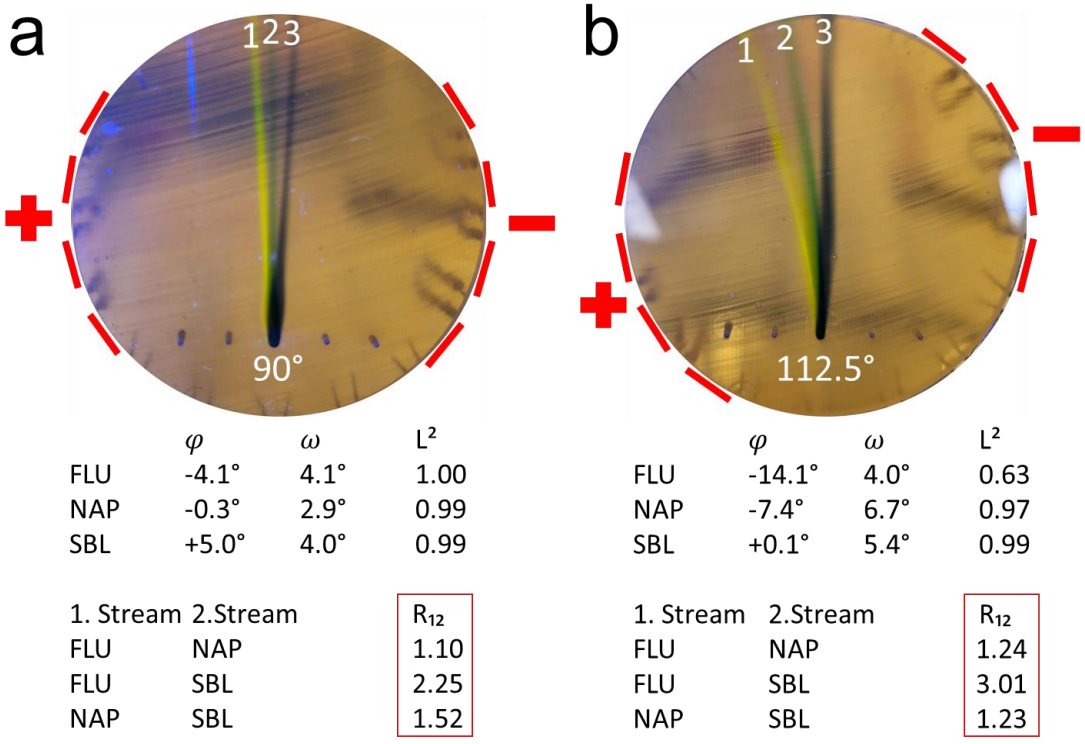

	φ	ω	L^2
FLU	-4.1°	4.1°	1.00
NAP	-0.3°	2.9°	0.99
SBL	+5.0°	4.0°	0.99

1. Stream	2.Stream	R_{12}
FLU	NAP	1.10
FLU	SBL	2.25
NAP	SBL	1.52

	φ	ω	L^2
FLU	-14.1°	4.0°	0.63
NAP	-7.4°	6.7°	0.97
SBL	+0.1°	5.4°	0.99

1. Stream	2.Stream	R_{12}
FLU	NAP	1.24
FLU	SBL	3.01
NAP	SBL	1.23

Figure 4.9 Comparison of CFE of fluorescein (FLU, stream 1), α- naphtholbenzein (NAP, stream 2), and Sudan Black (SBL, stream 3) with 90°(**a**) and 112.5° (**b**) field-to-flow angle at an electric field of 25 V/cm and a flow rate of 4 mL/min.

While the results of experiments correspond qualitatively to those of in-silica study, there is a significant quantitative disagreement. The two major potential reasons for this disagreement are: (*i*) experimental imperfections (*e.g.*, inaccurately measured values of electrophoretic mobilities of the two charged species) and (*ii*) secondary phenomena which were present in the experiment but not included in COMSOL simulation. The second reason is more interesting as it

can potentially reveal a phenomenon that has been previously disregarded by CFE practitioners. A known secondary phenomenon is the electroosmotic flow (EOF), which is very common in aqueous electrophoresis,[38,98] and can also be beneficial.[99,100] However, here we used non-aqueous CFE in which EOF is negligible, which was confirmed by no deflection of the stream of the electrically-neutral analyte. Therefore, we looked for another reason.

While using the field-to-flow angles different from 90°, we noticed a decrease in the flow velocity in the separation zone, which could be seen by following stream evolution for the neutral molecule. We hypothesized that this flow slowing was caused by ion concentration polarization. The phenomenon of ion concentration polarization is well known in the area of ion transport but has never been mentioned in the context of CFE; the reader is referred to multiple other publications for details.[101–104] This phenomenon is caused by the ion concentration gradient and is accompanied by recirculation of the flow near the electrodes. To check if the recirculation was detectable, we followed the flow pattern near the electrodes with fluorescent beads added to the background electrolyte. We found profound flow recirculation (**Video S2, DOI: 10.26434/chemrxiv-2022-3w7gt**), which confirms that ion concentration polarization is always present in CFE, but does not have the same magnitude when electrodes aren't segmented or in hydrodynamic flows with high Peclet numbers. This phenomenon can also explain the curving of the streams at angles other than 90°. While it would be interesting to include it in our simulation of CFE to see if this could improve quantitative agreement with the experiment, COMSOL does not have suitable capabilities. We did not find in our experimental results any signs of other phenomena that could contribute to the quantitative disagreement.

4.4. CONCLUSIONS

In summary, we proposed the concept and proved the feasibility of high-order symmetry in MSS. It was implemented in a working proof-of-concept CFE device with a circular separation zone and arc-shaped electrodes positioned in a deep channel surrounding the separation zone. This circular CFE can support flow and electric-field uniformity on par with or higher than those of canonic rectangular CFE. Both simulations and experiments confirmed the theoretical prediction that the best stream resolution is achieved at a field-to-flow angle different from 90°. Some quantitative disagreements between the results of simulation and experiments prompted us to look for secondary phenomena unaccounted for in the simulation. We identified one such phenomenon: ion concentration polarization. This phenomenon does not clearly manifest itself unless the field-to-flow angle is varied or the flow pattern near the electrodes is analyzed in detail. Accordingly, it's the first time when ion concentration polarization is reported in the context of CFE. We foresee that circular CFE will serve as a testbed for the investigation and creation of new CFE modalities. It is instructive to mention that the idea of circular CFE was conceived by recent advances in presenting CFE in polar rather than a Cartesian system of coordinates.

To conclude, we would like to emphasize that the fabrication process of circular and rectangular devices is the same; the circular CFE device in this work was created using our previously developed manufacturing process, avoiding adding extra complexity and maintaining feasibility (**APPENDIX C, Note C4.5**). In contrast to rectangular CFE, circular CFE provides three important advantages: 1) it is better aligned with the polar nature of CFE, 2) it provides better field and flow homogeneity, and 3) it can provide improved resolution when utilized with non-orthogonal field-to-flow orientation (the gain in resolution is theoretically limited to several

folds at most for all typical analytes). We see no advantages of rectangular CFE and recommend the use of a circular one by default.

LIMITATIONS

This chapter will sequentially address the set of intrinsic limitations present in every published article. Although electrophoresis is a popular separation method for biological macromolecules, it has a long way to go before it can be considered a weighty complement to liquid chromatography.

Chapter 2 limitations

Chapter 2 introduces the non-aqueous continuous-flow electrophoresis (NACFE) method as a potential complement to organic synthesis. Intuitively, two-dimensional separation methods are more engineeringly involved than classical techniques. They require a lengthy fabrication of complex geometries, making numeric simulations unavoidable. In turn, the finite element numeric simulations take significantly longer to solve than in the case of one-dimensional systems. Implementing a 2D separation platform is a prolonged endeavor that must be carefully weighted and planned. Only a limited set of systems requires truly continuous separation methods. Depending on the requirements imposed by the project, it might be advantageous to carefully search for a compromise between project demands and engineering investments.

Like other electrophoretic separation methods, NACFE requires a dissolved background electrolyte (BGE) to maintain the electric field in the solution. However, unlike water-based BGEs, typical aqueous electrolytes such as HEPES or TRIS aren’t compatible with organics solvents. This problem is addressed by employing a selection of molten salts or ionic liquids as charge carriers. These chemicals are significantly more expensive than aqueous electrolytes, raising the cost of separation.

In addition to those mentioned above, another critical imitation of electrophoretic separations is the need for the final liquid-liquid extraction workup to remove BGE from the analyte of interest. Depending on the analyte's physical properties, such extractions might be challenging and require multiple steps. This is potentially the primary disadvantage of electrophoretic methods over liquid chromatography, where the analyte is collected in a pure solvent that can be quickly boiled away.

Chapter 3 limitations

Chapter 3 introduces a new method for molecular steam visualization that doesn’t require expensive optical setups or optically transparent devices. However, based on the underlying physics, it can only detect molecules that absorb significantly at the excitation wavelength. At 254-nanometer wavelength, it limits the scope of detectable analytes to the family of aromatic or π-orbital rich compounds.

In addition, prolonged exposure to UV light can degrade the separated analytes by causing radical formation in some classes of chemicals. This problem can be addressed by reducing the UV excitation light exposure time with PWM modulation. The light source should only turn on while image acquisition is happening.

Chapter 4 limitations

Chapter 4 introduces the approach of improving the analyte resolution by rotating the electric field to an angle different than 90 degrees. This improvement, however, only works with analytes that possess the same charge and happens at the expense of the oppositely charged analytes. In other words, by increasing the resolution of the negative analytes, we decrease the resolution of the positive analyte and vice versa.

Although small resolution improvements can be obtained with minor angle modifications, this method only achieves its true potential at extreme angle values that approach 180 degrees. In such cases, an improvement on a scale of a few orders of magnitude is possible. Unfortunately, such improvement values require a very high electric field angle precision. Minor errors in electric field angle quickly collapse any gain in resolution.

Additionally, flexible electric field angle devices require a significantly higher amount of electrodes to cover the circumference of the circular device. Considering that the most frequent electrode material is platinum, this electrode length gain can dramatically increase the average cost of the fabricated device. Fortunately, platinum wires don’t degrade and are easily recovered from retired electrophoresis devices.

CONCLUDING REMARKS

Continuous-flow electrophoresis is an exciting alternative for small molecule separations. Over the past five years, our team has methodically worked to address the collective body of CFE limitations. Our initial efforts were focused on solving the fundamental compatibility issues between the continuous aqueous electrophoresis method and organic synthesis. Initial works have addressed the problem of poor solubility by replacing water with an organic solvent. Due to the low solubility of classic electrolytes in organic solvents, we searched for alternative charge carriers. We found them in tetrabutylammonium salts. The classic gassing problem caused by water electrolysis was simultaneously addressed by removing water from the systems. The new device materials were identified as a suitable replacement for PMMA to combat the destructive behavior of organic solvents. Our follow-up works have focused on molecular stream detection since most relevant compounds don't absorb in the visible spectrum. We have found an elegant solution that doesn't require expensive cameras or CFE devices made entirely from fused silica. Our latest efforts were concentrated on improving the resolution of NACFE by creating a functional non-orthogonal electric field device. We accomplished this by constructing the first circular CFE device capable of generating a homogenous electric field at various angles to the hydrodynamic flow. Our work has shown that such devices can possess flow and electric field homogeneity factors that rival rectangular CFE instruments.

FUTURE PLANS

Our recent works have addressed the primary issues of solubility, stream visualization, and resolution in continuous-flow electrophoresis. The published articles have pawed the way to the final goal of building a comprehensive separation complement to a continuous flow reactor. However, as previously mentioned in the Limitations chapter, many obstacles remain.

Searching for compatible chemical reactions

Not all synthesis reactions can be separated by continuous-flow electrophoresis. Depending on their functional groups, certain classes of compounds don't have any electrophoretic mobility. The major next step is the identification of compatible chemical reactions for which NACFE can serve as a good separation platform.

We will begin by running a small library of chemical compounds in a capillary electrophoresis device. This preliminary screening step would allow us to identify the functional groups that confer electrophoretic mobility to a molecule of interest. Based on this information, we can select several chemical reactions that should theoretically be resolvable in a NACFE system. During the next step, we will sequentially run all components of the chosen reaction and crude reaction mixture in a capillary electrophoresis device to experimentally prove that this separation is feasible. The final step will have us continuously injecting the crude mixture into the NACFE device while monitoring the separation.

New electrolytes for expanding the list of heteroconjugated molecules

As discussed in Chapter 2, the physics behind NACFE separations revolves around forming a non-covalent bond between components of the background electrolyte and the separated analytes. This bonding behavior is called heteroconjugation, and it is heavily dependent upon the nature of the selected BGE. By changing the BGE components in NACFE, we can fine-tune our separation device's selectivity, as shown in **APPENDIX A, Figure A2.4**. High-basicity anions are capable of heteroconjugating to a wider range of analytes. To date, the most basic anion we've tried is acetate; it can conjugate alcohols (pKa ~ 16). However, it cannot conjugate functional groups with higher pKa values, such as aldehydes or amides. It would be of great interest to explore the possibility of high basicity electrolytes such as lithium tert-butoxide. By expanding the selection of applicable BGEs, we make NACFE a more versatile separation platform.

Palladium electrodes for reduced gassing

Although most chemical reactions are conducted in organic solvents, the recent "green" trend in chemical synthesis is to use water as the solvent whenever possible. As previously mentioned, water undergoes active hydrolysis at high voltages. When DC is applied to the electrolyte solution, hydrogen gas is produced near the cathode and oxygen gas near the anode. Over time, gas bubbles interfere with the chip's laminar flow and ruin the separation. One interesting way of reducing the formation of bubbles is to use palladium. Palladium can actively adsorb hydrogen molecules into its lattice, making palladium hydride. By continuously running an oxidizer solution through palladium tube electrodes, it should theoretically be possible to create a regenerating non-gassing electrode.

LIST OF PUBLICATIONS

Ivanov, N. A., Liu, Y., Kochmann, S., & Krylov, S. N. (2019). Non-aqueous continuous-flow electrophoresis (NACFE): potential separation complement for continuous-flow organic synthesis. *Lab on a Chip*, *19*(13), 2156-2160.

Ivanov, N. A., Kochmann, S., & Krylov, S. N. (2020). Visualization of streams of small organic molecules in continuous-flow electrophoresis. *Analytical chemistry*, *92*(4), 2907-2910.

Kochmann, S., Ivanov, N. A., Le Blanc, J. Y., Gorin, B. I., & Krylov, S. N. (2022). Circular Geometry in Molecular Stream Separation to Facilitate Non-Orthogonal Field-to-Flow Orientation. *Analytical chemistry*, 2022, 94, 27, 9519–9524.

REFERENCES

(1) Akwi, F. M.; Watts, P. Continuous Flow Chemistry: Where Are We Now? Recent Applications, Challenges and Limitations. *Chem. Commun.* **2018**, *54* (99), 13894–13928. https://doi.org/10.1039/C8CC07427E.

(2) Bloemendal, V. R. L. J.; Janssen, M. A. C. H.; van Hest, J. C. M.; Rutjes, F. P. J. T. Continuous One-Flow Multi-Step Synthesis of Active Pharmaceutical Ingredients. *React. Chem. Eng.* **2020**, *5* (7), 1186–1197. https://doi.org/10.1039/D0RE00087F.

(3) Britton, J.; Raston, C. L. Multi-Step Continuous-Flow Synthesis. *Chem. Soc. Rev.* **2017**, *46* (5), 1250–1271. https://doi.org/10.1039/C6CS00830E.

(4) Espro, C.; Rodríguez-Padrón, D. Re-Thinking Organic Synthesis: Mechanochemistry as a Greener Approach. *Current Opinion in Green and Sustainable Chemistry* **2021**, *30*, 100478. https://doi.org/10.1016/j.cogsc.2021.100478.

(5) Kochmann, S.; Krylov, S. N. Quantitative Characterization of Molecular-Stream Separation. *Anal. Chem.* **2018**, *90* (15), 9504–9509. https://doi.org/10.1021/acs.analchem.8b02186.

(6) Seidel-Morgenstern, A.; Keßler, L. C.; Kaspereit, M. New Developments in Simulated Moving Bed Chromatography. *Chem. Eng. Technol.* **2008**, *31* (6), 826–837. https://doi.org/10.1002/ceat.200800081.

(7) Sá Gomes, P.; Rodrigues, A. E. Simulated Moving Bed Chromatography: From Concept to Proof-of-Concept. *Chem. Eng. Technol.* **2012**, *35* (1), 17–34. https://doi.org/10.1002/ceat.201100281.

(8) Lee, J. W. Expanding Simulated Moving Bed Chromatography into Ternary Separations in Analogy to Dividing Wall Column Distillation. *Ind. Eng. Chem. Res.* **2020**, *59* (20), 9619–9628. https://doi.org/10.1021/acs.iecr.0c00572.

(9) Kralj, J. G.; Sahoo, H. R.; Jensen, K. F. Integrated Continuous Microfluidic Liquid–Liquid Extraction. *Lab Chip* **2007**, *7* (2), 256–263. https://doi.org/10.1039/B610888A.

(10) Liu, Y.; Chen, G.; Yue, J. Manipulation of Gas-Liquid-Liquid Systems in Continuous Flow Microreactors for Efficient Reaction Processes. *J Flow Chem* **2020**, *10* (1), 103–121. https://doi.org/10.1007/s41981-019-00062-9.

(11) Gjelstad, A.; Rasmussen, K. E.; Parmer, M. P.; Pedersen-Bjergaard, S. Parallel Artificial Liquid Membrane Extraction: Micro-Scale Liquid–Liquid–Liquid Extraction in the 96-Well Format. *Bioanalysis* **2013**, *5* (11), 1377–1385. https://doi.org/10.4155/bio.13.59.

(12) Breil, C.; Abert Vian, M.; Zemb, T.; Kunz, W.; Chemat, F. "Bligh and Dyer" and Folch Methods for Solid–Liquid–Liquid Extraction of Lipids from Microorganisms. Comprehension of Solvatation Mechanisms and towards Substitution with Alternative Solvents. *IJMS* **2017**, *18* (4), 708. https://doi.org/10.3390/ijms18040708.

(13) Zhou, L.; Wu, K.; Qin, W.; Wang, G.; Fu, D.; Fei, W. Separation Characteristics of Boron Isotopes in Continuous Annular Chromatography. *Sci. China Chem.* **2015**, *58* (7), 1187–1192. https://doi.org/10.1007/s11426-014-5312-7.

(14) Agostino, F. J.; Cherney, L. T.; Galievsky, V.; Krylov, S. N. Steady-State Continuous-Flow Purification by Electrophoresis. *Angew. Chem. Int. Ed.* **2013**, *52* (28), 7256–7260. https://doi.org/10.1002/anie.201300104.

(15) Agostino, F. J.; Krylov, S. N. Advances in Steady-State Continuous-Flow Purification by Small-Scale Free-Flow Electrophoresis. *TrAC Trends in Analytical Chemistry* **2015**, *72*, 68–79. https://doi.org/10.1016/j.trac.2015.03.023.

(16) Kochmann, S.; Agostino, F. J.; LeBlanc, J. C. Y.; Krylov, S. N. Hyphenation of Production-Scale Free-Flow Electrophoresis to Electrospray Ionization Mass Spectrometry Using a Highly Conductive Background Electrolyte. *Anal. Chem.* **2016**, *88* (17), 8415–8420. https://doi.org/10.1021/acs.analchem.6b02235.

(17) Barbaresco, F.; Cocuzza, M.; Pirri, C. F.; Marasso, S. L. Application of a Micro Free-Flow Electrophoresis 3D Printed Lab-on-a-Chip for Micro-Nanoparticles Analysis. *Nanomaterials* **2020**, *10* (7), 1277. https://doi.org/10.3390/nano10071277.

(18) Jender, M.; Novo, P.; Maehler, D.; Münchberg, U.; Janasek, D.; Freier, E. Multiplexed Online Monitoring of Microfluidic Free-Flow Electrophoresis via Mass Spectrometry. *Anal. Chem.* **2020**, *92* (9), 6764–6769. https://doi.org/10.1021/acs.analchem.0c00996.

(19) Mazereeuw, M.; de Best, C. M.; Tjaden, U. R.; Irth, H.; van der Greef, J. Free Flow Electrophoresis Device for Continuous On-Line Separation in Analytical Systems. An Application in Biochemical Detection. *Anal. Chem.* **2000**, *72* (16), 3881–3886. https://doi.org/10.1021/ac991202k.

(20) Jezierski, S.; Belder, D.; Nagl, S. Microfluidic Free-Flow Electrophoresis Chips with an Integrated Fluorescent Sensor Layer for Real Time PH Imaging in Isoelectric Focusing. *Chem. Commun.* **2013**, *49* (9), 904–906. https://doi.org/10.1039/C2CC38093E.

(21) Köhler, S.; Nagl, S.; Fritzsche, S.; Belder, D. Label-Free Real-Time Imaging in Microchip Free-Flow Electrophoresis Applying High Speed Deep UV Fluorescence Scanning. *Lab Chip* **2012**, *12* (3), 458–463. https://doi.org/10.1039/C1LC20558G.

(22) Liu, S.; Madren, S.; Feng, P.; Sosic, Z. Characterization of the Acidic Species of a Monoclonal Antibody Using Free Flow Electrophoresis Fractionation and Mass Spectrometry. *Journal of Pharmaceutical and Biomedical Analysis* **2020**, *185*, 113217. https://doi.org/10.1016/j.jpba.2020.113217.

(23) Ouvry-Patat, S. A.; Torres, M. P.; Quek, H.-H.; Gelfand, C. A.; O'Mullan, P.; Nissum, M.; Schroeder, G. K.; Han, J.; Elliott, M.; Dryhurst, D.; Ausio, J.; Wolfenden, R.; Borchers, C. H. Free-Flow Electrophoresis for Top-down Proteomics by Fourier Transform Ion Cyclotron Resonance Mass Spectrometry. *Proteomics* **2008**, *8* (14), 2798–2808. https://doi.org/10.1002/pmic.200800079.

(24) Malmström, J.; Lee, H.; Nesvizhskii, A. I.; Shteynberg, D.; Mohanty, S.; Brunner, E.; Ye, M.; Weber, G.; Eckerskorn, C.; Aebersold, R. Optimized Peptide Separation and Identification for Mass Spectrometry Based Proteomics via Free-Flow Electrophoresis. *J. Proteome Res.* **2006**, *5* (9), 2241–2249. https://doi.org/10.1021/pr0600632.

(25) Moritz, R. L.; Clippingdale, A. B.; Kapp, E. A.; Eddes, J. S.; Ji, H.; Gilbert, S.; Connolly, L. M.; Simpson, R. J. Application of 2-D Free-Flow Electrophoresis/RP-HPLC for Proteomic Analysis of Human Plasma Depleted of Multi High-Abundance Proteins. *Proteomics* **2005**, *5* (13), 3402–3413. https://doi.org/10.1002/pmic.200500096.

(26) Jaffé, W. G.; Hannig, K. Fractionation of Proteins from Kidney Beans (Phaseolus Vulgaris). *Archives of Biochemistry and Biophysics* **1965**, *109* (1), 80–91. https://doi.org/10.1016/0003-9861(65)90290-0.

(27) Islinger, M.; Eckerskorn, C.; Völkl, A. Free-Flow Electrophoresis in the Proteomic Era: A Technique in Flux: Proteomics and 2-DE. *ELECTROPHORESIS* **2010**, *31* (11), 1754–1763. https://doi.org/10.1002/elps.200900771.

(28) Wildgruber, R.; Weber, G.; Wise, P.; Grimm, D.; Bauer, J. Free-Flow Electrophoresis in Proteome Sample Preparation: Proteomics 2013. *Proteomics* **2014**, *14* (4–5), 629–636. https://doi.org/10.1002/pmic.201300253.

(29) Novo, P.; Jender, M.; Dell'Aica, M.; Zahedi, R. P.; Janasek, D. Free Flow Electrophoresis Separation of Proteins and DNA Using Microfluidics and Polycarbonate Membranes. *Procedia Engineering* **2016**, *168*, 1382–1385. https://doi.org/10.1016/j.proeng.2016.11.385.

(30) Walowski, B.; Hüttner, W.; Wackerbarth, H. Generation of a Miniaturized Free-Flow Electrophoresis Chip Based on a Multi-Lamination Technique—Isoelectric Focusing of Proteins and a Single-Stranded DNA Fragment. *Anal Bioanal Chem* **2011**, *401* (8), 2465–2471. https://doi.org/10.1007/s00216-011-5353-0.

(31) Jing, M.; Bowser, M. T. Isolation of DNA Aptamers Using Micro Free Flow Electrophoresis. *Lab Chip* **2011**, *11* (21), 3703. https://doi.org/10.1039/c1lc20461k.

(32) Henning, R.; Geidrich, H.-G. Membrane Lipids of Rat Liver Lysosomes Prepared by Freeflow Electrophoresis. *Biochimica et Biophysica Acta (BBA) - Biomembranes* **1974**, *345* (3), 326–335. https://doi.org/10.1016/0005-2736(74)90195-3.

(33) Kessler, R.; Manz, H.-J. Characterization of Artifical Liposomes with Free-Flow Electrophoresis. *Electrophoresis* **1990**, *11* (11), 979–980. https://doi.org/10.1002/elps.1150111119.

(34) Peterson, R. R.; Cliffel, D. E. Continuous Free-Flow Electrophoresis of Water-Soluble Monolayer-Protected Clusters. *Anal. Chem.* **2005**, *77* (14), 4348–4353. https://doi.org/10.1021/ac0502495.

(35) Ho, S.; Critchley, K.; Lilly, G. D.; Shim, B.; Kotov, N. A. Free Flow Electrophoresis for the Separation of CdTe Nanoparticles. *J. Mater. Chem.* **2009**, *19* (10), 1390. https://doi.org/10.1039/b820703h.

(36) Rudisch, B. M.; Pfeiffer, S. A.; Geissler, D.; Speckmeier, E.; Robitzki, A. A.; Zeitler, K.; Belder, D. Nonaqueous Micro Free-Flow Electrophoresis for Continuous Separation of Reaction Mixtures in Organic Media. *Anal. Chem.* **2019**, *91* (10), 6689–6694. https://doi.org/10.1021/acs.analchem.9b00714.

(37) Frost, N. W.; Bowser, M. T. Using Buffer Additives to Improve Analyte Stream Stability in Micro Free Flow Electrophoresis. *Lab Chip* **2010**, *10* (10), 1231. https://doi.org/10.1039/b922325h.

(38) Fonslow, B. R.; Bowser, M. T. Optimizing Band Width and Resolution in Micro-Free Flow Electrophoresis. *Anal. Chem.* **2006**, *78* (24), 8236–8244. https://doi.org/10.1021/ac0609778.

(39) Fonslow, B. R.; Bowser, M. T. Free-Flow Electrophoresis on an Anodic Bonded Glass Microchip. *Anal. Chem.* **2005**, *77* (17), 5706–5710. https://doi.org/10.1021/ac050766n.

(40) Fonslow, B. R.; Barocas, V. H.; Bowser, M. T. Using Channel Depth To Isolate and Control Flow in a Micro Free-Flow Electrophoresis Device. *Anal. Chem.* **2006**, *78* (15), 5369–5374. https://doi.org/10.1021/ac060290n.

(41) Zhang, C.-X.; Manz, A. High-Speed Free-Flow Electrophoresis on Chip. *Anal. Chem.* **2003**, *75* (21), 5759–5766. https://doi.org/10.1021/ac0345190.

(42) Arter, W. E.; Saar, K. L.; Herling, T. W.; Knowles, T. P. J. Microchip Free-Flow Electrophoresis for Bioanalysis, Sensing, and Purification. In *Biomedical Engineering Technologies*; Rasooly, A., Baker, H., Ossandon, M. R., Eds.; Methods in Molecular Biology; Springer US: New York, NY, 2022; Vol. 2394, pp 249–266. https://doi.org/10.1007/978-1-0716-1811-0_16.

(43) Saar, K. L.; Müller, T.; Charmet, J.; Challa, P. K.; Knowles, T. P. J. Enhancing the Resolution of Micro Free Flow Electrophoresis through Spatially Controlled Sample Injection. *Anal. Chem.* **2018**, *90* (15), 8998–9005. https://doi.org/10.1021/acs.analchem.8b01205.

(44) Agostino, F. J.; Evenhuis, C. J.; Krylov, S. N. Milli-Free Flow Electrophoresis: I. Fast Prototyping of MFFE Devices: Electrodriven Separations. *J. Sep. Science* **2011**, *34* (5), 556–564. https://doi.org/10.1002/jssc.201000758.

(45) Anciaux, S. K.; Bowser, M. T. Reduced Surface Adsorption in 3D Printed Acrylonitrile Butadiene Styrene Micro Free-flow Electrophoresis Devices. *ELECTROPHORESIS* **2020**, *41* (3–4), 225–234. https://doi.org/10.1002/elps.201900179.

(46) Preuss, J.; Nguyen, G. N.; Berk, V.; Bahnemann, J. Miniaturized Free-flow Electrophoresis: Production, Optimization, and Application Using 3D Printing

Technology. *ELECTROPHORESIS* **2021**, *42* (3), 305–314. https://doi.org/10.1002/elps.202000149.

(47) Anciaux, S. K.; Geiger, M.; Bowser, M. T. 3D Printed Micro Free-Flow Electrophoresis Device. *Anal. Chem.* **2016**, *88* (15), 7675–7682. https://doi.org/10.1021/acs.analchem.6b01573.

(48) Zhang, D.; Liu, X.; Qiu, J. 3D Printing of Glass by Additive Manufacturing Techniques: A Review. *Front. Optoelectron.* **2021**, *14* (3), 263–277. https://doi.org/10.1007/s12200-020-1009-z.

(49) Kuhn, R.; Hoffstetter-Kuhn, S.; Wagner, H. Free-Flow Electrophoresis for the Purification of Proteins: II. Isoelectric Focusing and Field Step Electrophoresis. *Electrophoresis* **1990**, *11* (11), 942–947. https://doi.org/10.1002/elps.1150111111.

(50) Hoffstetter-Kuhn, S.; Kuhn, R.; Wagner, H. Free Flow Electrophoresis for the Purification of Proteins: I. Zone Electrophoresis and Isotachophoresis. *Electrophoresis* **1990**, *11* (4), 304–309. https://doi.org/10.1002/elps.1150110406.

(51) Miller, J. L.; Shea, D.; Khaledi, M. G. Separation of Acidic Solutes by Nonaqueous Capillary Electrophoresis in Acetonitrile-Based Media. *Journal of Chromatography A* **2000**, *888* (1–2), 251–266. https://doi.org/10.1016/S0021-9673(00)00467-2.

(52) Terabe, S. Capillary Separation: Micellar Electrokinetic Chromatography. *Annual Rev. Anal. Chem.* **2009**, *2* (1), 99–120. https://doi.org/10.1146/annurev.anchem.1.031207.113005.

(53) Kohlheyer, D.; Besselink, G. A. J.; Schlautmann, S.; Schasfoort, R. B. M. Free-Flow Zone Electrophoresis and Isoelectric Focusing Using a Microfabricated Glass Device with Ion Permeable Membranes. *Lab Chip* **2006**, *6* (3), 374. https://doi.org/10.1039/b514731j.

(54) Fleming, G. S.; Beeler, A. B. Integrated Drug Discovery in Continuous Flow. *Journal of Flow Chemistry* **2017**, *7* (3–4), 124–128. https://doi.org/10.1556/1846.2017.00027.

(55) Yoshida, J.; Takahashi, Y.; Nagaki, A. Flash Chemistry: Flow Chemistry That Cannot Be Done in Batch. *Chem. Commun.* **2013**, *49* (85), 9896–9904. https://doi.org/10.1039/C3CC44709J.

(56) Gutmann, B.; Cantillo, D.; Kappe, C. O. Continuous-Flow Technology-A Tool for the Safe Manufacturing of Active Pharmaceutical Ingredients. *Angew. Chem. Int. Ed.* **2015**, *54* (23), 6688–6728. https://doi.org/10.1002/anie.201409318.

(57) Zhang, J.; Wang, K.; Teixeira, A. R.; Jensen, K. F.; Luo, G. Design and Scaling Up of Microchemical Systems: A Review. *Annu. Rev. Chem. Biomol. Eng.* **2017**, *8* (1), 285–305. https://doi.org/10.1146/annurev-chembioeng-060816-101443.

(58) Plutschack, M. B.; Pieber, B.; Gilmore, K.; Seeberger, P. H. The Hitchhiker's Guide to Flow Chemistry. *Chem. Rev.* **2017**, *117* (18), 11796–11893. https://doi.org/10.1021/acs.chemrev.7b00183.

(59) Castro, E. R.; Manz, A. Present State of Microchip Electrophoresis: State of the Art and Routine Applications. *Journal of Chromatography A* **2015**, *1382*, 66–85. https://doi.org/10.1016/j.chroma.2014.11.034.

(60) Novo, P.; Janasek, D. Current Advances and Challenges in Microfluidic Free-Flow Electrophoresis—A Critical Review. *Analytica Chimica Acta* **2017**, *991*, 9–29. https://doi.org/10.1016/j.aca.2017.08.017.

(61) Suryawanshi, P. L.; Gumfekar, S. P.; Bhanvase, B. A.; Sonawane, S. H.; Pimplapure, M. S. A Review on Microreactors: Reactor Fabrication, Design, and Cutting-Edge Applications. *Chemical Engineering Science* **2018**, *189*, 431–448. https://doi.org/10.1016/j.ces.2018.03.026.

(62) Johnson, A. C.; Bowser, M. T. Micro Free Flow Electrophoresis. *Lab Chip* **2018**, *18* (1), 27–40. https://doi.org/10.1039/C7LC01105A.

(63) Novo, P.; Dell'Aica, M.; Jender, M.; Höving, S.; Zahedi, R. P.; Janasek, D. Integration of Polycarbonate Membranes in Microfluidic Free-Flow Electrophoresis. *Analyst* **2017**, *142* (22), 4228–4239. https://doi.org/10.1039/C7AN01514C.

(64) Tobishima, S.-I.; Yamaji, A. Ethylene Carbonate—Propylene Carbonate Mixed Electrolytes for Lithium Batteries. *Electrochimica Acta* **1984**, *29* (2), 267–271. https://doi.org/10.1016/0013-4686(84)87058-9.

(65) Muzikar, J.; van de Goor, T.; Gaš, B.; Kenndler, E. Propylene Carbonate as a Nonaqueous Solvent for Capillary Electrophoresis: Mobility and Ionization Constant of Aliphatic Amines. *Anal. Chem.* **2002**, *74* (2), 428–433. https://doi.org/10.1021/ac010887x.

(66) Kochmann, S.; Krylov, S. N. Image Processing and Analysis System for Development and Use of Free Flow Electrophoresis Chips. *Lab Chip* **2017**, *17* (2), 256–266. https://doi.org/10.1039/C6LC01381C.

(67) Kuldvee, R.; Vaher, M.; Koel, M.; Kaljurand, M. Heteroconjugation-Based Capillary Electrophoretic Separation of Phenolic Compounds in Acetonitrile and Propylene Carbonate. *Electrophoresis* **2003**, *24* (10), 1627–1634. https://doi.org/10.1002/elps.200305378.

(68) Kenndler, E. A Critical Overview of Non-Aqueous Capillary Electrophoresis. Part I: Mobility and Separation Selectivity. *Journal of Chromatography A* **2014**, *1335*, 16–30. https://doi.org/10.1016/j.chroma.2014.01.010.

(69) Walker, D. T.; Douglas, C. D.; MacLean, B. J. Synthesis, Characterization, and Surface Studies of Conjugated Polymers Possessing 2,2′-Biimidazole Moieties. *Can. J. Chem.* **2009**, *87* (6), 729–737. https://doi.org/10.1139/V09-055.

(70) Okada, T. Non-Aqueous Capillary Electrophoretic Separation of Brønsted Acids as Heteroconjugated Anions. *Journal of Chromatography A* **1997**, *771* (1–2), 275–284. https://doi.org/10.1016/S0021-9673(97)00094-0.

(71) Porras, S. P.; Kuldvee, R.; Palonen, S.; Riekkola, M.-L. Capillary Electrophoresis of Methyl-Substituted Phenols in Acetonitrile. *Journal of Chromatography A* **2003**, *990* (1–2), 35–44. https://doi.org/10.1016/S0021-9673(02)01965-9.

(72) Tandon, V.; Bhagavatula, S. K.; Nelson, W. C.; Kirby, B. J. Zeta Potential and Electroosmotic Mobility in Microfluidic Devices Fabricated from Hydrophobic Polymers: 1. The Origins of Charge. *Electrophoresis* **2008**, *29* (5), 1092–1101. https://doi.org/10.1002/elps.200700734.

(73) Pugmire, D. L.; Waddell, E. A.; Haasch, R.; Tarlov, M. J.; Locascio, L. E. Surface Characterization of Laser-Ablated Polymers Used for Microfluidics. *Anal. Chem.* **2002**, *74* (4), 871–878. https://doi.org/10.1021/ac011026r.

(74) Schuetzner, Wolfgang.; Kenndler, Ernst. Electrophoresis in Synthetic Organic Polymer Capillaries: Variation of Electroosmotic Velocity and .Zeta. Potential with PH and Solvent Composition. *Anal. Chem.* **1992**, *64* (17), 1991–1995. https://doi.org/10.1021/ac00041a039.

(75) Tavares, M. F. M.; McGuffin, V. L. Theoretical Model of Electroosmotic Flow for Capillary Zone Electrophoresis. *Anal. Chem.* **1995**, *67* (20), 3687–3696. https://doi.org/10.1021/ac00116a012.

(76) Nissum, M.; Foucher, A. L. Analysis of Human Plasma Proteins: A Focus on Sample Collection and Separation Using Free-Flow Electrophoresis. *Expert Review of Proteomics* **2008**, *5* (4), 571–587. https://doi.org/10.1586/14789450.5.4.571.

(77) Köhler, S.; Benz, C.; Becker, H.; Beckert, E.; Beushausen, V.; Belder, D. Micro Free-Flow Electrophoresis with Injection Molded Chips. *RSC Adv.* **2012**, *2* (2), 520–525. https://doi.org/10.1039/C1RA00874A.

(78) Pfeiffer, S. A.; Rudisch, B. M.; Glaeser, P.; Spanka, M.; Nitschke, F.; Robitzki, A. A.; Schneider, C.; Nagl, S.; Belder, D. Continuous Purification of Reaction Products by Micro Free-Flow Electrophoresis Enabled by Large Area Deep-UV Fluorescence Imaging. *Anal Bioanal Chem* **2018**, *410* (3), 853–862. https://doi.org/10.1007/s00216-017-0697-8.

(79) Ivanov, N. A.; Liu, Y.; Kochmann, S.; Krylov, S. N. Non-Aqueous Continuous-Flow Electrophoresis (NACFE): Potential Separation Complement for Continuous-Flow Organic Synthesis. *Lab Chip* **2019**, *19* (13), 2156–2160. https://doi.org/10.1039/C9LC00460B.

(80) Turgeon, R. T.; Bowser, M. T. Improving Sensitivity in Micro-Free Flow Electrophoresis Using Signal Averaging. *Electrophoresis* **2009**, *30* (8), 1342–1348. https://doi.org/10.1002/elps.200800497.

(81) Nagl, S. Micro Free-Flow Isoelectric Focusing with Integrated Optical PH Sensors. *Eng. Life Sci.* **2018**, *18* (2), 114–123. https://doi.org/10.1002/elsc.201700035.

(82) Saar, K. L.; Zhang, Y.; Müller, T.; Kumar, C. P.; Devenish, S.; Lynn, A.; Łapińska, U.; Yang, X.; Linse, S.; Knowles, T. P. J. On-Chip Label-Free Protein Analysis with Downstream Electrodes for Direct Removal of Electrolysis Products. *Lab Chip* **2018**, *18* (1), 162–170. https://doi.org/10.1039/C7LC00797C.

(83) Song, Y.-A.; Chan, M.; Celio, C.; Tannenbaum, S. R.; Wishnok, J. S.; Han, J. Free-Flow Zone Electrophoresis of Peptides and Proteins in PDMS Microchip for Narrow PI Range Sample Prefractionation Coupled with Mass Spectrometry. *Anal. Chem.* **2010**, *82* (6), 2317–2325. https://doi.org/10.1021/ac9025219.

(84) Benz, C.; Boomhoff, M.; Appun, J.; Schneider, C.; Belder, D. Chip-Based Free-Flow Electrophoresis with Integrated Nanospray Mass-Spectrometry. *Angew. Chem. Int. Ed.* **2015**, *54* (9), 2766–2770. https://doi.org/10.1002/anie.201409663.

(85) Hassur, S. M.; Whitlock, H. W. UV Shadowing—A New and Convenient Method for the Location of Ultraviolet-Absorbing Species in Polyacrylamide Gels. *Analytical Biochemistry* **1974**, *59* (1), 162–164. https://doi.org/10.1016/0003-2697(74)90020-7.

(86) Meyers, C. L. F.; Meyers, D. J. Thin-Layer Chromatography. *Current Protocols in Nucleic Acid Chemistry* **2008**, *34* (1). https://doi.org/10.1002/0471142700.nca03ds34.

(87) Hollenstein, M.; Damha, M. J. Rolling Circle Amplification with Chemically Modified Nucleoside Triphosphates. *Current Protocols in Nucleic Acid Chemistry* **2016**, *67* (1). https://doi.org/10.1002/cpnc.17.

(88) Gioiello, A.; Piccinno, A.; Lozza, A. M.; Cerra, B. The Medicinal Chemistry in the Era of Machines and Automation: Recent Advances in Continuous Flow Technology. *J. Med. Chem.* **2020**, *63* (13), 6624–6647. https://doi.org/10.1021/acs.jmedchem.9b01956.

(89) Jiao, J.; Nie, W.; Yu, T.; Yang, F.; Zhang, Q.; Aihemaiti, F.; Yang, T.; Liu, X.; Wang, J.; Li, P. Multi-Step Continuous-Flow Organic Synthesis: Opportunities and Challenges. *Chem. Eur. J.* **2021**, *27* (15), 4817–4838. https://doi.org/10.1002/chem.202004477.

(90) Turgeon, R. T.; Bowser, M. T. Micro Free-Flow Electrophoresis: Theory and Applications. *Anal Bioanal Chem* **2009**, *394* (1), 187–198. https://doi.org/10.1007/s00216-009-2656-5.

(91) Evenhuis, C. J.; Okhonin, V.; Krylov, S. N. Non-Orthogonal Micro-Free Flow Electrophoresis: From Theory to Design Concept. *Analytica Chimica Acta* **2010**, *674* (1), 102–109. https://doi.org/10.1016/j.aca.2010.06.002.

(92) Schindelin, J.; Arganda-Carreras, I.; Frise, E.; Kaynig, V.; Longair, M.; Pietzsch, T.; Preibisch, S.; Rueden, C.; Saalfeld, S.; Schmid, B.; Tinevez, J.-Y.; White, D. J.; Hartenstein, V.; Eliceiri, K.; Tomancak, P.; Cardona, A. Fiji: An Open-Source Platform for Biological-Image Analysis. *Nat Methods* **2012**, *9* (7), 676–682. https://doi.org/10.1038/nmeth.2019.

(93) Tinevez, J.-Y.; Perry, N.; Schindelin, J.; Hoopes, G. M.; Reynolds, G. D.; Laplantine, E.; Bednarek, S. Y.; Shorte, S. L.; Eliceiri, K. W. TrackMate: An Open and Extensible

Platform for Single-Particle Tracking. *Methods* **2017**, *115*, 80–90. https://doi.org/10.1016/j.ymeth.2016.09.016.

(94) Ershov, D.; Phan, M.-S.; Pylvänäinen, J. W.; Rigaud, S. U.; Le Blanc, L.; Charles-Orszag, A.; Conway, J. R. W.; Laine, R. F.; Roy, N. H.; Bonazzi, D.; Duménil, G.; Jacquemet, G.; Tinevez, J.-Y. *Bringing TrackMate into the Era of Machine-Learning and Deep-Learning*; preprint; Bioinformatics, 2021. https://doi.org/10.1101/2021.09.03.458852.

(95) Pamme, N. Continuous Flow Separations in Microfluidic Devices. *Lab Chip* **2007**, *7* (12), 1644. https://doi.org/10.1039/b712784g.

(96) Rathore, A. S.; Kumar, D.; Kateja, N. Recent Developments in Chromatographic Purification of Biopharmaceuticals. *Biotechnol Lett* **2018**, *40* (6), 895–905. https://doi.org/10.1007/s10529-018-2552-1.

(97) Okhonin, V.; Evenhuis, C. J.; Krylov, S. N. Non-Orthogonal-to-the-Flow Electric Field Improves Resolution in the Orthogonal Direction: Hidden Reserves for Combining Synthesis and Purification in Continuous Flow. *Anal. Chem.* **2010**, *82* (4), 1183–1185. https://doi.org/10.1021/ac902546y.

(98) Mesbah, K.; Mai, T. D.; Jensen, T. G.; Sola, L.; Chiari, M.; Kutter, J. P.; Taverna, M. A Neutral Polyacrylate Copolymer Coating for Surface Modification of Thiol-Ene Microchannels for Improved Performance of Protein Separation by Microchip Electrophoresis. *Microchim Acta* **2016**, *183* (7), 2111–2121. https://doi.org/10.1007/s00604-016-1825-4.

(99) Bacheva, V.; Paratore, F.; Rubin, S.; Kaigala, G. V.; Bercovici, M. Tunable Bidirectional Electroosmotic Flow for Diffusion-Based Separations. *Angew. Chem. Int. Ed.* **2020**, *59* (31), 12894–12899. https://doi.org/10.1002/anie.201916699.

(100) Rosenfeld, T.; Bercovici, M. Dynamic Control of Capillary Flow in Porous Media by Electroosmotic Pumping. *Lab Chip* **2019**, *19* (2), 328–334. https://doi.org/10.1039/C8LC01077C.

(101) de Valença, J. C.; Wagterveld, R. M.; Lammertink, R. G. H.; Tsai, P. A. Dynamics of Microvortices Induced by Ion Concentration Polarization. *Phys. Rev. E* **2015**, *92* (3), 031003. https://doi.org/10.1103/PhysRevE.92.031003.

(102) Hanasoge, S.; Diez, F. J. Vortex Chain Formation in Regions of Ion Concentration Polarization. *Lab Chip* **2015**, *15* (17), 3549–3555. https://doi.org/10.1039/C5LC00558B.

(103) Liu, W.; Ren, Y.; Xue, R.; Song, C.; Wu, Q. On Ion Transport Regulation with Field-effect Nonlinear Electroosmosis Control in Microfluidics Embedding an Ion-selective Medium. *ELECTROPHORESIS* **2020**, *41* (10–11), 778–792. https://doi.org/10.1002/elps.201900408.

(104) Liu, W.; Ren, Y.; Tao, Y.; Zhou, Z.; Wu, Q.; Xue, R.; Yao, B. Multiple Frequency Electrothermal Induced Flow: Theory and Microfluidic Applications. *J. Phys. D: Appl. Phys.* **2020**, *53* (17), 175304. https://doi.org/10.1088/1361-6463/ab71b1.

(105) Kochmann, S.; Ivanov, N. A.; Lucas, K. S.; Krylov, S. N. Topino: A Graphical Tool for Quantitative Assessment of Molecular Stream Separations. *Anal. Chem.* **2021**, *93* (29), 9980–9985. https://doi.org/10.1021/acs.analchem.1c01229.

APPENDICES

APPENDIX A - Supplementary tables and figures for Chapter 2

Table A2.1. Properties of tested plastic materials

Evaluation parameters of tested plastic materials. PMMA is our reference material and choice for aqueous-based continuous-flow electrophoresis. FEP, PSu, and PVC Type I are suitable candidates for non-aqueous electrophoresis, in principle. However, PVC Type I is optically clear, has the best cost-efficiency, and, thus, was chosen in the present studies.

Name[a]	OC[b]	Millability[c]	PC[d]	Costs[e] ($/dm³)	Costs[f] ($/chip)	Relative costs[g]
ABS	not clear	✔	✘	20	3	1.0
CLPS	not clear	✔	✔	100	13	4.3
CPVC	not clear	✔	✔	55	7	2.3
FEP	**semi-clear**	✔	✔	**535**	**70**	**23.3**
HDPE	not clear	✔	✔	10	2	0.7
PCa	clear	✔	✘	20	3	1.0
PE	not clear	✘	✔	70	9	3.0
PEEK	not clear	✔	✔	655	86	28.7
PETG	clear	✔	✘	15	2	0.7
PMMA	**clear**	✔	✘	**25**	**3**	**1.0**
PP	semi-clear	✘	✔	15	2	0.7
PPS	not clear	✔	✔	755	99	33.0
PS	not clear	✔	✘	15	2	0.7
PSu	**semi-clear**	✔	✔	**185**	**24**	**8.0**
PTFE	not clear	✔	✔	170	22	7.3
PVC Type I	**clear**	✔	✔	**30**	**4**	**1.3**
PVDF	not clear	✔	✔	200	26	8.7
UHMW	not clear	✔	✔	15	2	0.7

[a]ABS = Acrylontrile butadiene styrene, CLPS = Cross-linked polystyrene (Rexolite), CPVC = Chemical-resistant polyvinyl chloride, FEP = Fluorinated ethylene propylene, HDPE = High-density polyethylene, PCa = Polycarbonate, PE = Polyester, PEEK = Polyether ether ketone, PETG = Polyethylene terephthalate glycol, PMMA = Poly(methyl methacrylate), PP = Polypropylene, PPS = Polyphenylene sulphide, PS = Polystyrene, PSu = Polysulfone, PTFE = Polytetrafluoroethylene (Teflon), PVC Type I = Polyvinyl chloride Type I, PVDF = Polyvinylidene fluoride, UHMW = Ultra-high-molecular-weight polyethylene.

[b]Optical clarity in visible spectrum (non-transparent).

[c]Ability to mill plastics using our established protocols for PMMA.[44] (✘ = material tends to melt and/or fringe more easily than PMMA).

[d]Compatibility with propylene carbonate (PC): plastic can withstand continuous exposure to PC for at least 48 h without any obvious swelling or disintegration.

[e]Cost is given in Canadian Dollars and based on McMaster-Carr's price list of February 2019. They are listed here for pure illustration and a rough comparison.

[f]About 0.132 dm^3 are required for the assembly of one chip. Electrodes and flow connectors not included in price.

[g]Relative to PMMA.

Figure A2.1. NACFE chip

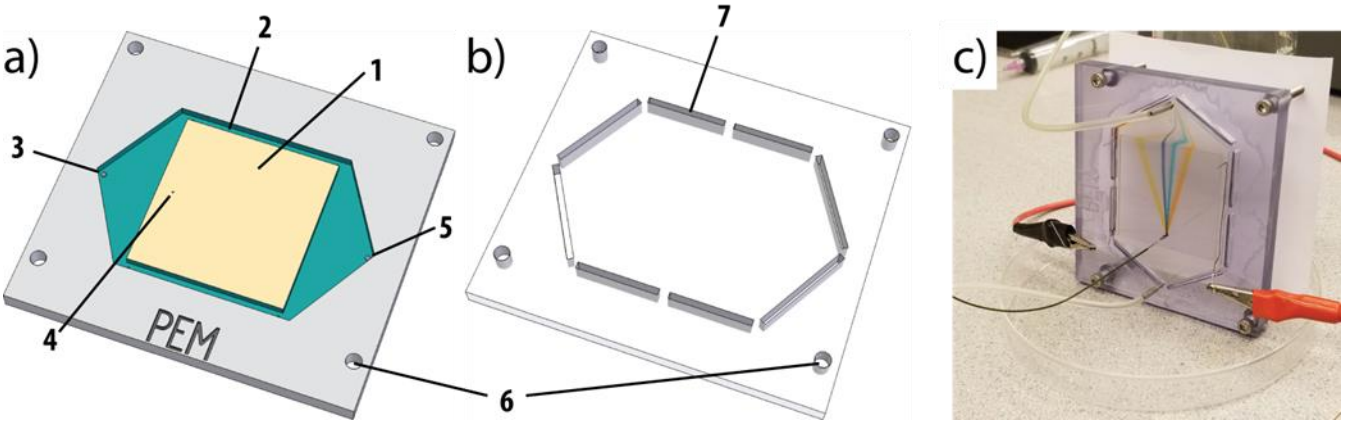

NACFE chip used in this study (named PEM after the city of Pembroke): a) bottom plate, b) top plate, and c) photo of the assembled chip during operation. The numbers indicate: the separation zone (1), electrode channels (2), electrolyte inlet (3), sample inlet (4), outlet (5), mounting holes (6), and gluing channels (7). The chip dimensions are 110 mm × 100 mm × 12 mm, and the dimensions of the separation zone are 50 mm × 52 mm × 0.25 mm.

Figure A2.2. Electric current in NACFE with an electrolyte being TBAA solution in PC

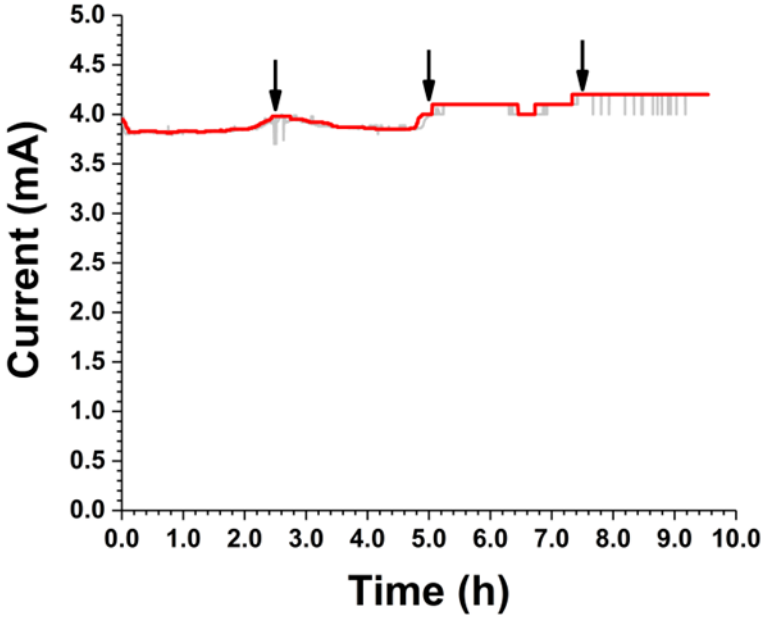

Long-term stability of NACFE using a solution of 30 mM TBAA in PC as an electrolyte. The arrows indicate the times at which the electrolyte was recycled. The grey curve is the signal as measured; the signal was smoothened for clarity by a percentile filter (100-point window; 80%); the red curve is the result of smoothening. The current was stable at 4.00 ± 0.15 mA (E = 18.2 V/cm) with only a slight drift towards higher currents due to electrochemical reactions and/or buffer depletion.

Figure A2.3. Formation of brown precipitate at the cathode for the imidazolium-based electrolyte

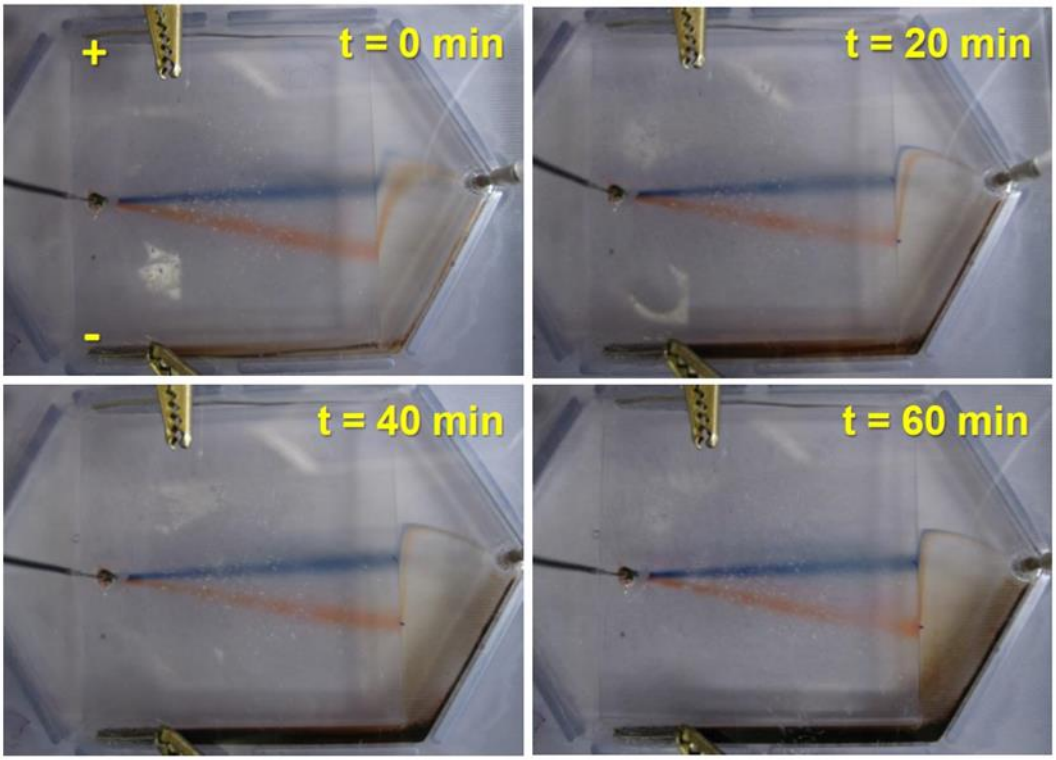

Separation of Sudan black B and Rhodamine 6G (3 mM each) in 21 mM imidazolium ethyl sulfate in PC. The excessive precipitation of a brown product at the cathode (bottom) affects the optical clarity of the chip.

Figure A2.4. Comparing NACFE with weak- and strong-basicity anions in the electrolyte

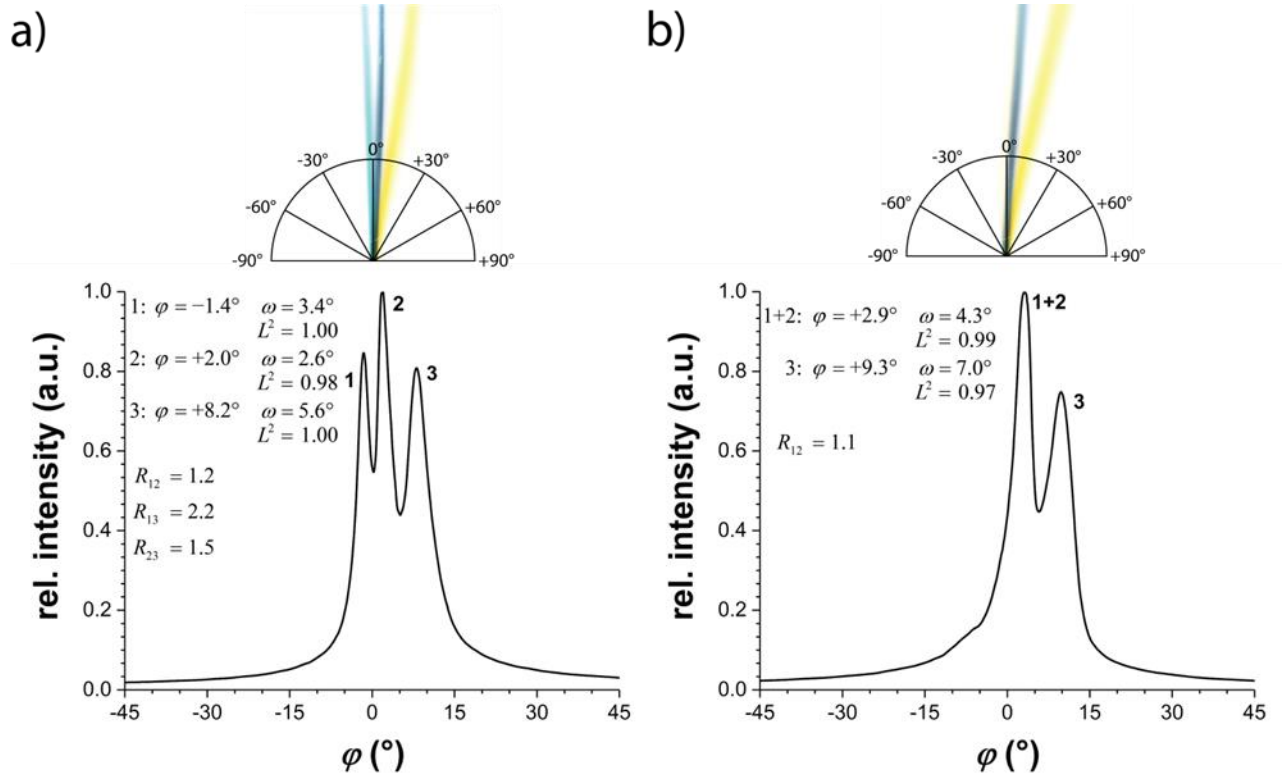

Separations with a) TBAA (strong base anion) and b) tetrabutylammonium hydrogen sulfate (weak base anion) in PC as electrolytes. Analytes were α-naphtholbenzein (1), Sudan black B (2), and DMAS (3). Only the strong-base anion was able to separate all three analytes. The conditions were: electrolyte flow rate = 3 mL/min, sample flow rate = 2 µL/min, and E = 27.3 V/cm (I ≈ 8.8 mA). The anode and cathode are towards negative and positive angles, respectively.

Figure A2.5. Acetonitrile as solvent in non-aqueous electrolyte

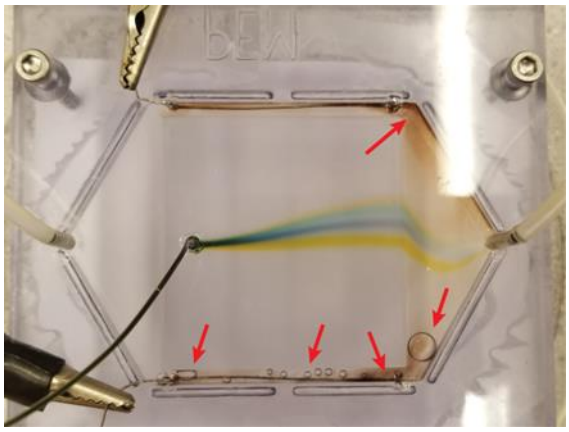

NACFE of four analytes (fluorescein, α-naphtholbenzein, Sudan black B, and DMAS; 1.25 mM each) in an electrolyte containing 30 mM TBAA in acetonitrile. Bubble formation (red arrows) and lack of bubble dislodging from the electrodes are evident. Bands are broader, and higher electric fields are needed to achieve resolution similar to that in the PC-based electrolyte. Conditions were: electrolyte flow rate = 4 mL/min, sample flow rate = 2 µL/min, and E = 5.3 V/cm (I ≈ 8.0 mA).

APPENDIX B - Supplementary tables and figures for Chapter 3

Table B3.1. Properties of tested plastic materials

Evaluation parameters of tested plastic materials. In theory, most are suitable candidates for fluorescent sublayer-based visualization. However, PEI is brighter and produces a green color, and, thus, was chosen in the present studies. PVC is listed as a non-fluorescent reference material from our previous study of NACFE (*Lab Chip* 2019, 19, 2156−2160, DOI: **10.1039/C9LC00460B**).

Name[a]	Fluorescence color[b]	Machinability[c]	PC[d]	Cost[e] ($/dm³)	Cost[f] ($/chip)
PVC	N/A	✔	✔	30	0.9
Nylon	White	✘	✔	157	4.7
PPSU	Blue	✔	✔	204	6.1
CLPS	Blue	✔	✔	100	3.0
HDPE	Blue	✔	✔	10	0.3
POM	Blue	✔	✔	56	1.7
LDPE	Violet	✘	✔	29	0.9
PE	Blue	✔	✔	70	2.1
PEI	**Green**	✔	✔	**249**	**7.5**
PPS	Violet	✔	✔	755	22.7
PSu	Blue	✔	✔	185	5.6
PVDF	Blue	✔	✔	200	6.0

[a]PVC = Polyvinylchloride, Nylon = Polyamide, PPSU = Polyphenylsulfone, CLPS = Cross-linked polystyrene (Rexolite), HDPE = High-density polyethylene, POM = Polyoxymethylene (Delrin Acetal), LDPE = Low-density polyethylene, PE = Polyester, PEI = Polyethereimide, PPS = Polyphenylene sulphide, PSu = Polysulfone, PVDF = Polyvinylidene fluoride.

[b]Apparent fluorescence in the visible range of spectrum.

[c]Ability to mill plastics using our established protocols for PVC. (✘ = material tends to melt and/or fringe more easily than PVC).

[d]Compatibility with propylene carbonate (PC): plastic can withstand continuous exposure to PC for at least 48 h without any obvious swelling or disintegration.

[e]Costs are given in Canadian Dollars and based on McMaster-Carr's price list of December 2019. They are listed here for pure illustration and a rough comparison.

[f]About 0.03 dm³ are required for to assemble a single chip (70 mm × 70 mm × 5.2 mm). Electrodes and flow connectors are not included in price.

Figure B3.1. Quartz-quartz pseudo device

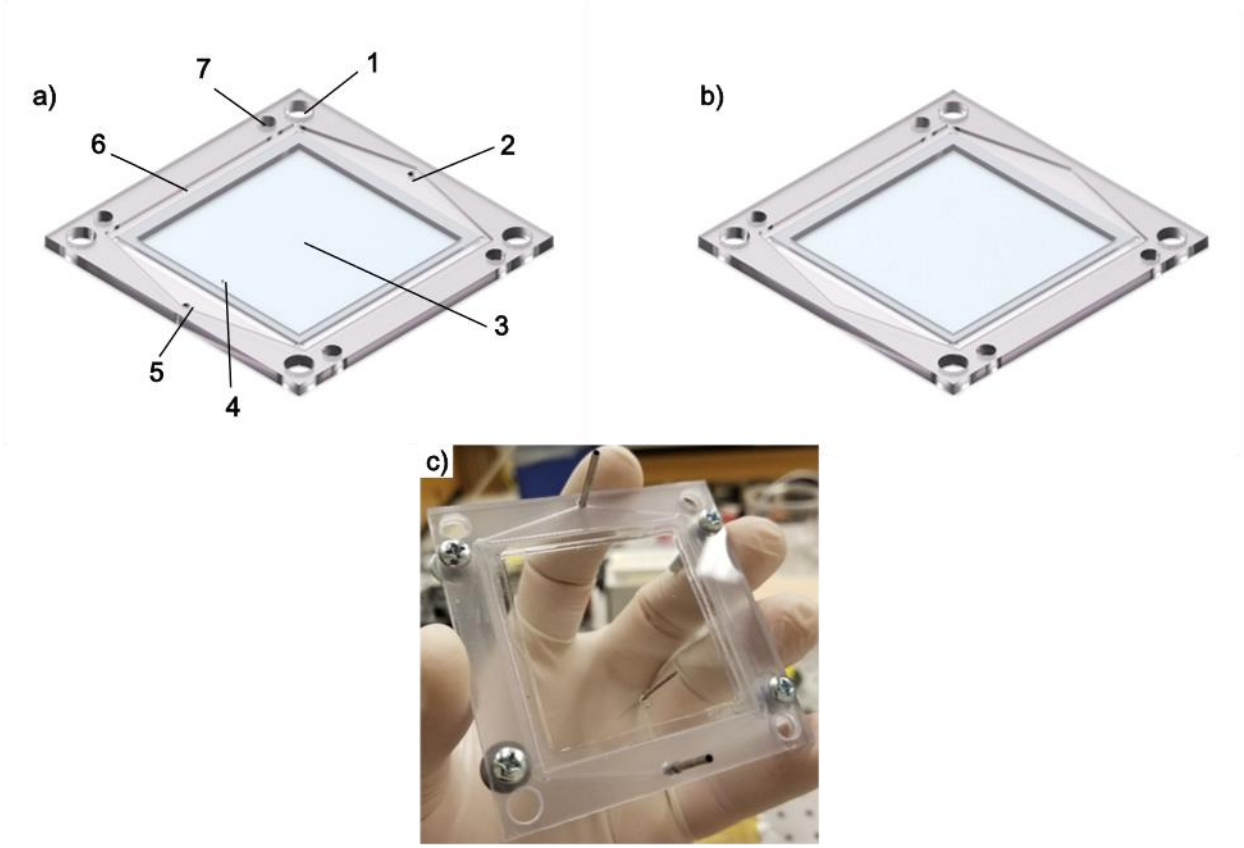

Quartz-quartz pseudo device used as an optically ideal reference in this study: a) top PVC-Quartz plate, b) bottom PVC-Quartz plate, and c) photo of the assembled device. The numbers indicate: 6 mm mounting holes (1), outlet (2), the separation zone (3), sample inlet (4), electrolyte inlet (5), electrode channels (6), 4 mm mounting holes (7). The chip dimensions are 70 mm × 70 mm × 5.2 mm, and the dimensions of the separation zone are 50 mm × 50 mm × 0.2 mm.

Figure B3.2. PEI-quartz pseudo device

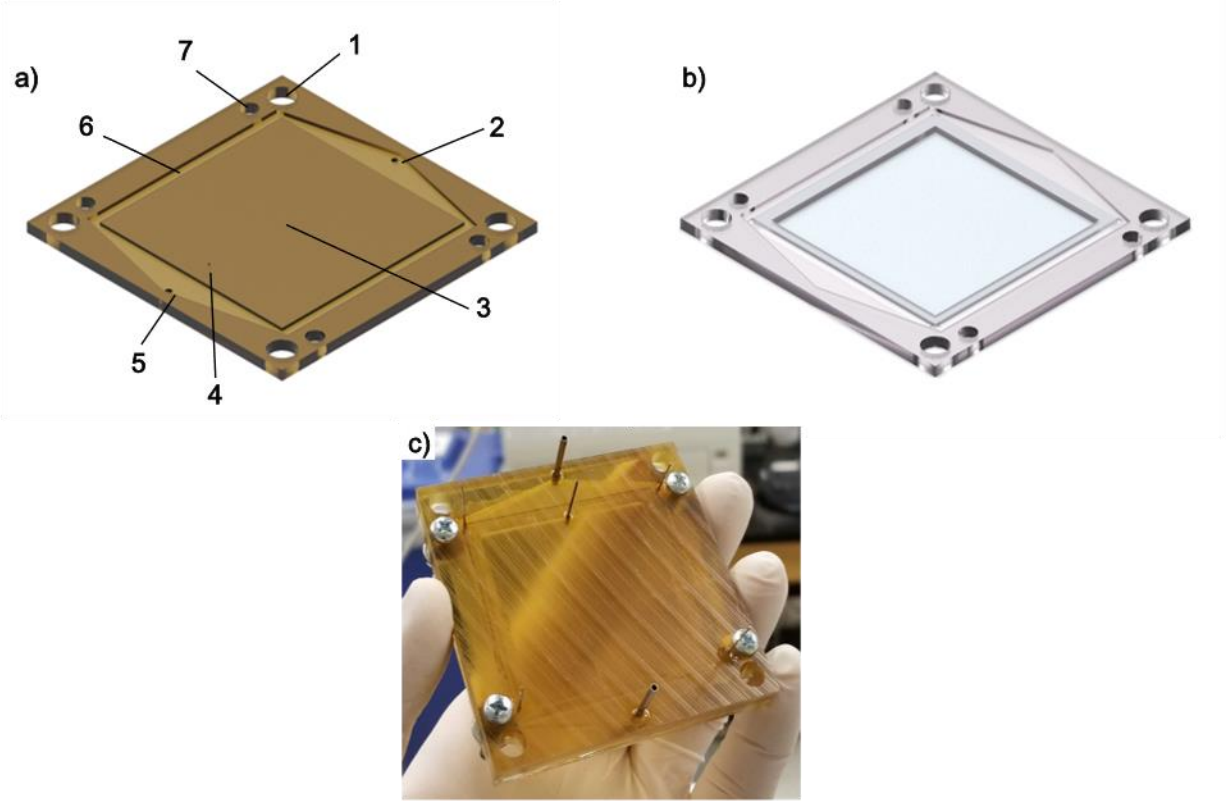

Hybrid PEI-quartz device used for CFE separation in this study: a) top polyetherimide plate, b) bottom Quartz-PVC plate, and c) photo of the assembled device. The numbers indicate: 6 mm mounting holes (1), outlet (2), the separation zone (3), sample inlet (4), electrolyte inlet (5), electrode channels (6), 4 mm mounting holes (7). The chip dimensions are 70 mm × 70 mm × 5.2 mm, and the dimensions of the separation zone are 50 mm × 50 mm × 0.2 mm.

APPENDIX C - Supplementary tables and figures for Chapter 4

Figure C4.1. CAC geometry transformation

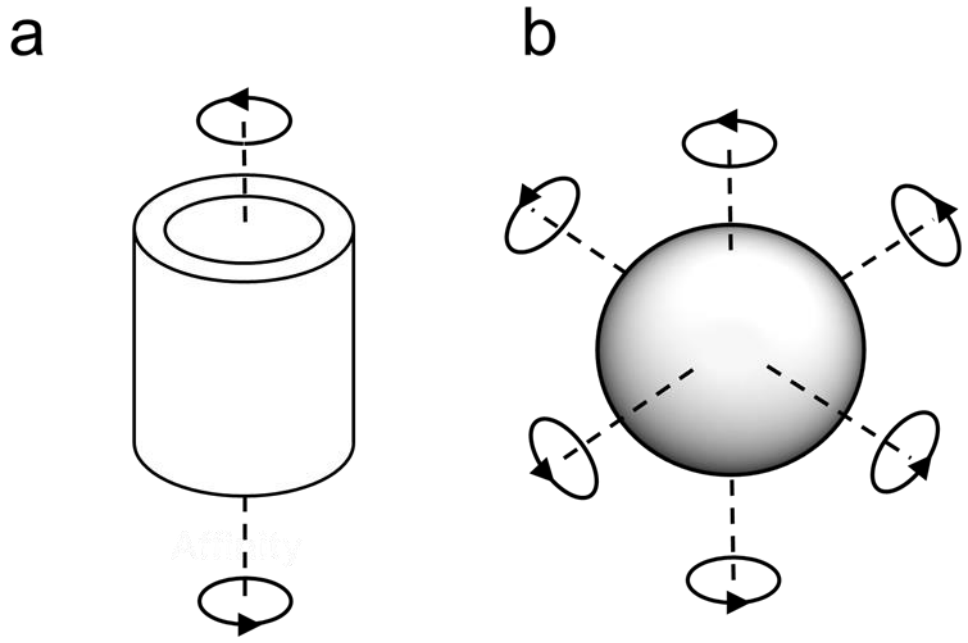

Illustration of **a)** conventional CAC geometry with one infinite rotation axis at the center of the cylinder and **b)** transformed geometry that contains an additional infinite rotational axis orthogonal to the surface of the sphere.

Figure C4.2. Varying the total number of the electrode segments

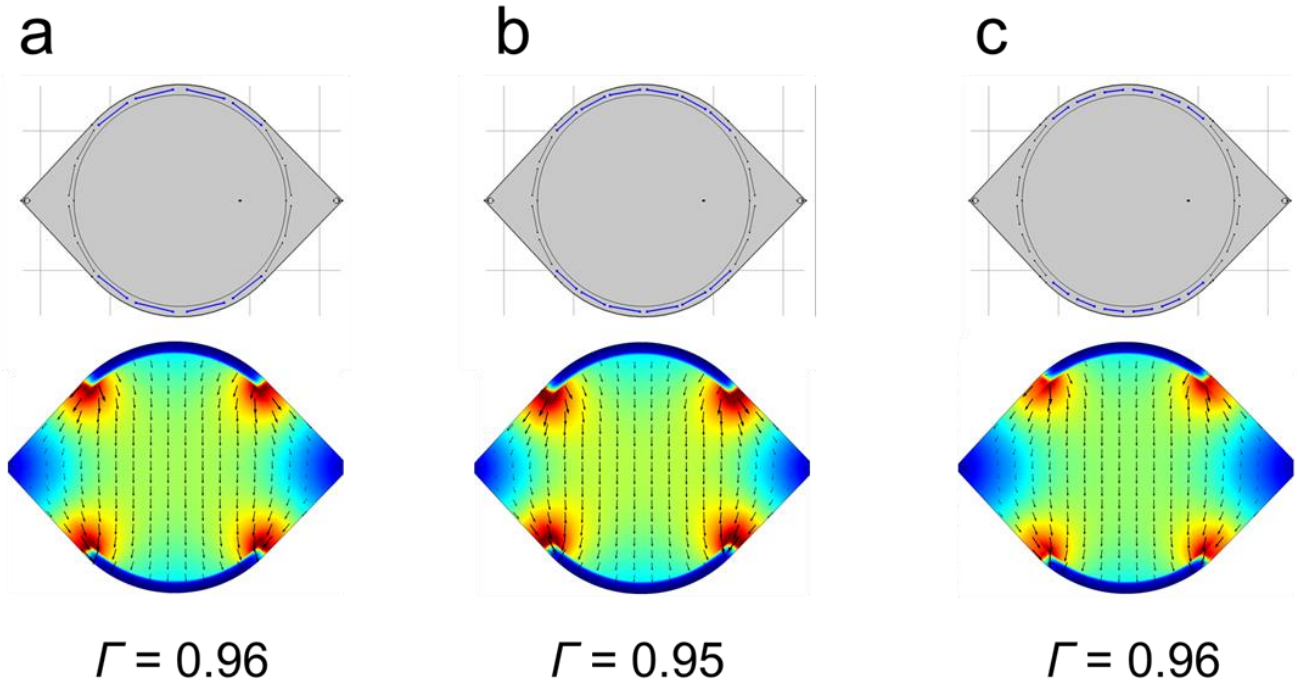

Illustration of potential geometries containing **a)** 16, **b)** 20, and **c)** 24 electrodes and their corresponding COMSOL simulated electric fields.

Figure C4.3. Angulagrams for Figure 4.6a

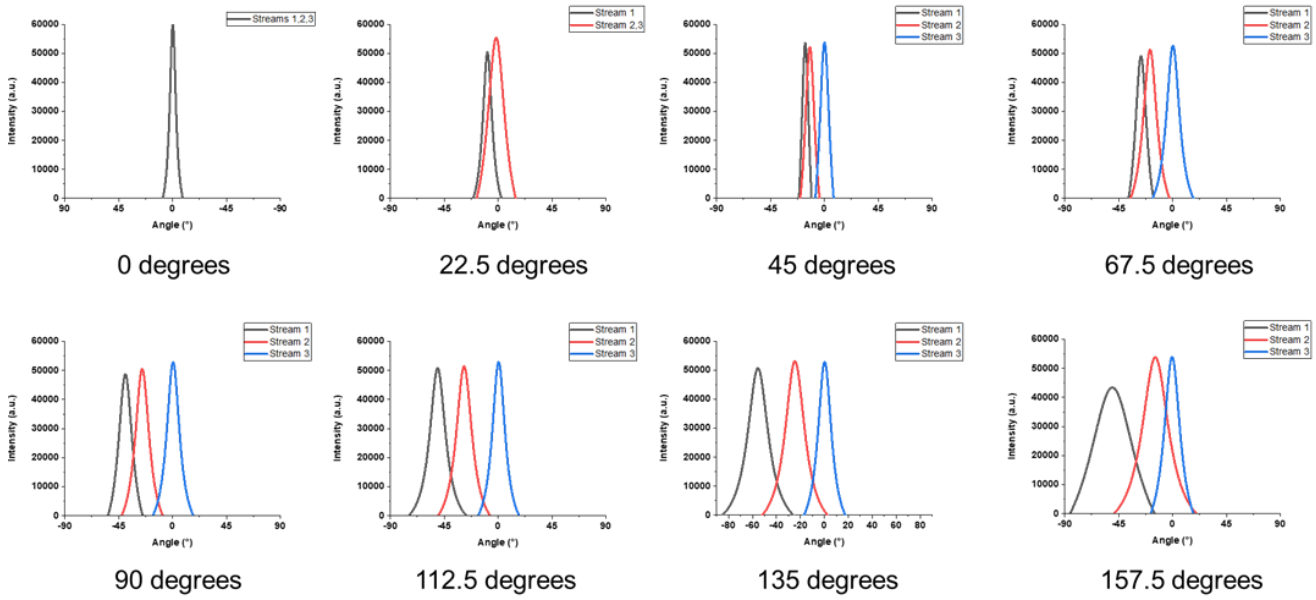

Angulagrams for molecular streams in Figure 6a in the main text. The angulagrams were generated using Topino software.[105]

Note C4.1. Examples of Γ for different geometries with non-homogenous flow

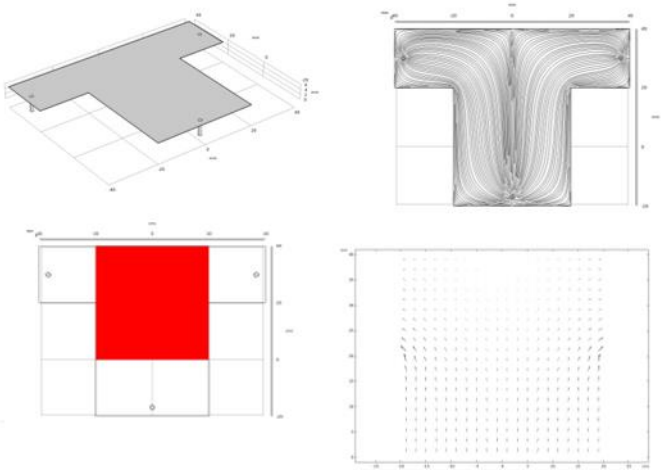

$\Gamma = 0.631$

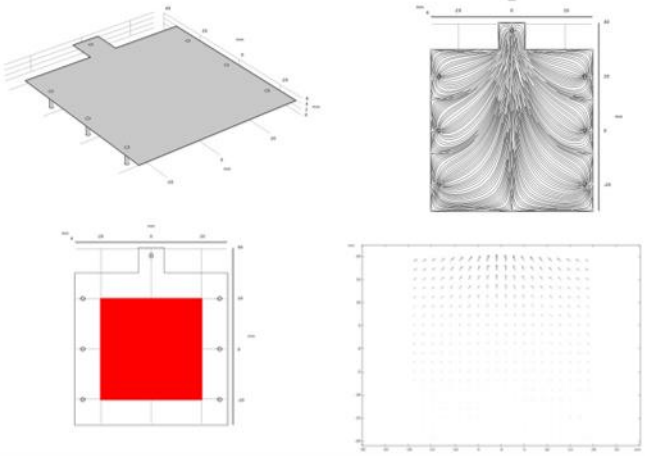

$\Gamma = 0.311$

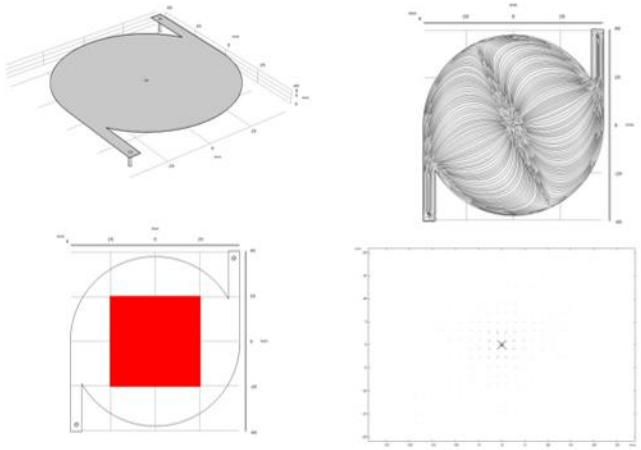

$\Gamma = 0.282$

Note C4.2. List of COMSOL models

The complete list of COMSOL models (.mph) deposited into ChemRxiv:

1. Circular device geometry evolution models (**Figure 4.3**)
    1.1. Circle prototype 250 micron uniform thickness (**Figure 4.3a**)
    1.2. Circle prototype 3mm electrode channels (**Figure 4.3b**)
    1.3. “The eye” 3mm electrode channels (**Figure 4.3c**)
2. Examples of Γ for non-ideal flow geometries (**Note C4.1**)
    2.1. T splitter geometry flow field
    2.2. Square multiple inlets flow field
    2.3. Sink with 2 inlets flow field
3. Varying the total number of electrodes in the circular device (**Figure C4.2**)
    3.1. 16 segments with 8 active electrodes (**Figure C4.2a**)
    3.2. 20 segments with 12 active electrodes (**Figure C4.2b**)
    3.3. 24 segments with 12 active electrodes (**Figure C4.2c**)
4. Varying the number of active electrodes in the circular device (**Figure 4.4**)
    4.1. 16 segments with 4 active electrodes (**Figure 4.4a**)
    4.2. 16 segments with 8 active electrodes (**Figure 4.4b**)
    4.3. 16 segments with 12 active electrodes (**Figure 4.4c**)
5. Varying the angle in non-orthogonal separation models (**Figure 4.6**)
    5.1. 16 segments with 8 active electrodes, 0 degrees between flow and electric field
    5.2. 16 segments with 8 active electrodes, 22.5 degrees between flow and electric field
    5.3. 16 segments with 8 active electrodes, 45 degrees between flow and electric field
    5.4. 16 segments with 8 active electrodes, 67.5 degrees between flow and electric field
    5.5. 16 segments with 8 active electrodes, 90 degrees(orthogonal) between flow and electric field
    5.6. 16 segments with 8 active electrodes, 112.5 degrees between flow and electric field
    5.7. 16 segments with 8 active electrodes, 135 degrees between flow and electric field
    5.8. 16 segments with 8 active electrodes, 157.5 degrees between flow and electric field

Note C4.3. Measurements of electrophoretic mobilities in CE

Analyte	Charge	Migration time, s	Migration velocity, m/s	Difference between migration velocities of the analyte and EOF, m/s	Electrophoretic mobility, $m^2/(Vs)$
Toluene (EOF marker)	Neutral	133.8	0.00149	0	0
SBL	Near Neutral	133.8	0.00149	0	0
NAP	Negative	215.4	0.00092	–0.00057	-5.7×10^{-9}
FLU	Negative	417	0.00048	–0.00101	-1.0×10^{-8}

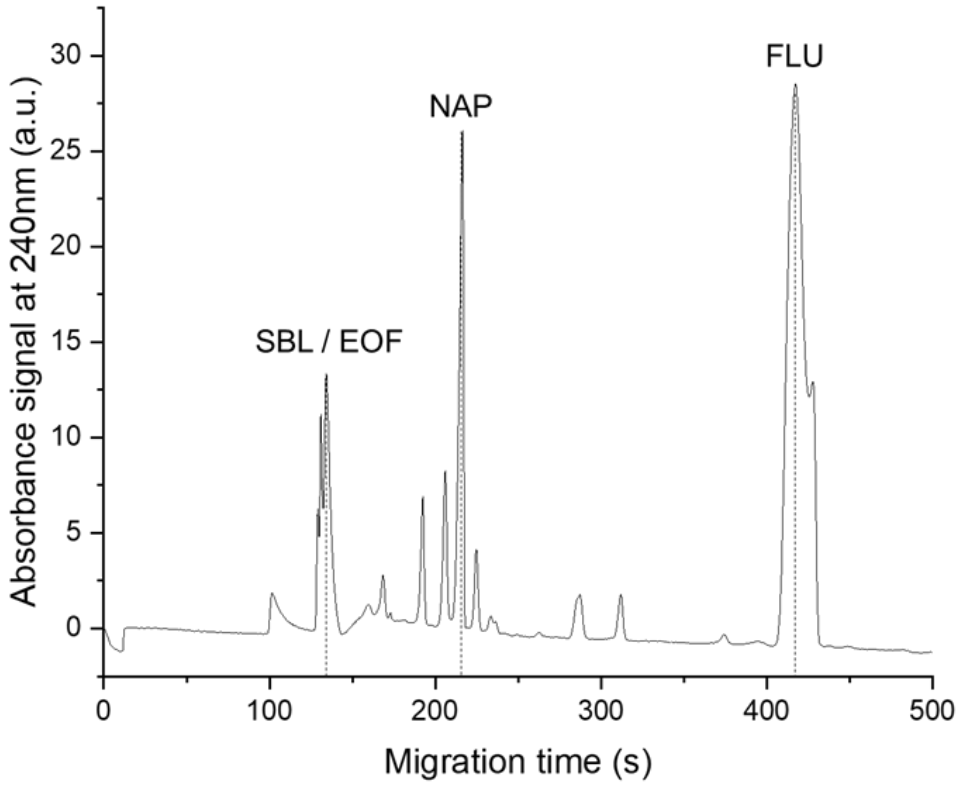

Note C4.4. Circular CFE device

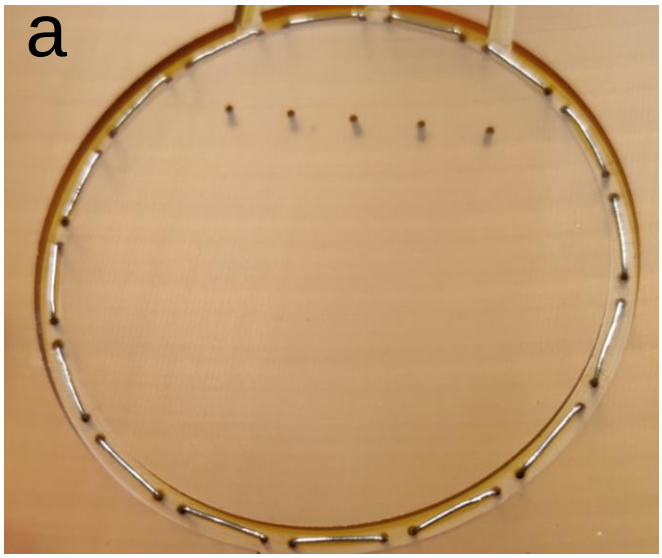

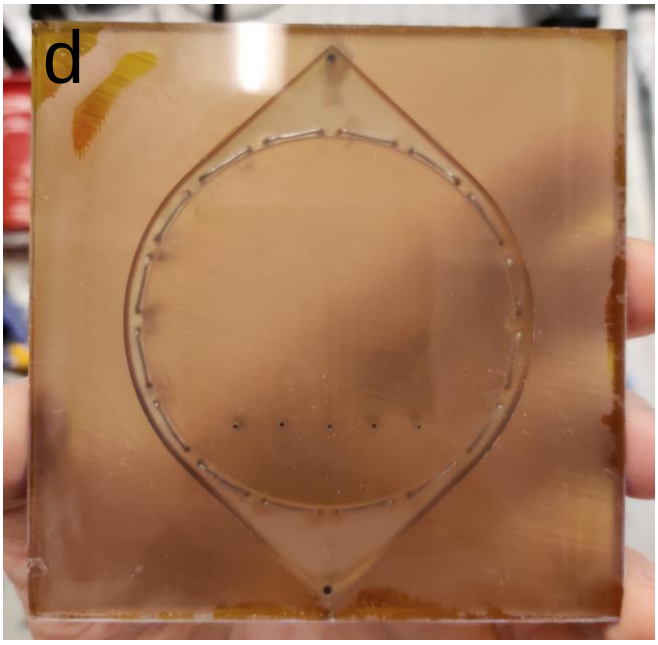

Note C4.5. Fabrication timeline for rectangular and circular device

Rectangular device **Engineering material/steps**	**Time/** **Material**	**Non-orthogonal device** **Engineering material/steps**	**Time/** **Material**
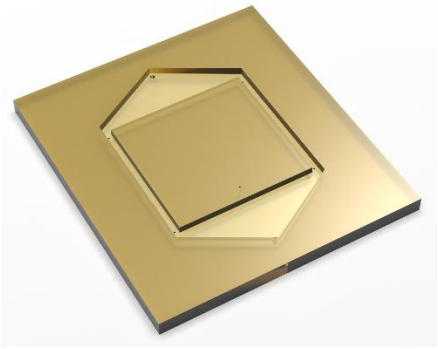		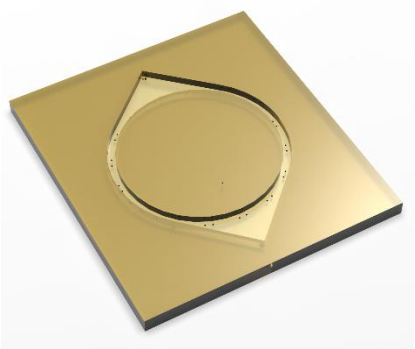	
	Milling chip parts		
1 × plate of **PEI** 1 × plate of **PVC**	2 × 110 cm³	1 × plate of **PEI** 1 × plate of **PVC**	2 × 110 cm³
1. Roughing bottom piece	2.5 h	1. Roughing bottom piece	2.5 h
2. Flatlanding bottom piece	1.0 h	2. Flatlanding bottom piece	1.0 h
3. Roughing top piece	1.0 h	3. Roughing top piece	1.0 h
4. Flatlanding top piece	2.0 h	4. Flatlanding top piece	2.0 h
	Adding fluid ports		
2 × **gauge 22** inlet (metal)	2 × 10 mm	2 × **gauge 22** inlet (metal)	2 × 10 mm
1 × **gauge 16** inlet (metal)	1 × 10 mm	1 × **gauge 16** inlet (metal)	1 × 10 mm
5. Installing **2** buffer inlets	0.1 h	5. Installing **2** buffer inlets	0.1 h
6. Installing **1** sample inlet	0.1 h	6. Installing **1** sample inlet	0.1 h
	Adding electrical connections		
platinum wire	2 × 7 cm	**platinum** wire	16 × 2 cm
		Gold-plated nickel crimps	16
7. Drilling **4** electrode holes	0.1 h	7. Drilling **32** electrode holes	1.0 h
8. Preparing **2** electrodes	0.1 h	8. Preparing **16** electrodes	0.5 h
9. Installing **2** electrodes	0.1 h	9. Installing **16** electrodes	0.5 h
10. Gluing **2** electrodes	0.1 h	10. Gluing **16** electrodes	0.5 h
11. Waiting for glue to set	2.0 h	11. Waiting for glue to set	2.0 h
		12. Attaching crimps	1.0 h
	Assembling chip parts		
12. Gluing pieces together	0.5 h	13. Gluing plates together	0.5 h
13. Waiting for glue to set	2.0 h	14. Waiting for glue to set	2.0 h
Total time	11.6 h	**Total time**	14.7 h